Hydrodynamics of drop formation in liquid-liquid systems: investigation and interpretation of drop sizes in liquid-liquid systems as a function of nozzle diameter, nozzle velocity and physical properties of the systems

Thesis

THE OPEN UNIVERSITY

DEPARTMENT OF ENGINEERING MECHANICS

HYDRODYNAMICS OF DROP FORMATION IN LIQUID-LIQUID SYSTEMS

Investigation and interpretation of drop sizes in liquid-liquid systems as a function of nozzle diameter, nozzle velocity and physical properties of the systems.

A thesis submitted for the degree of

DOCTOR OF PHILOSOPHY

by

SHUAIB AHMAD KHAN

B.Sc., M.Sc., M.Phil.

Date of Submission: Aug 86 AUGUST 1986
Date of Award: 1.12.86

HYDRODYNAMICS OF DROP FORMATION IN LIQUID-LIQUID SYSTEMS

SHUAIB AHMAD KHAN

B.Sc., M.Sc., M.Phil.

PH.D

AUGUST 1986

ACKNOWLEDGEMENTS

I wish to express my sincere gratitude to Dr A Bright, who directed this research programme and offered continuous guidance and encouragements during the course of this work.

I am grateful to Prof. A G Parkinson, head of the Engineering Mechanics Department, for providing laboratory facilities for the experimental work of the present study.

My thanks are also due to the member of staff, technicians and my colleagues for their co-operation.

August 1986 S A Khan

INDEX

ABSTRACT

Drop formation processes from a nozzle of diameter 0.0602 cm in immiscible liquids were investigated experimentally and theoretically. Experimental data for drop sizes in prejetting and jetting regimes were obtained.

In the prejetting conditions for water into decane system, data for drop formation time, drop diameter and drop velocities were obtained at three different Weber numbers using still photography and high speed cine film photographic techniques. A model has been developed to account for a two stage drop formation process in the prejetting regime.

In the jetting regime three liquid pairs were employed with injection of dispersed phase from above and below the continuous phase to give a range of physical properties. Interfacial tension was varied from 3.1 to 27.5 mNm^{-1}. The ratio of the continuous phase to the dispersed phase densities was varied from 0.73 to 1.36. The ratio of viscosities of the two phases was varied from 0.063 to 15.7. The experimental data for minimum drop size, mean drop size, jetlength and jet diameter were obtained from still photography. Experimental data for wave length, wave period, wave amplitude of the fastest growing disturbance on the jet were obtained by stroboscopic and high speed photographic techniques.

A linear stability analysis for small scale

hydrodynamics of the wave motion has been developed to predict the wave growth rate in the jetting regime. Patterns of drop formation and drop size variations in the intermediate regime were investigated and a semi-theoretical correlation was obtained to predict the drop size in the intermediate regime.

LIST OF FIGURES

LIST OF TABLES

LIST OF PHOTOGRAPHS

CHAPTER 1

INTRODUCTION

A knowledge of drop size and drop size distribution is of fundamental importance for an understanding of the heat and mass transfer characteristics in liquid-liquid systems. The heat and mass transfer rates are directly proportional to the interfacial area created in liquid-liquid contactors. A wide variety of contacting equipment is used to bring immiscible liquid phases together. Essentially the purpose of all these devices is to disperse one phase as a drop within another phase. For an optimum design of a liquid-liquid contactor it is desirable to have a knowledge of the effect of such parameters like nozzle diameter,physical properties of the system and flow rate on the interfacial area created.

The present work concentrates on the drop formation from a nozzle in immiscible liquid systems. Experimental work has been carried out to understand the effect of flow rate through the nozzle, nozzle size and the physical properties of the two immiscible phases on the sizes of the drops produced.

When one liquid is injected into a second immiscible liquid through a nozzle a number of distinct regimes can be identified in the drop formation process. At a low flow rate through the nozzle drops form at the nozzle tip. As the flow rate increases, a certain critical flow rate is reached when a jet is formed with drops growing at the

end of this jet some distance away from the nozzle. At higher flow rates, the length of the jet increases and drops of various sizes break off from the end of the jet. At still higher flow rates the jet becomes unstable and disintegrates at a number of points producing a wide range of drop sizes.

The different regimes of drop formation correspond to the changing influence of the forces acting on the jet and growing drops. Various theories have been put forward to explain the changing mechanism of drop formation.

In chapter 2, the main results of the previous theories and the experimental findings on drop formation in liquid-liquid systems, are presented. In chapter 3, the experimental techniques were devised to obtain further data on the factors influencing drop size. This data is critically examined in the light of the existing theories in chapter 4. The experimental observations suggest that many of the assumptions are incorrect and need to be re-examined for a better understanding of the mechanism of drop formation.

In chapters 5 and 6 an attempt is made to incorporate the new experimental findings to achieve a better explanation of the different regimes of drop formation and extend the theories to provide a basis of predicting the drop size in the low flow rate regime. A new approach is suggested for predicting drop sizes at low flow rates and modifications to existing theories are presented to explain the distribution of drop size formed at higher

flow rates.

The objectives of the present work are to acquire further understanding of the fundamental mechanisms of drop formation from a nozzle in liquid-liquid systems and to provide more suitable methods of predicting the drop size and its variation with the flow rate through the nozzle based on the hydrodynamics of the jet and growing drops.

CHAPTER 2

LITERATURE SURVEY

2.1 INTRODUCTION

It has been an area of interest of many previous workers to be able to predict the drop size in liquid-liquid systems. Various attempts have been made by many workers to develop a theoretical or semi-theoretical basis to predict the diameter of the drops under various flow conditions. In most of the cases experimental drop size data were presented in the form of various empirical correlations of Sauter mean drop diameter. The mean drop diameter was then related to a number of dimensionless groups.

When a liquid issues from a nozzle into a second immiscible fluid, the liquid forms itself into discrete drops. The size of these drops depends on the densities and viscosities of the liquid and the surrounding fluid; the interfacial tension between the two fluids, the size of the nozzle and the velocity of liquid as it leaves the nozzle. The variation of the drop size as the velocity through the nozzle increases is shown in the typical curve as given in Figure 1.

Various distinct regimes can be identified on the basis of the flow rate of the injected liquid through the

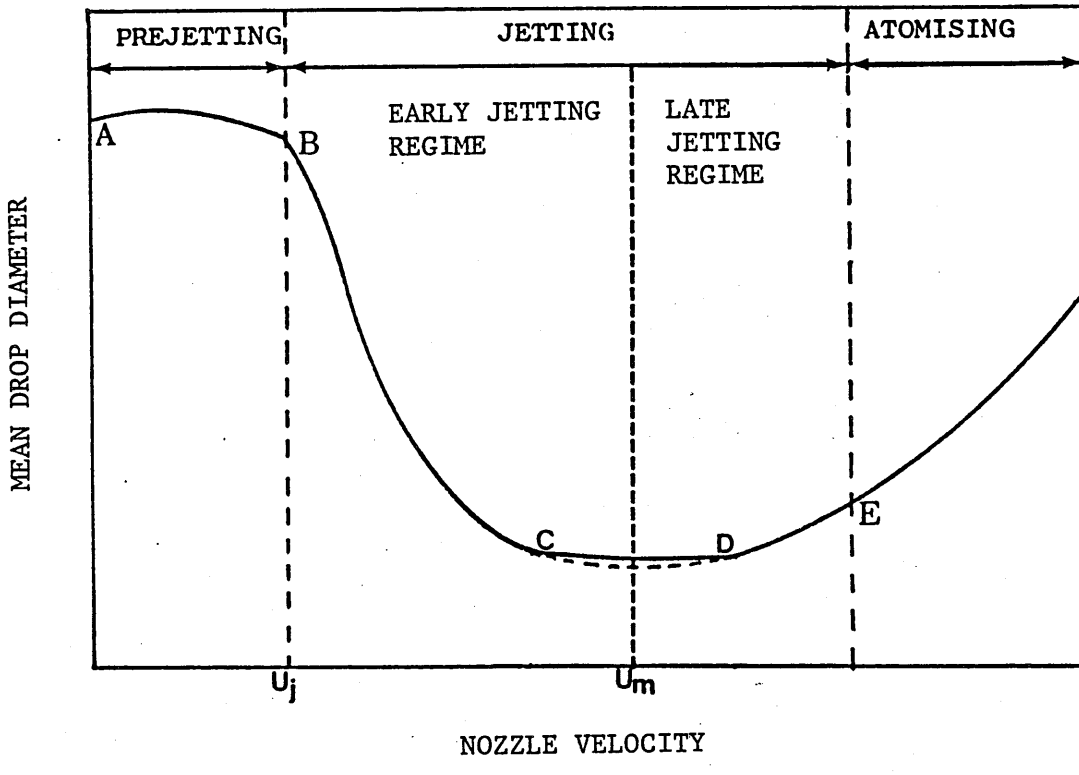

FIGURE 1 VARIATION OF MEAN DROP DIAMETER WITH NOZZLE VELOCITY

nozzle. The drop formation mechanism is different for the different regimes.

At low flow rates, drops form at the nozzle tip and detach at, or close to, the nozzle tip. This is the prejetting regime. The point of detachment of the drops keeps moving away from the nozzle tip as the flow rate increases, leaving a small residual volume of liquid at the nozzle tip which acts as a seed for the growth of the next drop. Eventually, a flow rate is reached where drops no longer form at the nozzle but instead grow at the end of a short continuous cylindrical column, known asajet. The liquid velocity at this point is known as the jetting velocity, U_j. With a further increase in the liquid velocity, drop formation occurs through the breakup of the liquid jet. This is the jetting regime.

On the basis of regularities in drop formation pattern and variation in the jet length, the jetting regime itself can be distinguished into two distinct sub regimes. In the early jetting regime where the flow rate is moderate, the jet breaks-up into drops showing regular patterns or families of drop sizes. The families contain different combinations of large and small drops with the proportion of small drops increasing with liquid velocity through the nozzle. Thus the mean drop size tends to decrease. In the early jetting regime it has been observed experimentally that the jet length increases slowly with the flow rate. Further increase in the velocity causes a more rapid increase in the jet length

and the drop families become more extensive. Experimentally it has been observed that in the region where the jet length increases rapidly with the liquid velocity, the extended families contain only two sizes of drops, a small drop and a large drop. The proportion of large drops to small drops varies with velocity. The ratio reduces as the velocity increases until a point is reached where the formation of large drops almost completely disappears and the mean drop size reaches a minimum value. This condition occurs at a critical velocity denoted by U_m, which can be seen in Figure 1 and serves to mark the end of the early jetting regime with a minimum in the drop size and a maximum in the jet length. Beyond this critical velocity asymmetric waves start to appear on the jet. The jet reduces its length and acquires a sinuous shape. The drops are formed irregularly, thrown off by 'whipping' actions at the end of the jet. The mean drop size increases during this late jetting regime. Finally at very high flow rates the jet retreats back to the nozzle and the breakup process becomes more random with the fluid atomizing at the nozzle tip.

It is clear that the prediction of the drop sizes formed by the injection through the nozzle needs to account for various flow regimes encountered as the liquid flow rate through the nozzle increases.

At low velocities in the pre-jetting regime single drops are formed at, or in the close vicinity of the

nozzle tip. In this regime, as shown in Figure 1 from A to B, drop sizes change very little with increasing velocity. Theories of drop formation in the prejetting regime rely on a static force balance where buoyancy and surface tension forces are considered to be the principal governing forces in determining the drop size.

In the jetting regime where the drops are formed at the end of a liquid jet, previous workers have adopted different approaches based on viscous, inertial and surface tension forces acting on the surface of the liquid jet. They assumed that these forces are responsible for the formation of a disturbance wave on the surface of the liquid jet. The amplitude of the wave grows on the jet surface and when it becomes equal to the jet radius, the jet breaks-up to form drops. A number of theoretical solutions have been introduced in the literature to predict the wave length of the fastest growing wave on the surface of the jet and then this wave length was used as a criterion to predict drop sizes under the jetting conditions. These theories are used to predict the minimum drop size in the region which often corresponds to the maximum jet length conditions, as shown in Figure 1 from C to D.

It has been observed experimentally that the drop size changes from a maximum drop diameter in the prejetting condition to a minimum drop diameter at the maximum jet length condition. Empirical correlations have been proposed to match the experimental observations in

these two extreme cases. However, very little information is available in the literature to predict drop size in the intermediate region, from B to C in Figure 1.

The following literature survey will therefore examine the recommendations for predicting the drop size in the prejetting regime, the minimum drop size regime and the intermediate regime.

2.2 DROP SIZE PREDICTION IN THE PREJETTING REGIME

The formation of droplets at the nozzle in liquid-liquid systems was studied by Harkins & Brown (1). The purpose of their study was to develop a reliable means of measuring interfacial tensions between two immiscible liquids. They derived an equation to predict the volume of a drop formed from a nozzle at a very low velocity by equating the buoyancy force acting on the drop to the interfacial tension force at the nozzle. The drop volume was corrected for the fraction $(1-\psi)$ of liquid which remained behind at the nozzle at the time of drop detachment. The fraction, U, was found to be a function of the detached drop volume and the nozzle diameter. The buoyancy force F_b, and interfacial tension force, F_s were expressed as;

$$F_b = V\Delta\rho g$$

$$F_s = \sigma\pi D_n$$

where V is the total volume of liquid attached to the nozzle. Therefore the volume of a drop formed at static conditions was given as;

$$V_s = V\psi = \left[\frac{\sigma\pi D_n\psi}{\Delta\rho g}\right] = \left[\frac{\pi D_n^3\psi}{E_o}\right] \qquad [2.1]$$

where Eotvos number $Eo = \left[\frac{gD_n^2\Delta\rho}{\sigma}\right]$

In 1950 Hayworth & Treybal(2) extended Harkins & Brown's analysis by including inertial and drag forces in their force balance equation. They suggested that the total volume of the drop, V_f, is made up of following partial volumes as;

$$V_f = V_s + V_r - V_k \qquad [2.2]$$

where V_s is the volume required to overcome the interfacial tension force given by equation [2.1] of Harkins & Brown.

V_r is the volume required to reach a sufficient rising velocity to break away from the nozzle and was suggested to have a form

$$V_r = 0.5236 \left[\frac{18 U_n K \mu_c}{\Delta\rho g}\right]^{3/2}$$

where K is calculated graphically and was given as a function of viscosity

$$K = 4.05 \frac{[D_n]^{0.747}}{[U_n]^{0.635} \cdot [\mu_c]^{0.814}}$$

V_k is the negative volume equivalent of the kinetic energy supplied by the incoming stream and was calculated as

$$V_k = \frac{V_f \rho_d U_n^2}{2\Delta\rho g D}$$

where D is the diameter of the drop. Substituting these

values of V_f, V_r and V_k in equation [2.2] and assuming $D = (V_f/0.5236)^{0.33}$ they obtained;

$$V_f - V_f^{2/3}\left[\frac{0.403\rho_d U_n^2}{\Delta\rho g}\right] = \frac{D_n \pi\sigma\psi}{\Delta\rho g} + 0.5236\left[\frac{18KU_n\mu_c}{\Delta\rho g}\right]^{3/2} \quad [2.3]$$

Further they replaced ψ by a constant 0.655 and used a graphically calculated value for K in equation[2.3]. Thus equation [2.3] can be written as ;

$$V_f + 0.0041V_f^{2/3}\left[\frac{\rho_d U_n^2}{\Delta\rho}\right] = 0.0021\left[\frac{D_n}{\Delta\rho}\right]$$

$$+ 0.0106\left(\frac{D_n^{0.747} U_n^{0.365} \mu_c^{0.186}}{\Delta\rho}\right) \quad [2.4]$$

Their work was largely devoted to the prejetting conditions where the drop size was uniform and they used Alketerge C to vary the interfacial tension. They also tried to extend the correlation to the jetting regime, but concluded that their correlation is only valid for prejetting conditions.

Null & Johnson (3) used a geometric approach to predict drop volume in the prejetting conditions, and empirically correlated various geometric parameters with the dimensionless groupings. They considered a two stage drop formation process. Null & Johnson assumed a constant velocity of the drop and a linear decrease in the neck radius of the drop during its detachment process from the nozzle. The first stage corresponds to a maximum travel

of the top edge of the drop, while the second stage corresponds to the jet behind the drop attaining a conical geometry. The time of formation of the drop was determined by a data fitting exercise. For their experimental data Null & Johnson found this approach to have a mean error of 20% compared to 84.7%for the prediction of Hayworth & Treybal.

Meister & Scheele (4) studied a wide range of liquid properties and nozzle diameters. They found that the Hayworth & Treybal and Null & Johnson's correlation did not satisfactorily predict drop size. They extended Hayworth & Treybal's analysis for the prediction of drop size in the prejetting conditions.

Meister & Scheele(4) considered four major forces which act on a drop during the process of its formation at the nozzle. The buoyancy force, F_b ,due to density difference between the two fluids and the kinetic force F_k, associated with the fluid flowing out of the nozzle, act to separate the drop from the nozzle. To balance these forces the interfacial tension force, F_s, at the nozzle tip and the drag force, F_d, exerted by the continuous phase, act to keep the drop on the nozzle. At equilibrium they suggested that the force balance equation was;

$$F_b + F_k = F_s + F_d \qquad [2.5]$$

where $F_b = V_s g \Delta\rho$

$$F_k = \frac{4\rho_d Q U_n}{3}$$

$$F_s = \sigma \pi D_n$$

$$F_d = k_d \left[\frac{\mu_d Q}{D}\right] \left[\frac{D_n}{D}\right]^n$$

The constants k_d and n need to be evaluated experimentally to correct any reduction in F_d due to the induced continuous phase motion. Upon substituting values for F_b, F_k, F_s and F_d and rearranging the equation [2.5] they obtained an expression to predict the volume of liquid on the nozzle tip at static conditions as;

$$V_s = \frac{\sigma \pi D_n}{\Delta \rho g} + \frac{k_d \mu_d Q}{\Delta \rho g D}\left[\frac{D_n}{D}\right]^n - \frac{4 Q U_n}{3 \Delta \rho g} \qquad [2.6]$$

Further they derived an expression to calculate the additional volume V_n due to the volumetric flow out of the nozzle during the process of drop break off as;

$$V_n = k_n \left[\frac{Q^2 D_n^2}{(\Delta \rho g)^2} \frac{\rho_d \sigma}{2}\right] \qquad [2.7]$$

where k_n is another constant.

Combining equations [2.6] and [2.7] they suggested a final expression for the drop volume after the detachment from the nozzle as;

$$V_f = (V_s + V_n)\psi \qquad [2.8]$$

$$V_f = \left[\left(\frac{\sigma \pi D_n}{\Delta \rho g}\right) + k_d \mu_d Q \left(\frac{D_n}{D^2 \Delta \rho g}\right)^n - \left(\frac{4 \rho_d Q U_n}{3 \Delta \rho g}\right) \right.$$

$$\left. + k_n \left(\frac{Q^2 D_n^2 \rho_d \sigma}{(\Delta \rho g)^2}\right)^{1/3} \right] \psi \qquad [2.9]$$

where ψ is the Harkins-Brown correction factor, correcting for the residual volume left behind the nozzle. Equation [2.9] was derived for a parabolic velocity profile in the liquid leaving the nozzle. It was suggested that this equation can be used for a flat velocity profile if the constant 4/3 in the kinetic term is replaced by 1.0

Meister and Sheele calculated the empirical constant k_n by fitting all data for systems with continuous phase viscosity less than 10 centipoise, since for these systems the drag term was negligible, and used this value to calculate k_d and n for the heptane-water system only. With these values for the constants Meister and Sheele found good results for the prediction of the drop diameter with the average mean error 6%.

Chazal and Ryan (5) studied drop formation from a nozzle at low velocities, that is for prejetting conditions. They considered a two stage drop formation process where they suggested that the time required to form a drop can be divided into two parts. First, the time required for the drop to reach its unstable or necking in stage; and second, the time for the drop to detach completely after instability has occurred.

The first stage of the formation process was analysed by applying Newton's second law of motion to the drop at the instant of instability. They considered buoyancy and interfacial tension forces acting on the drop at the nozzle and the momentum of the entering fluid. Drag on the forming drop was neglected. However, the effect of the continuous phase viscosity was taken into account during the second stage of formation. The final expression was suggested as;

$$V_f = \frac{2D_n\pi\sigma}{\Delta\rho g}\left[\psi + \left(\frac{k_1\Delta\rho g D_n U_n V_f^{0.5}}{\sigma U_t}\right) - k_2\left(\frac{D_n U_n^2}{\sigma}\right)(1 + B)\right] \qquad [2.10]$$

where $B = 0$ in the prejetting region

$B = 0.286(\Delta\rho g D_n^2/\sigma)^{0.5}$ in the jetting region

ψ = Harkin-Brown Correction Factor

U_t = Terminal velocity of the drop

k_1 and k_2 are empirical constants.

The equation [2.10] produced good results for their experimental data within 6.3% error. When they compared their results with Meister and Sheele (4) using equation [2.10], they found that the curve of drop volume vs flow rate was roughly comparable, but Meister and Sheele's numerical values over estimated by more than 50%. They were not able to explain this variation except to suggest that the physical properties of the systems used in the

two studies can vary significantly. A further problem of making a comparison was that the techniques of measuring of drop volumes were different in both cases.

Kumar and Hartland (6) studied drop formation in both the prejetting and jetting regimes. They suggested a purely empirical correlation to predict drop diameter in low viscosity liquids as;

$$\frac{D_{32}}{D_n} = k(We^*)^m \, (Eo)^n \qquad [2.11]$$

where the modified Weber number,

$$We^* = \frac{\Delta\rho D_n U_n^2}{\sigma}, \text{ and } Eo = \frac{\Delta\rho D_n^2 g}{\sigma}$$

Kumar and Hartland calculated values of We^* and Eo from their experimental data and applied a multiple regression analysis to predict k,m and n for equation [2.11]. For the prejetting region they proposed k = 1.591, m = -0.068, and n = -0.278.

This equation produced good results for their own experimental data and also in predicting the results of Meister and Scheele. All these studies were found to be applicable only to the prejetting regime. Thus, in order to specify the limit of application of these correlations, it is necessary to be able to predict when the onset of jetting occurs.

2.3 PREDICTION OF THE JETTING VELOCITY

The drop volume correlations described in the previous section apply only at low velocities where drops form directly from the nozzle. As the flow rate through the nozzle is increased, a critical velocity, called the jetting velocity U_j, is reached, above which a jet of liquid issues from the nozzle. The jet breaks-up into drops, but because the drop formation mechanism has changed , the drop can no longer be predicted by the low velocity correlations. Various attempts have been made to pinpoint this critical velocity at which the jetting occurs.

Smith and Moss (7) found that for a liquid injected into a gas the jetting velocity U_j can be expressed as;

$$U_j = k\left[\frac{\sigma}{\rho_d D_n}\right]^{0.5} \qquad [2.12]$$

where k is a constant. For their experimental conditions they found it to vary between 2 and 3.

Smith and Moss reported that the value of k is a function of surface tension, the lowest value of k corresponding to the lowest surface tension.

Hayworth and Treybal (2) worked with liquid-liquid systems and found that the jet usually formed when the velocity through the nozzle was around 10 cm/sec. This was an average value for their systems. They did not make any attempt to correlate the jetting velocity.

Fujinawa et al (8) developed an empirical correlation to predict the jetting velocity in liquid-liquid systems. In their empirical correlation they considered the jetting velocity as a function of surface tension and nozzle diameter, and produced an expression

$$U_j = 4.4\left[\frac{\sigma^{0.20}}{(D_n)^{0.5}}\right] \qquad [2.13]$$

Ryan (15) studied liquid-liquid dispersion and produced an empirical correlation to predict the jetting velocity. He considered the density difference of the two phases and produced an equation

$$\frac{\rho_d}{\Delta\rho}\left[\frac{2U_j^2}{gD_n}\right] = 1.64\left[\frac{\sigma}{\Delta\rho g D_n^2}\right]^{0.95} \qquad [2.14]$$

Ryan assumed $0.95 \approx 1$ and simplified the above equation as

$$U_j = 1.16\left[\frac{\sigma}{\rho_d D_n}\right]\left[\frac{1}{\sqrt{(gD_n)}}\right] \qquad [2.15]$$

Meister and Scheele (4) gave the first theoretical basis to define the jetting velocity in liquid-liquid systems. They considered two possible jet formation mechanisms on which they have based their predictions for the jetting velocity.

The first mechanism they proposed was that the jet will form if there is sufficient upward force at the nozzle exit, to form a jet. They suggested that if the drop is not large enough to detach from the nozzle , the

kinetic force of the liquid leaving the nozzle can either enlarge the drop or raise the drop up on a cylinder of liquid, thus forming a jet. Further, they have postulated that if sufficient upward force exists to form a jet, this will occur in preference to further enlargement of the drop. They derived a force balance equation at the jetting velocity as;

$$F_k + F_p = F_s$$

where F_k kinetic force = $\frac{\rho_d U_n^2 D_n^2}{3}$

F_p excess pressure force = $\frac{\sigma \pi D_n^2}{D}$

and F_s interfacial tension force = $\sigma \pi D_n$

Upon substituting these values in equation [2.15] and rearranging;

$$U_j = 1.73 \left[\left(\frac{\sigma}{\rho_d D_n}\right) \left(1 - \frac{D_n}{D}\right) \right]^{0.5} \qquad [2.16]$$

In a second proposed mechanism Meister and Sheele considered that the jet will form when the initial rise velocity is sufficiently low and the drop rise is less than one drop diameter during the time of formation of the next drop. Thus the drops will then merge to form a jet.

Their experimental data fits well with equation [2.16]. They did not find any experimental support for their second proposed mechanism when they analysed their cine film sequence during the jet formation.

Prediction of the jetting velocity is a crucial step in an attempt to describe the whole range of behaviour of drop formation from nozzles, since after jetting, there is a complete shift in outlook from a force balance approach to a stability theory approach.

2.4 DROP SIZE PREDICTION IN THE JETTING REGIME

It is accepted in the literature by most workers that the drop formation mechanisms are different in the prejetting and the jetting regimes. For prejetting conditions the drop size prediction is generally based on a force balance type of correlation as described in section 2.2 . On the other hand, it is agreed that the size of drops formed from a cylindrical liquid jet in the jetting regime is controlled by the surface disturbances which result from the jet instability. These disturbances grow on the surface of the jet and cause it to break into drops. In the jetting regime the breakup process is controlled by the rate of amplification of the disturbances on the jet surface.

The method of predicting the drop size from the disintegration of a cylindrical jet was established by Tyler(10), who argued that if the disturbance wave of length λ is responsible for the breakup of a jet into drops, then the volume of the resulting drop will be equal to the volume of the cylindrical portion of the jet of length λ , that is :

$$V_F = \frac{\pi D^3}{6} = \frac{\pi D_j^2 \lambda}{4} \qquad [2.17]$$

$$\frac{D}{D_j} = \left[\frac{1.5\lambda}{D_j}\right]^{0.33} \qquad [2.18]$$

This equation can therefore be used to predict the drop size if the wave length of disturbance λ is known. This information can be found by considering the instability of liquid jets under the action of surface tension, viscous and inertial forces.

2.4.1 THE RAYLEIGH'S INSTABILITY ANALYSIS

The instability of liquid jets has been a subject of investigation over the last one hundred years, but over the last two decades the interest has markedly increased and this has been reflected in the vast increase in the number of publications.

The instability theory predicts what kind of disturbances will trigger the breakup of the jet to form drops. Rayleigh(9) attempted to explain the growth and propagation of the disturbances on the surface of the jet.

The general form of a disturbance on the surface of the jet can be expressed as;

$$\eta = \eta_o e^{\alpha t} \cos(kz) \qquad [2.19]$$

where η_o is the initial amplitude of the disturbance, α is the growth rate of the disturbance and k is the wave number of the growing wave and is equal to $2\pi/\lambda$.

He showed by considering the effect of the radii of curvatures on the pressure in a cylinder of fluid, that if the nodes on the surface of the jet are farther apart than the circumference of the cylinder, then the pressure will be greater at the node than between the nodes; and the nodes will amplify. But if the nodes are less than a circumferential distance apart, the pressure will be greater between the nodes than at the node; and the mode will diminish. Therefore, a critical wavelength, equal to the jet circumference exists, above which waves will amplify and below which waves will diminish.

The disturbances which do grow on the surface of the jet will cause the jet to breakup. The disturbance wave, which grows fastest, will dominate the break up process. When the amplitude of the fastest growing wave becomes equal to or more than the radius of the jet, the jet breaks up into drops.

Lord Rayleigh in the late nineteenth century suggested a number of solutions for jet instability which have been the basis for all subsequent studies. At the first attempt, Rayleigh (9) suggested an analytical solution to predict growth rate for an axisymmetric wave on the surface of an inviscid, stationary liquid jet in air. His expression was;

$$\alpha = \left(\frac{\sigma}{\rho_d a^3}\right)\left[\frac{ka(1 - k^2a^2)}{I_o(ka)/I_1(ka)}\right] \qquad [2.20]$$

It is clear from the above equation that the growth rate does depend on the surface tension(σ), liquid jet density(ρ_d) and the jet radius(a).

The wave which has a maximum growth rate can be identified from Figure 2, maximising (α) with respect to ka in equation [2.20]. The growth rate (α) is real and positive for $0<ka<1$. It was found that the α passes a maximum value when $(ka)_{max} = 0.696$ or $\lambda_{max} = 9.02a$. By substituting these values in equation [2.20] Rayleigh obtained;

$$\alpha_{max} = \left[\frac{\sigma}{8\rho_d a^3}\right]^{0.5} \qquad [2.21]$$

Rayleigh's analysis was used directly by Tyler(10) for predicting the drop size. Tyler measured the wave lengths of the waves appearing on the surface of the jets of various liquids. In all cases he found a close agreement between the wavelength λ and the corresponding intervals between the drops after the breakup. Thus substituting for

$\lambda = \lambda_{max} = 2\pi/(ka)_{max}$ and $(ka)_{max} = 0.696$, the following simple result was obtained using equation [2.18];

$$\frac{D}{D_j} = \left[\frac{1.5\lambda}{(ka)_{max}}\right]^{0.33} = [6.77]^{0.33} = 1.89 \qquad [2.22]$$

Tyler's measurements of drop size and jet diameter produced values in the range of $1.88 < D/D_j < 1.94$. These results confirmed Tyler's hypothesis and suggested that the instability theory could be used to predict drop sizes resulting from the breakup of liquid jets.

The use of an instability theory to isolate the fastest growing disturbance as the governing factor in the jet breakup, furnishes a prediction only for the minimum drop size. However, the prediction of the drop size distribution can not be made without further considerations of the likely influence of the other disturbances on the surface of the jet. Further refinements of Rayleigh's instability theory have therefore

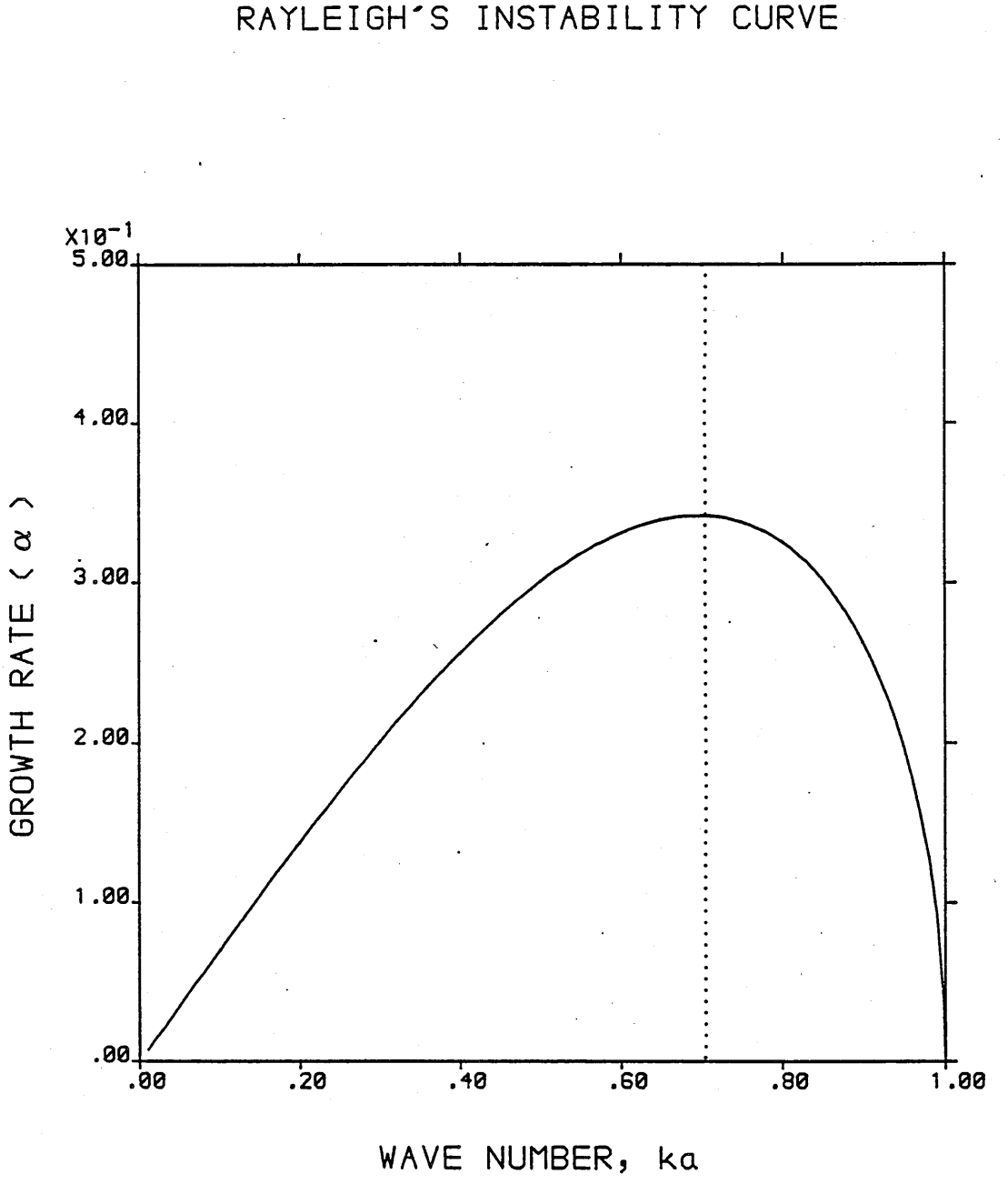

FIGURE 2 INSTABILITY CURVE SHOWING MAXIMUM GROWTH RATE AT WAVE NUMBER 0.696

yielded better prediction of the minimum drop size, particularly for liquid-liquid systems, but have not been useful in explaining the spread of drop sizes encountered in the jetting regime. Thus the following sections concentrate exclusively on minimum drop size in liquid-liquid systems.

2.4.2 MINIMUM DROP SIZE IN LIQUID-LIQUID SYSTEMS

In liquid-liquid systems it has been reported by several previous workers that there is a minimum drop size which occurs around a critical velocity near the conditions where the jet attains its maximum length. Predictions of the minimum drop size are based on extending Rayleigh's analysis to include the effect of the properties of the liquid surrounding the jet and influence of the jet velocity on the growth rate.

2.4.2.1 INFLUENCE OF THE CONTINUOUS PHASE DENSITY

Christiansen and Hixson (12) derived an equation for the instability of an inviscid liquid jet in a second inviscid liquid by extending Rayleigh's equation to include the density of the surrounding phase. The equation for the growth rate of disturbances on the surface of the jet was given by;

$$\alpha = \left(\frac{\sigma}{\rho_d a^3}\right)\left[\frac{ka\,(1 - k^2a^2)}{\frac{I_o(ka)}{I_1(ka)} + S\,\frac{K_o(ka)}{K_1(ka)}}\right] \qquad [2.23]$$

where $s = \rho_c / \rho_d$ the ratio of the density of the two phases. This equation reduces to Rayleigh's equation for $\rho_c = 0$. The wave length which maximises $\hat{\alpha}$ in equation [2.23] was found to be a function of the density ratio. This equation predicts

$$4.5D_j < \lambda_{max} < 4.83\,D_j \qquad [2.24]$$

Based on the same reasoning as Tyler this result suggests that the drop size in liquid-liquid systems should be in the range of;

$$1.877 < D/D_j < 1.922 \qquad [2.25]$$

The experimental result of Christiansen and Hixson gave value of $D/D_j = 2.07$, which agrees well with the prediction from their instability theory.

Christiansen & Hixson's experimental results and theoretical predictions have been used as a basis for subsequent design correlations for minimum drop size in liquid-liquid systems. It has been generally observed that the ratio of the minimum drop diameter to the jet diameter is constant around a value of 2.

They also suggested a method of predicting the critical velocity U_m at which the minimum drop size was observed. This was obtained by correlating the wave celerity with the jet velocity. Most of their data fits the expression $(U_m/c_1)=2.33$ where c_1 is the celerity or inherent velocity of the sinuous wave and is given by;

$$c_1 = \left[\frac{\sigma K}{\frac{I_o(ka)}{I_1(ka)} + \frac{K_o(ka)}{K_1(ka)}}\right]^{0.50} \qquad [2.26]$$

Treybal (13) used equation [2.26] to predict the optimum jet velocity for operating a liquid-liquid extraction column to produce maximum surface area. Treybal modified equation [2.26] to an empirical

correlation for predicting this critical velocity;

$$U_{cm} = 2.69 \left[\frac{D_{jm}}{D_n}\right]^2 \left[\frac{\sigma}{D_{jm}} (0.51\rho_c + 0.427\rho_d)\right]^{0.50} \quad [2.27]$$

where D_{jm} is the mean jet diameter

$$D_{jm}/D = [\ 1 + 0.485Eo]^{-1} \quad \text{for } Eo < 0.615 \quad [2.28]$$

$$D_{jm}/D = [\ 0.12 + 1.51(Eo)^{0.5})\ ]^{-1} \quad \text{for } Eo > 0.615 \quad [2.29]$$

As is clear from the above equations, Treybal suggested that this critical velocity is a function of the jet diameter rather than nozzle diameter. In equations [2.28] and [2.29] the jet diameter was extrapolated from the work of Christiansen & Hixson. However, it should be noted that Christiansen & Hixson did not measure the jet diameter experimentally but estimated it retrospectively from the drop diameter.

2.4.2.2 INFLUENCE OF THE JET VISCOSITY

The inclusion of viscous forces into the instability analysis may be expected to change the results because of the damping effect of viscosity on the wave growth.

It was Rayleigh (16) again who predicted the growth rate of axisymmetric surface tension waves for a viscous stationary liquid jet in air and suggested the following equation.

$$\alpha = \frac{\sigma}{2\mu a}\left(\frac{1 - k^2a^2}{\dfrac{I_o(k^2a^2)}{I_1(k^2a^2)}\left[\dfrac{}{}\right] - k^2a^2 - 1.}\right) \qquad [2.30]$$

This equation suggests that the growth rate increases as ka tends to zero which means, in viscous systems, long wavelength waves will grow fastest and break the jet into drops.

Weber (17) combined the two analyses of Rayleigh, that is equations [2.20] and [2.30], to derive an expression for the wave growth on the surface of liquid jets as;

$$\alpha^2 + 3\left[\frac{\mu k^2a^2}{\rho a^2}\right]\alpha = \frac{\sigma}{2\rho a^3}\,[1 - k^2a^2]\,k^2a^2 \qquad [2.31]$$

This equation includes the effect of viscosity on the growth rate of the disturbance on the jet surface. For an inviscid liquid jet this equation can be reduced to Rayleigh's equation [2.20] with the assumption that

$K_o(ka)/K_1(ka) = 2/ka$. The maximum growth rate was found at a wave number $(ka)_{max}$ given by;

$$ka_{max} = \frac{1}{(2 + 6Z_j)^{0.50}}$$ where Z_j is the Ohnesorge number

Upon substitution of this value in Tyler's equation [2.18] gives the following prediction for the drop size from a stationary liquid jet in air was obtained

$$\frac{D}{D_j} = 1.88\ (1 + 3Z_j)^{0.167} \qquad [2.32]$$

2.4.2.3 INFLUENCE OF THE CONTINUOUS PHASE VISCOSITY

Tomotika(18) presented an equation for the breakup of a stationary viscous liquid jet in a stationary viscous liquid continuous phase. Tomotika considered the case where the densities of the dispersed and continuous phases were very small to obtain an equation for the growth rate of axisymmetric waves on the surface of the jet. The final equation was suggested as

$$\alpha = \frac{\sigma}{2a\mu}(1 - k^2a^2) f(ka) \qquad [2.33]$$

where f(ka) is a complicated function of viscosity ratio and Bessel functions of the wave number.

Meister (19) investigated the general solution presented by Tomotika to calculate the growth rates of disturbances on the surface of a cylindrical liquid jet for various limiting cases. The characteristic equation for growth rate was given by ;

$$\alpha^2 + \alpha A1 = (\frac{\sigma}{\rho a^3})A2 \qquad [2.34]$$

where A1 and A2 are the complicated functions of the wave number, Ohnesorge number, density and viscosity ratios of the two phases. The criteria for these limiting cases was based on the Ohnesorge numbers of the jet, Z_j and the continuous phase Z_c. These criteria are outlined in Table 1.

Further, they suggested that the wave travels on the surface of the jet at the interfacial velocity which for liquid-liquid systems is less then the average jet velocity. They proposed an expression for the interface

TABLE 1

SUMMARY OF THE SPECIAL CASES FOR THE PREDICTION OF THE WAVE NUMBER AND THEIR CRITERION

SPECIAL CASE	PREDICTION OF WAVE NUMBER	CRITERIA
low μ jet in low μ liquid	$k_m = f(\rho_c/\rho_d)$	$Zj \ll 1$ $Zc \ll 1$
High μ jet in high μ liquid	$k_m = f(\mu_d/\mu_c)$	$Zj \gg 1$ $Zc \gg 1$
High μ jet in low μ liquid	$k_m = 1/(2(1+3Zj))^{.5}$	$Zj \gg 1$ $Zc \ll 1$
Low μ jet in high μ liquid	$k_m = 1/(2(1+Zc))^{.5}$	$Zj \ll 1$ $Zc \gg 1$

velocity based on continuous phase drag on the jet and derived the following equation to predict the minimum drop volume ;

$$V_F = \frac{2\pi^2 D_j^3}{\left[\frac{U_I}{U_A}\right] N(ka)_{max}} \qquad [2.35]$$

where U_I is the interfacial velocity, U_A is the average jet velocity and N is a function of a critical Reynolds number which depends on the wave length of the disturbance.

Kitamura, Mishima and Takahashi (25) presented a semi-theoretical approximation of Tomotika's analysis and showed that the influence of the continuous phase viscosity on the size of the fastest growing disturbance was very small for the range $0.1 < \mu_c/\mu_d < 20$. They proposed therefore a slight modification to equation [2.32] which could be used for a stationary viscous jet in a moderately viscous continuous phase. Their equation for the wave number at which the growth rate was found to be maximum is given by;

$$ka_{max} = \frac{0.95}{[2\ (1 + 3Z_j)]^{0.5}} \qquad [2.36]$$

where Z_j is the Ohnesorge number of the jet phase. This value gives the following prediction for the drop size

$$\frac{D}{D_j} = 1.91\ (1 + 3Z_j)^{0.167} \qquad [2.37]$$

2.4.2.4 INFLUENCE OF THE JET INERTIA

All the analyses described so far have assumed a stationary liquid jet in a stationary continuous phase. The predicted values of the wave number are all less than 0.7 giving the drop size ratio $D/D_j = 2$ according to Tyler's equation [2.18]. However, Bright(24) found that the measured values of the wave number for liquid-liquid systems were around a value of unity or greater; even though drop size ratios were still equal to two. Bright suggested that the motion of the jet rela- tive to the continuous phase introduces another term in the characteristic equation for growth rate. His analysis produced the following equation;

$$\alpha^2 + \alpha B = \frac{\sigma}{\rho a^3}\left[\frac{ka\,(1-ka)}{I^* + sK^*}\right] + \left[\frac{DU}{a}\right]^2 (ka)^2 \qquad [2.38]$$

where B is a function of viscosity ratio μ_c/μ_d, and D is a function of the velocity gradient across the jet interface due to drag of the continuous phase. With this equation Bright was able to show that the fastest growing wave could have values of wave number equal to or greater than 1.

Bright proposed an alternative hypothesis that an axisymmetric disturbance wave will always travel at a velocity less than the jet velocity and derived an expression for the velocity of the wave based on equation [2.38] as;

$$\frac{C}{U} = \frac{I^* + sUK^* + F}{I^* + sK^* + G} \qquad [2.39]$$

where U is the ratio of jet to continuous phase velocity, F and G depend on the viscosity ratio and the velocity gradient across the interface.

Using equations [2.38] and [2.39] Bright suggested an equation to predict the minimum drop size as;

$$V_F = \frac{2\pi^2 D_j^3}{(ka)_{max} \frac{C}{U}} \qquad [2.40]$$

For U = 0 (no relative motion) and s =0 (liquid jet in air) equation [2.40] reduces to Tyler's equation. In other words, in liquid air systems the fastest growing wave is travelling at the same velocity as the jet, but in liquid-liquid systems the wave always travel more slowly than the jet. This phenomenon was observed in Bright's experiments. Equation [2.40] explains why: although wave number is larger than predicted by stationary theories, it is compensated by the increase in the drop volume between the antinodes of the wave due to a difference between the wave and the jet velocities.

Developments of instability theory for liquid-liquid systems to account for the physical properties of the two phases and relative motion between the jet and the surroundings have provided better methods of estimating

the minimum drop size from the breakup of a liquid jet. The general procedure is based on theoretical calculations of the wave number, ka; and the wave velocity, C_f of the fastest growing wave in addition to the use of an equation relating the drop volume to the volume contained between the one wave length of the fastest growing disturbance. However, none of these theories can explain the range of drop sizes found in practice in the early part of the jetting regime. The next section will deal with the correlations to predict mean drop size in this regime.

2.5 DROP SIZE PREDICTION IN THE INTERMEDIATE REGIME

Most of the theories of drop size reported in the literature have been developed either for the prejetting conditions (based on a force balance approach) or for the conditions where the minimum drop size was observed (based on the instability theory). Very little information is available for predicting drop distributions in early jetting conditions where quite repeatable patterns of drops have been observed. A large number of experimental drop size data sets in the prejetting and the jetting regimes have been obtained by many previous workers for various systems, where drops are formed by injecting one liquid into the other through a nozzle or orifice. Most of the workers have developed empirical correlations based on the Sauter Mean Drop Diameter, D32. These correlations have their own assumptions and limitations depending on nozzle diameter, flow conditions and physical properties of the systems.

2.5.1 EXPERIMENTAL OBSERVATIONS

To bridge the gap for the drop size prediction between the prejetting and the maximum jet length conditions, Horvath et al (22) studied the drop formation and the drop size distribution in both the regions. They reported that in the prejetting conditions at low velocities, the drops were very uniform. When the velocity was increased they observed that at a critical velocity where the jetting starts, the drop formed at the

jetting velocity and further, at higher velocities, drops were of two different sizes. The plots of their experimental data on the drop size distribution at different jet velocities are shown in Figure 3.

Figure 3 suggests that the distribution is no longer uniform, but instead it is a bimodal distribution. It may also be seen from Figure 3 that the small drops prevailed at the higher velocities, which corresponded to the maximum jet length conditions where the larger drops disappear almost completely. However, this velocity at which only small drops appear, could not be achieved by them.

Keith and Hixson (11) experimentally studied drop sizes from liquid jets in liquid-liquid systems. For small nozzles they found that the curve of drop surface area vs flow rate shows a sharp maximum at a particular flow rate. The maximum becomes less pronounced for larger diameter nozzles. For most systems this maximum occurred at a velocity slightly below the velocity associated with the maximum jet length. The velocity at which the maximum surface area was obtained was shown to depend on nozzle diameter. They also observed that at the flow rate for the maximum surface area, the drops were surprisingly uniform. This uniformity suggests that some regular periodic disturbances occur on the jet which causes a regular jet breakup. They further studied the distribution of drop sizes in the jetting region and found that the standard deviation of the drop size decreases

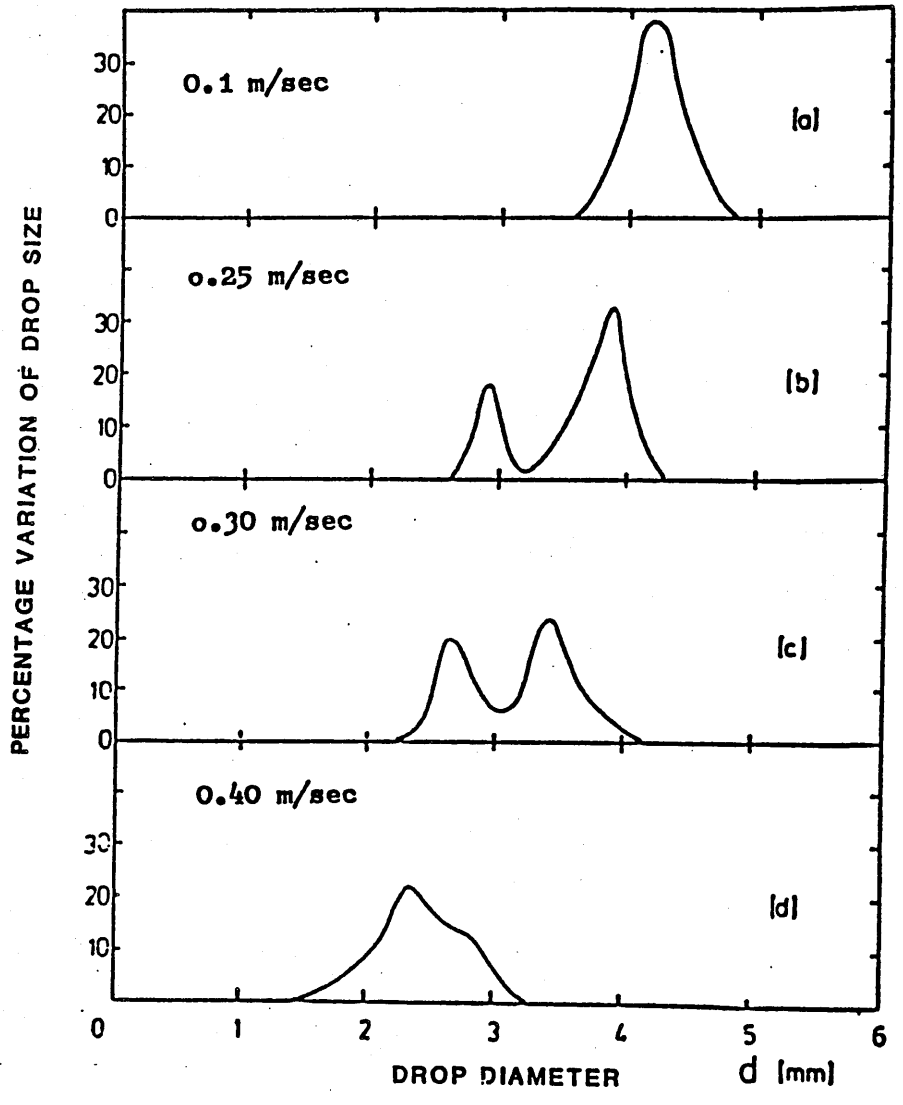

FIGURE 3 DROP SIZE DISTRIBUTION AT VARIOUS NOZZLE VELOCITIES

SYSTEM - XYLENE INTO WATER

NOZZLE DIAMETER - 0.10 cm

Ref No - 22

gradually until the jet attains its maximum length, after which the standard deviation increases quite suddenly due to more random breakup mechanisms.

Van den Akker (23), in his experimental studies observed various combinations (or families) of large and small drops in the early jetting region depending on the nozzle velocity. In most of the cases he found that the sizes of large and small drops were constant, but the relative number of the two kinds of drop in a combination varied. Further, he found that at a higher velocity (98.7 cm/sec in his case) only small drops appeared. He reported this velocity as the critical velocity where the maximum jet length was observed.

Van den Akker measured the volume of large and small drops and found that the volume of the large drop was about twice the volume of the small drops. This phenomenon of the formation of double sized drops was also reported as a 'twinning' effect by Christiansen and Hixson (12), where they observed only two types of drops at the flow rate below the critical flow rate; one equal to the ideal one wave length drop and one double that size or twin. They analysed their high speed cine films and suggested that the double size drops were created by the oscillation in the jet length. The jet length fluctuates; releasing a small drop at its shortest length and a large or twin drop at the longest stable position. This phenomenon was experimentally observed by Christiansen and Hixson only at the flow rate just below the critical

value, where oscillations were very small. At the lower flow rates they suggested that the jet oscillations increases ; corresponding to an increase in the number of the larger drops. This apparently explains the larger mean drop size and the consequent decrease in the surface area at low flow rates.

Meister and Sheele attempted to explain their experimental data in the range of jet velocities where the jet length was shorter than the two wave lengths of the growing wave. They suggested that a regular alternating pattern of drop sizes will occur. After a drop breaks off as a result of an instability mechanism, the remaining jet is less than one wave length long and the next drop begin to form by the force balance mechanism.

Recently Bright (24) observed that when the nozzle velocity increases above the jetting velocity, drops break off the jet in various families at regular intervals. He said that the families contain drops of different sizes but the volume of each drop is an integer multiple of the fundamental (minimum drop) volume. He suggested that the large drops in the family grow by the accumulation of the jetting liquid within successive waves on the jet.

Bright confirmed the previous observations made by Horvath(22) and Van den Akker(23) and said that the composition of the drop families changes within the jetting regime. At low velocities he reported a preponderance of large drops in a family, while at higher velocities more small drops were observed.

2.5.2 EMPIRICAL CORRELATION TO PREDICT THE DROP DIAMETER

It has been reported in the literature that as the flow rate increases through the nozzle the mean diameter of the drop decreases from the maximum value in the prejetting conditions to a minimum value which is observed near the maximum jet length situation. Instability theory also predicts that the minimum drop size is formed by the fastest growing wave on the surface of the jet at the maximum jet length condition. Skelland and Johnson(14) suggested that the critical velocity at which maximum jet length was observed, could be used as a parameter to correlate the drop size .They plotted their experimental data D_{32}/D_{jm} vs U_n/U_m where U_m is the critical velocity of the jet at which the maximum jet length was observed. They suggested that this critical velocity can be calculated using the continuity of mass between the nozzle and the point of breakup as follows;

$$U_m = U_{cm} \left(\frac{D_n}{D_{jm}}\right)^2 \qquad [2.41]$$

where U_{cm} is the velocity of the jet at the minimum drop conditions and D_{jm} is the jet diameter at the maximum jet length. U_{cm}, U_{jm} can be calculated using Treybal's equation [2.27]. Skelland and Johnson's predicted drop size ratio varied within a range

$$1.8 < \frac{D}{D_{jm}} < 2.6$$

Horvath et al (22) developed a correlation using Skelland and Johnson (14) and Christiansen and Hixson(12) theoretical approaches to predict the mean drop diameter in the jetting region. The correlation was suggested as ;

$$\frac{D_{32}}{D_{jm}} = \frac{2.06}{\left(\frac{U_n}{U_c}\right)} + 1.47 \ln\left(\frac{U_n}{U_c}\right) \qquad [2.42]$$

where the critical velocity U_c was calculated from Skelland and Johnson's equation [2.41] and the critical jet diameter D_{jm} was calculated by Christiansen and Hixson equation for the jet diameter.

Equation [2.42] provides a link between the prejetting theories for maximum drop size and the instability theory for minimum drop size. Horvath et al compared the prediction of equation [2.42] with Meister & Scheele(20) and Skelland & Johnson(14) and found a close agreement with Skelland & Johnson's results in the early jetting region.

Kumar and Hartland (6) also produced a purely empirical equation for the prediction of drop size in the jetting region which was based on their experimental data. They applied a multiple regression analysis to calculate the constants k, m and n for their general equation [2.11] and derived a final equation as;

$$\frac{D_{32}}{D_n} = 1.546\ (We^*)^{-0.021}\ (Eo)^{-0.214} \qquad [2.43]$$

where We^* is the modified Weber number.
They calculated We^* and Eo from their experimental data. The maximum error for the prediction of drop size in the jetting region using equation [2.43] was found to be 9.7%.

Bright(24) studied the drop formation process in the jetting region and reported that the jet breaks-up into distinct families of drops at different point in the jetting region as described earlier. He measured the group formation time (Tg) for different families and the fundamental period (Tf) of the fastest growing wave on the surface of the jet.

Bright considered the formation of distinct size related drops in a family group with reference to the fundamental frequency (ω_f) and hypothesized that the fundamental frequency of the fastest growing wave interacts with various harmonics of frequency (ω_h) to give a beat frequency, which he identified as the frequency for the formation of a family (ω_g) as;

$$\omega_g = \omega_f - \omega_h \qquad [2.44]$$

or

$$\frac{\omega_h}{\omega_f} = \left(1 - \frac{\omega_g}{\omega_f}\right) = \left(1 - \frac{Tf}{Tg}\right) \qquad [2.45]$$

To support his hypothesis he characterized various family groupings on the basis of a harmonic ratio;

$$\frac{\omega_h}{\omega_f} = \frac{\text{Number of drops in family}}{\text{Number of fundamental volumes in family}} \qquad [2.46]$$

$$\frac{D_{32}}{D_m} = \frac{n_1 + n_2 + n_3 + n_4 + \ldots.}{n_1 + 2n_2 + 3n_3 + 4n_4 + \ldots.} \qquad [2.47]$$

From the definition of the Sauter mean drop diameter;

$$\frac{D_{32}}{D_m} = \frac{n_1 + 2n_2 + 3n_3 + 4n_4 + \ldots.}{n_1 + 2n_2^{0.67} + 3n_3^{0.67} + 4n_4^{0.67} + \ldots} \qquad [2.48]$$

Bright approximated equation [2.48] to get

$$\frac{D_{32}}{D_m} = \left[\frac{n_1 + 2n_2 + 3n_3 + \ldots.}{n_1 + n_2 + n_3 + \ldots}\right]^{1/3} \qquad [2.49]$$

Bright plotted the harmonic ratio calculated from equation [2.48] against the ratio of jet velocity to critical velocity and found the following dependency

$$\frac{\omega_h}{\omega_f} = \left[\frac{U_n}{U_c}\right]^2$$

Thus from Equation [2.49]

$$\frac{D_{32}}{D_m} = \left[\frac{U_c}{U_n}\right]^{2/3} \qquad [2.50]$$

Equation [2.50] predicts mean drop sizes which are in close agreement with the data of Horvath et al and

Skelland and Johnson. Equation [2.50] possesses a semi-theoretical justification on the basis of the likely interaction of a number of waves growing on the jet.

2.6 SIGNIFICANCE OF THE LITERATURE SURVEY

The survey presented in this chapter has illustrated the various methods proposed for estimating drop sizes in different regimes of drop formation in liquid-liquid systems. All of the theoretical developments presented depend on assumptions of the hydrodynamic behaviour of a drop or a jet surrounded by a second immiscible liquid. The experimental justification for these theories is founded, principally, on drop size measurements in different regimes. However, drop size is always derived from more fundamental quantities such as the detachment time of a drop in the prejetting regime, or the wave properties of disturbances in the jetting regime. In chapter 3 techniques are described for measuring these fundamental parameters in order to ascertain whether the assumptions of previous theories are in fact justified.

CHAPTER 3

EXPERIMENTAL APPARATUS AND PROCEDURE

To study the influence of various parameters like nozzle diameter, nozzle velocity and physical properties of the two phases on the drop size resulting from a liquid jet, an experimental programme was initiated to obtain data for use in the drop size predictions in the prejetting and jetting regimes. Further, to check the validity of the existing instability theories, data on drop formation time, wave lengths, wave growth rates and wave velocities of the fastest growing wave on the surface of the jet were obtained. In addition measurements of jet length at the point of breakup and the variation of the jet diameter with distance from the nozzle were made to give a better understanding of the mechanism of drop formation.

3.1 APPARATUS

The experimental apparatus used in the present study is shown in Plate (1) and a schematic diagram is presented in Figure 4. The apparatus will be described according to the flow control unit and photographic unit.

3.1.1 FLOW CONTROL UNIT

To minimise the effect of variation of liquid flow through the nozzle and its effects on the jet length and the resulting drop sizes, it is essential to have a steady and constant flow of liquid at a fixed setting.

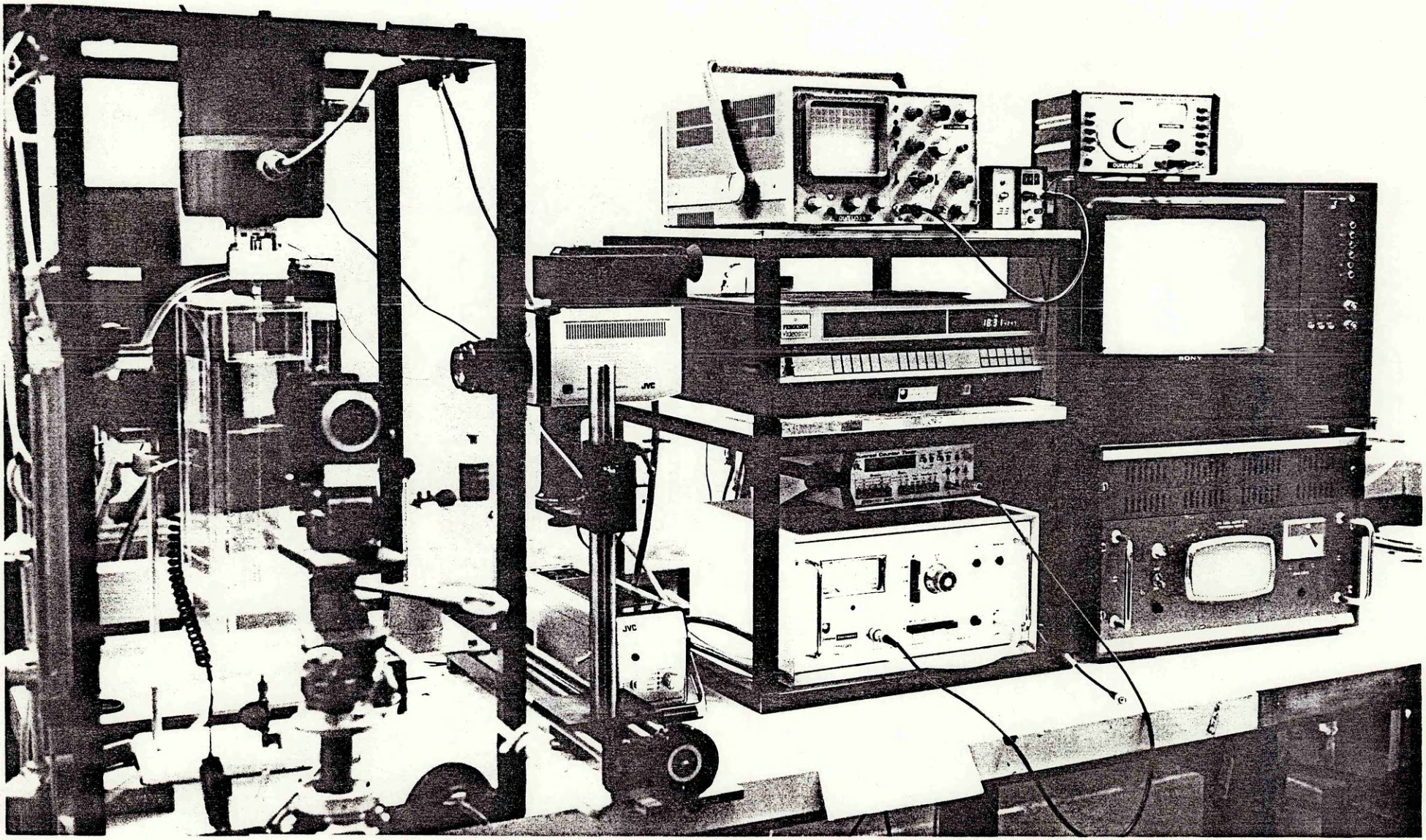

PLATE 1 EXPERIMENTAL APPARATUS USED IN THE PRESENT WORK

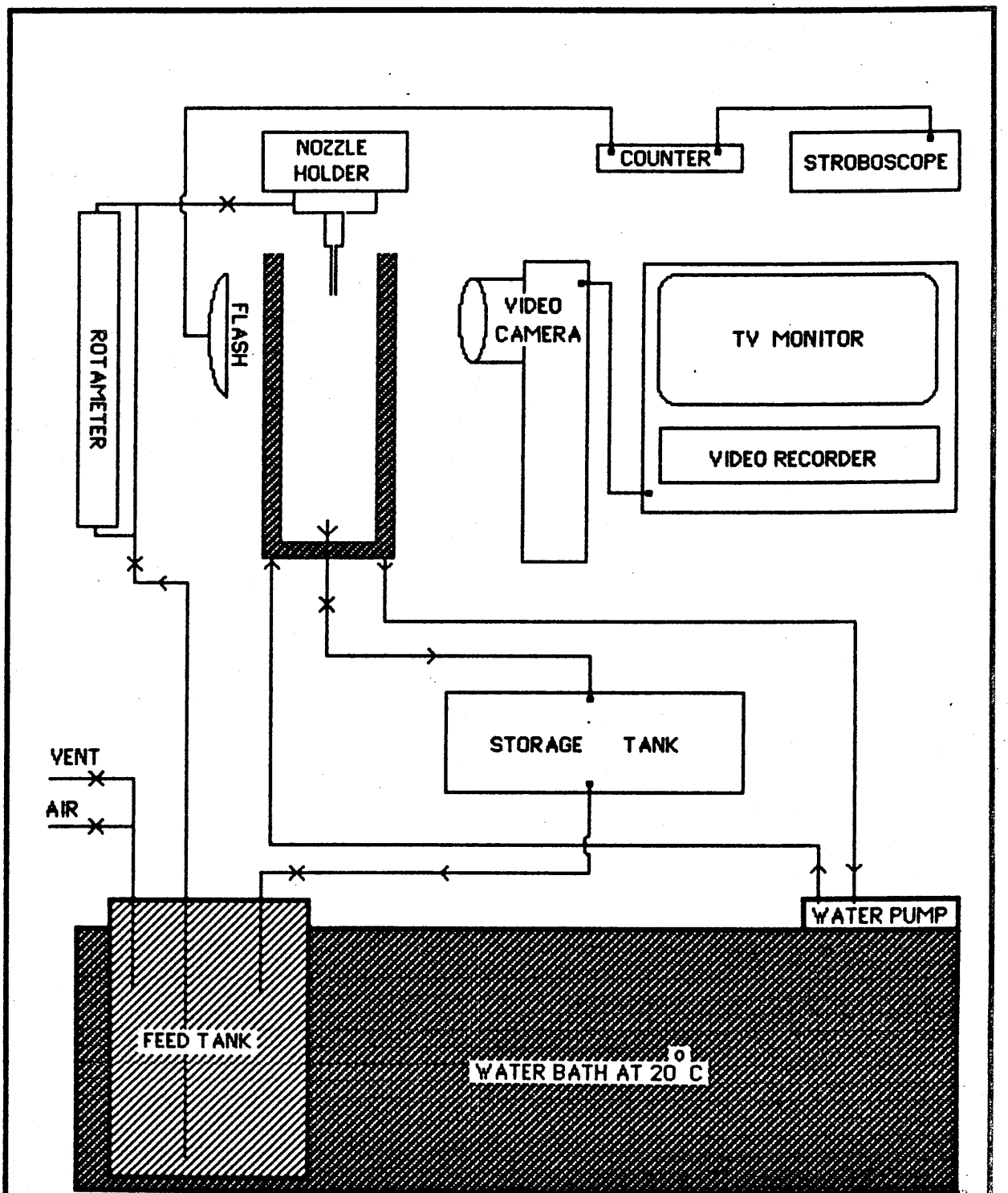

FIGURE 4

SCHEMATIC DIAGRAM OF EXPERIMENTAL APPARATUS

A schematic diagram of a flow control unit is shown in Figure 5, consisting of a pressurised stainless steel feed tank having a capacity of 0.6 litre,with 5mm stainless steel tubing connecting the feed tank to the nozzle holder. A hypodermic nozzle having diameter 0.0602 cm and length 6.0 cm was used. This nozzle gave a fully developed laminar flow in the tube. A rotameter and two additional needle valves were fitted between the feed tank and the holder for fine control of the flow rate of a liquid. The rotameter was calibrated for each dispersed phase by measuring the volume of the collected liquid for a fixed time. A typical calibration curve is given in Figure 6 at $20^{o}C$.

The feed tank was pressurised from a nitrogen cylinder. A pressure regulator maintained the nitrogen pressure at 30 psi in the feed tank. The feed tank temperature was maintained at $20^{o}C$ using a Gallenkamp Thermostatic bath.

The temperature of the continuous phase was also maintained at $20^{o}C$ using a test section which was enclosed within a sealed double walled jacket carrying circulating water from the thermostatic bath maintained at $20^{o}C$ as shown in Figure 5

The test section was made from a double walled perspex sheet of 0.5 cm thickness with the following dimensions :

Inside : Length - 12 cm Breadth - 12 cm Ht. - 37cm
Outside : Length - 14 cm Breadth - 14 cm Ht. - 38cm

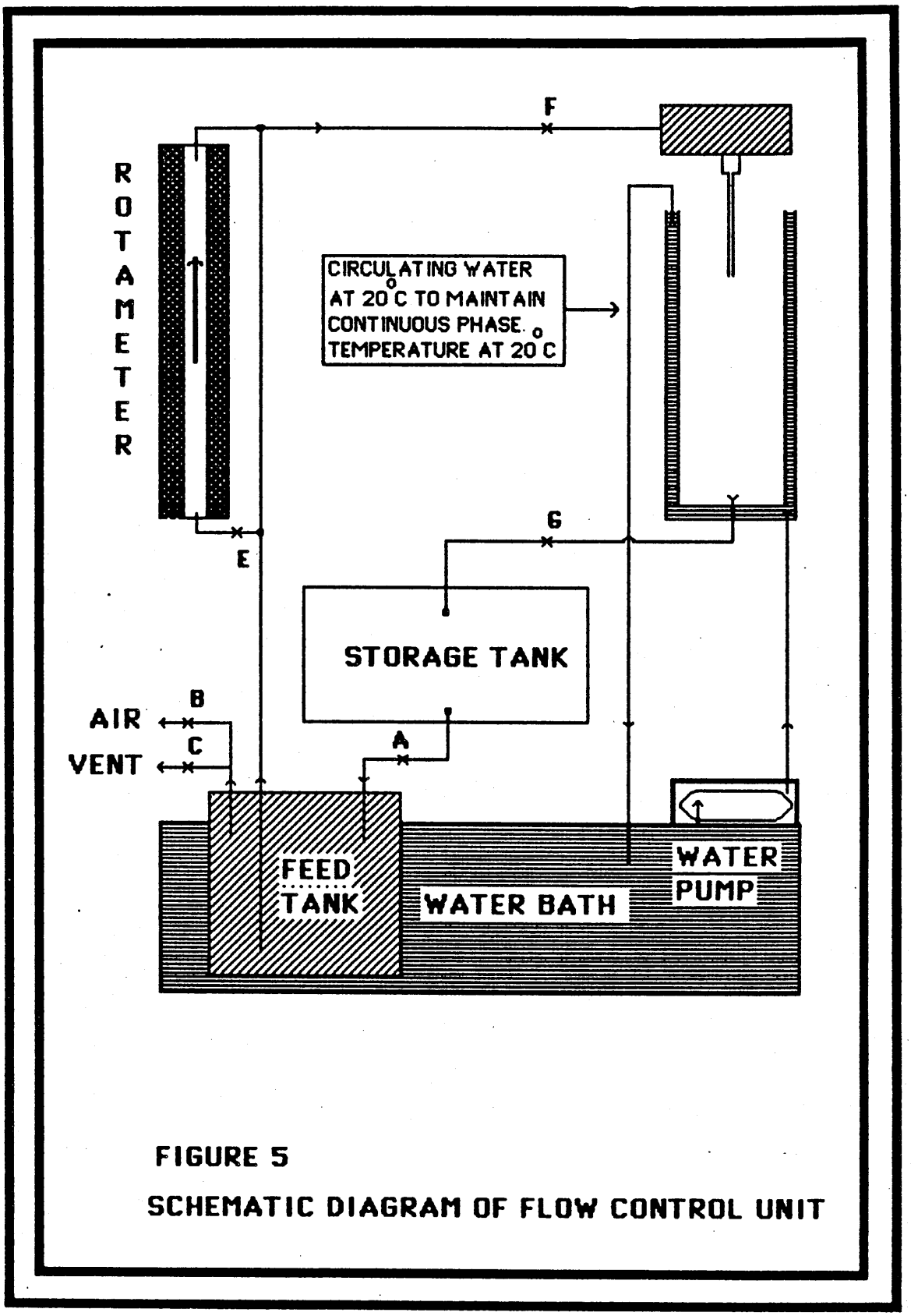

FIGURE 5

SCHEMATIC DIAGRAM OF FLOW CONTROL UNIT

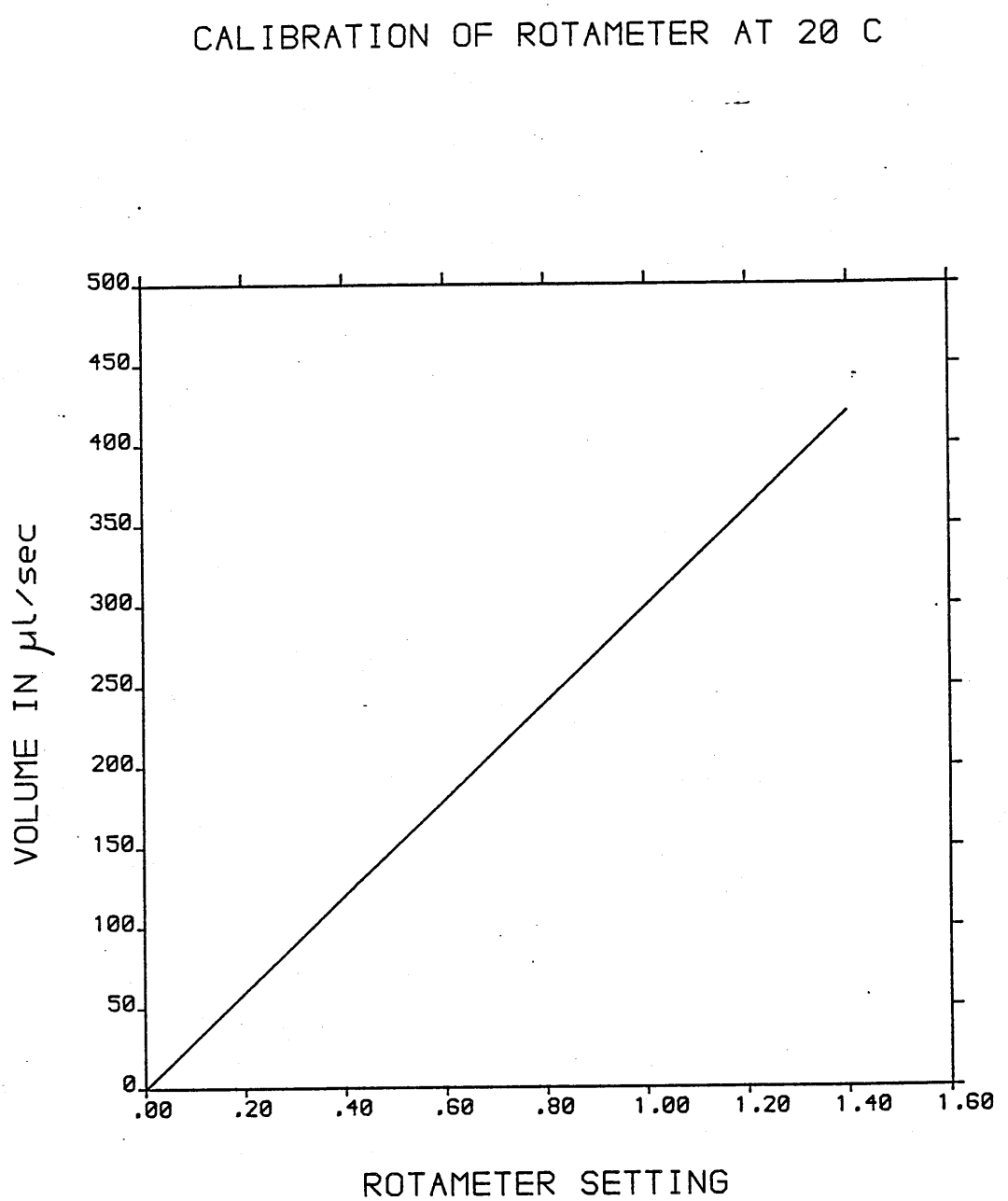

FIGURE 6 CALIBRATION OF ROTAMETER AT 20 C

A perspex scale and a mercury thermometer were suspended in the test section to measure the magnification and the continuous phase temperature respectively. Hence the variation of the physical properties due to the temperature variation of the two phases can be ignored as the temperatures of both the phases were kept constant for all experimental runs.

To recycle the dispersed phase a storage tank of capacity 1.0 litre was fitted between the test section and the feed tank as shown in Figure 5. A needle valve G was fitted between the test section and the storage tank through which the level of the liquid in the test section was maintained. The outlet from the storage tank was controlled by a valve A to refill the feed tank.

3.1.2 PHOTOGRAPHIC UNIT

In the present study, in addition to still photography, a stroboscopic video recording and high speed photographic techniques were also employed.

3.1.2.1 STILL PHOTOGRAPHY

A fixed base stand mounted with a 35mm camera with a bellow attachment was used for still photography. A cable release mechanism was used to prevent unnecessary movement during the photography. A second strobe with a flash duration of 15 μs was used to illuminate the jet and the droplets. The flash time was synchronised with the camera at a shutter speed 1/60 of a second. A light diffuser was placed in front of the flash and provided a uniform illumination over the photographic area, which produced distinct and measurable boundaries around the jet and drop surfaces. A scale was fixed in the same plane as the liquid jet and within the camera field. Ilford Pan F (50 ASA) film was used for the still photographs. The still film negatives were further enlarged and the image analysed directly on the enlarged screen. The still photographic images were analysed to measure the drop diameter and the length of the waves appearing on the jet.

3.1.2.2 VIDEO RECORDING

A video recorder was used to record the pictures from a video camera focussed at the jet. The camera was mounted on an adjustable rack to give both vertical and

horizontal movements in the jet plane. To illuminate the jet, a strobe light was used. The frequency of the strobe light was set manually equal to the drop formation frequency. This gave a frozen picture of the liquid jet on a T V monitor. The recording was made at every setting of the flow rate. The period of drop formation and the group period of formation of regular families were measured at each flow setting.

The disintegration process of the liquid jet and the drop formation patterns were studied in detail by re-playing the recorded film in slow motion on the TV monitor. The jet lengths, drop sizes and inter drop distances could be measured directly from the TV monitor by freezing the frames of the film. This technique was very accurate for the measurement of the jet lengths. Re-play of the slow motion stroboscope image, using the freeze frame facility, enabled measurements of the jet length at the exact point of break up. The measurements of the wave lengths of the fastest growing disturbance and the drop diameter after the breakup were also obtained from the frozen image on the video monitor.

3.1.2.3 HIGH SPEED PHOTOGRAPHY

The camera used was a 16mm Hadland Hyspeed rotating prism model of 30m film capacity. The camera was mounted on a strong pillar stand which combines great flexibility of adjustment with adequate stability. It employed two lenses, oriented at right angles, simultaneously. The

image was superimposed on the same film. The camera is capable of up to 10K frames per second. The frame image is established on a continuously moving film by a prism which rotates synchronously with the film motion. Different film speeds can be obtained by adjusting the voltage supplied to the motor of the camera and a speed at any point is indicated by limiting pulses registered on the film during the operation.

A speed control unit permits the synchronization of the camera with the events to be photographed.The regulation of the camera speed is controlled by the current supplied with an auto transformer with a maximum output of 280 volts. The camera control circuit also incorporates a 70 ms delay time when operating above 130 volts. This delay brings the camera up to speed in two steps to prevent the stripping of the film sprocket holes.

The back light for the high speed film was provided by a microscope lamp giving a high illumination over a small field of view. The film requirements for jet and droplet photography are much the same as for any other high speed camera except good contrast and high resolution are required. A Kodak Tri-X reversal film was used for high speed film.

The film was analysed by projecting it on a large screen. The projector used gives a bright and flickerless picture at different variable film speeds for reversed and forward running facilities. Individual frames can also be analysed and frames progressed frame by frame, forward

or backward by operating a push button switch. An accurate frame counter which operates in both the directions provides a ready means of frame identification. Measurements of the position of the co-ordinates of the interface were digitised and stored on a data logging computer. Analysis of the high speed film allowed several measurements to be made. In the prejetting regime, the velocity of the front and the centre of the drop was measured. Also the neck velocity was measured during drop detachment. The major and minor diameters of the growing drop and neck were also measured and the volume of the drop and the neck were calculated. In the jetting regime the full wave profile from the nozzle to the breakup point was analysed over the full period of formation of a group of drops. Measurements of wave amplitude vs distance and time, wave length and wave velocity were calculated from the wave profile.

3.2 MEASUREMENT OF THE PHYSICAL PROPERTIES

In the present study three liquid pairs with six different configurations were used as given in Table (2). The physical properties were measured by two independent methods in each case and an average value was used for calculations.

The viscosity of the test liquids were measured using a Synchro- Lectric Viscometer. This viscometer measures the viscosity by measuring the torque required to rotate a spindle in the liquid.The torque is proportional to the

viscosity of the fluid and the size of the spindle. The instrument was calibrated and found to be accurate within 1% and to reproduce within 0.2% of its full scale range.

The measured value of viscosity was also measured with an Ostwald Viscometer calibrated with water at $20^{o}C$. The average value of these two were taken and used in the calculations.

Density measurements were made with a specific gravity Bottle also calibrated with distilled water at $20^{o}C$. The obtained readings were also checked using calibrated hydrometers.

Interfacial tension was determined using the Harkins - Brown drop volume technique. A 3ml microburette fitted with a glass dropping tip having an inside diameter of 0.52mm and outside diameter 1.5mm respectively was used for the measurements. The burette was filled with the denser liquid and the tip was just submerged into the other liquid. Each drop was then formed very slowly so that all kinetic effects could be ignored. Fifteen drops were formed and the average volume was measured to calculate the interfacial tension using the following equation ;

$$\sigma = \frac{V_f (\rho_d - \rho_c) g}{D_n \psi}$$

where ψ is the Harkins Brown correction factor which depends on D_n/V_f. D_n- nozzle diameter and V_f is the drop volume under static conditions The value of the correction

factor is presented in Figure 7.

The measurements of the interfacial tension were also made with a Torsion balance. This balance records the forces required to lift a platinum ring or glass plate free from the interface between the two liquids. The results were very consistent and were very close to those results obtained from Harkin-Brown's method. The average values here again were taken for the calculations.

A list of these physical properties of the liquid-liquid pair used in the present study is given in Table (2).

NOTE In the present study the effect of contamination has been ignored; ~~therefore~~, in practical applications this effect could alter the results.

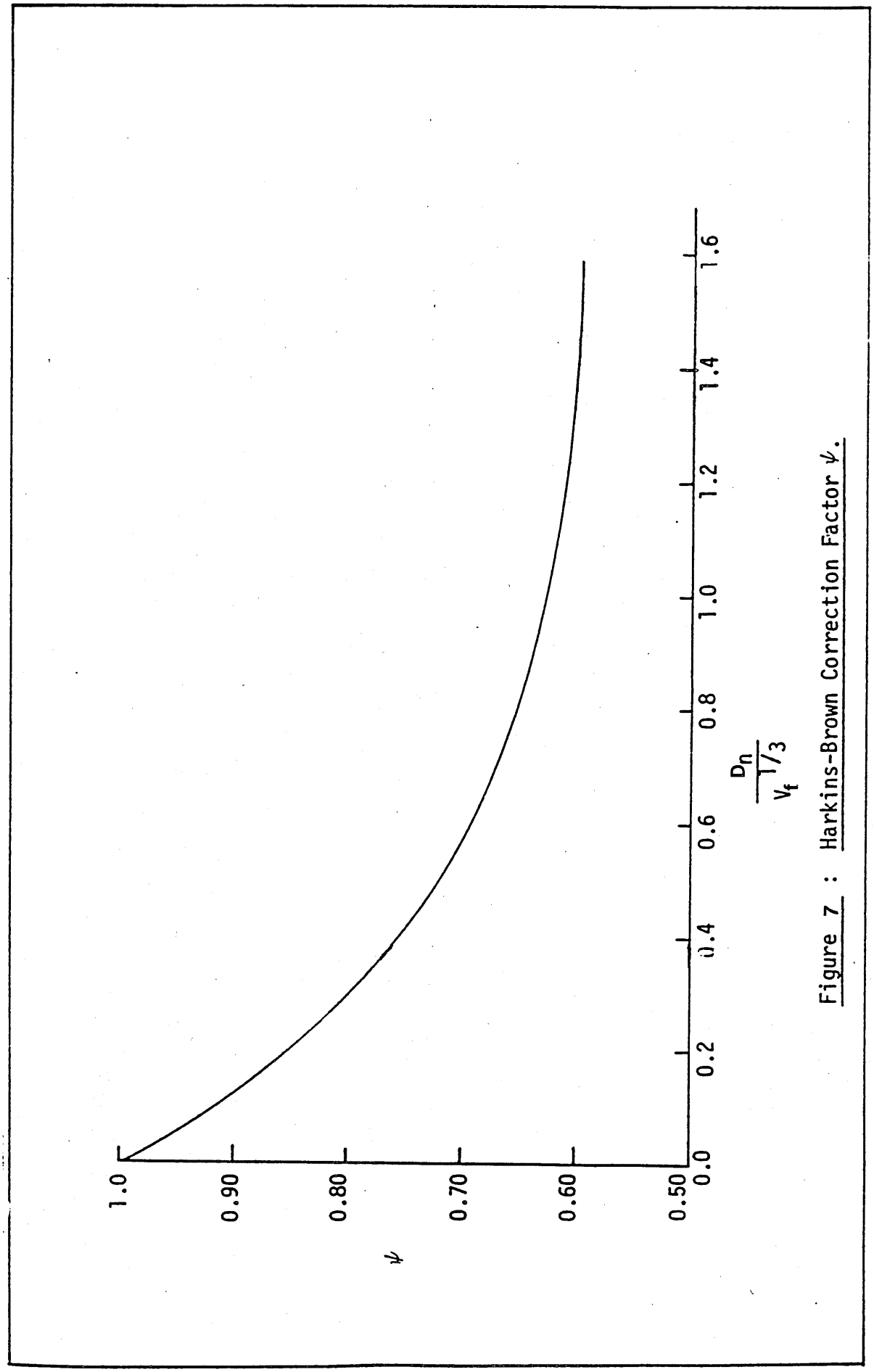

Figure 7 : Harkins-Brown Correction Factor ψ.

TABLE 2

AVERAGE PHYSICAL PROPERTIES OF MUTUALLY SATURATED LIQUID PAIRS USED IN THE PRESENT WORK

SYSTEM DP/CP	DISPERSED PHASE		CONTINUOUS PHASE		INTERFACIAL
	Density	Viscosity	Density	Viscosity	Tension
	kgm^{-3}	mPas	kgm^{-3}	mPas	mNm^{-1}
Decane/Water	732	0.99	999	1.10	22.5
Decanol/water	836	18.0	999	1.15	3.1
Paraffin/Water	882	10.5	999	1.15	27.5
Water/Decane	999	1.10	732	.99	22.5
Water/Decanol	999	1.15	836	18.0	3.1
Water/Paraffin*	999	1.15	882	10.2	27.5

* Liquid Paraffin was supplied by BDH Chemical for the experimental work.

3.3 EXPERIMENTAL PROCEDURE

The method of generating data for a particular run proceeded as follows :

The flow control system was flushed with distilled water before starting with a new system. The feed tank was then emptied and dried. Meanwhile, the two phases were left to equilibrate in a stirred 20 litre flask. After several hours of equilibration the physical properties of the two phases were measured. The dispersed phase was then placed in the tank and run through the circulating system to fill the line and eliminate air bubbles in the line.

The nozzle to be used was cleaned with chromic acid and flushed with the continuous phase in order to prevent wetting of the nozzle exit by the dispersed phase. The test section was filled with the continuous phase.

The temperature of the two phases was monitored until a steady temperature of $20^{o}C$ was achieved. Then the feed tank was pressurised and the flow rate was adjusted to have a steady rotameter reading. For each setting of the flow rate, the period and the wave length of the fastest growing wave was measured using the stroboscope. Still photographs of jet and drops were taken for every setting of the flow rate and a video film was also recorded simultaneously. The flow rate of the dispersed phase was increased in small intervals from prejetting conditions to cover the whole of the early jetting region until the point where asymmetric waves were observed on the surface

of the jet. High speed cine film photography was run at three settings in the jetting region corresponding approximately to Weber numbers 6,10,20 and also at three settings in the prejetting region corresponding to Weber numbers 0.5,1.0,1.5

For each setting of the flow rate, the period and the wave length of the fastest growing wave was measured using the stroboscope. Still photographs of jet and drops were taken for every setting of the flow rate and a video film was also recorded simultaneously.

CHAPTER 4

EXPERIMENTAL OBSERVATIONS AND RESULTS

4.1 EXPERIMENTAL OBSERVATIONS

The drop formation phenomena from liquid jets as observed in the present study can be best described in terms of the characteristic jetting regimes, which are a function of the velocity of the liquid through the nozzle as already described in chapter 2.

At low velocities, the drops are formed directly from the nozzle tip as illustrated in Plate (2). This flow regime is the prejetting regime, characterized by uniform sized drops growing at the nozzle tip with a specific time of formation. The drop size particularly depends on the ratio of interfacial tension to the density difference for a particular system. The drop size increases with increasing surface tension and viscosity of the continuous phase.

The complete process of drop formation in the prejetting regime can be identified under three distinct stages as revealed from high speed cine film photography.

a. Drop growth at the nozzle.
b. Cylindrical column formation.
c. Necking in process to detachment.

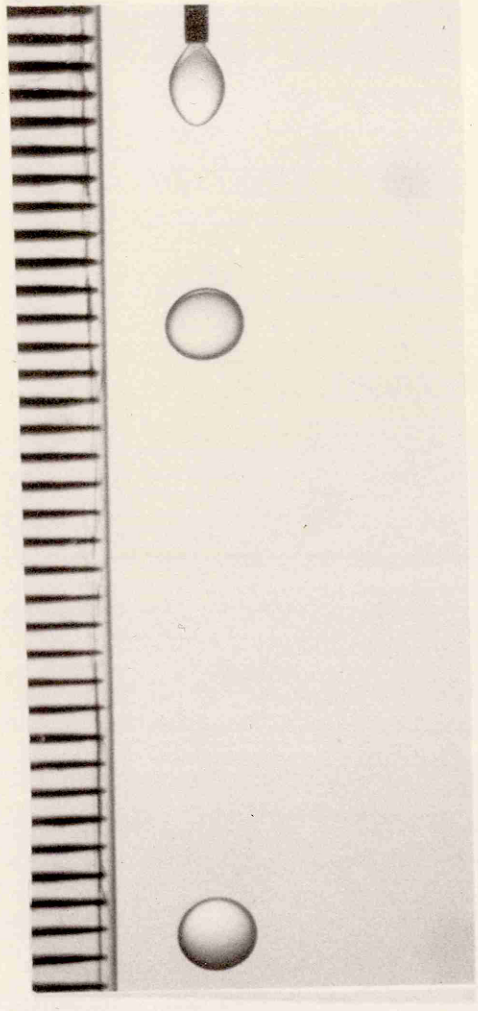

PLATE 2. DROP FORMATION FROM THE NOZZLE AT LOW VELOCITY

NOZZLE DIAMETER	-	0.0602 cm
FLOWRATE	-	0.048 cc/sec
FORMATIONTIME	-	400 ms
DROP SIZE	-	0.3322 cm
SCALE 1 div	-	1 mm

Initially, all the volume flow of incoming liquid accumulates to form a spherical shaped drop at the nozzle tip. The drop grows in size with a constant velocity. After a certain time a critical stage is reached where this drop is no longer attached to the nozzle, but instead to a small cylindrical liquid column as can be seen in Plate (3) from 12. Beyond this critical stage a fraction of incoming volume of liquid stays in the cylinder, which causes an increase in its length. However, at the same time due to the reduction of the total flow of liquid into the drop a decrease in the rate of expansion of the drop was observed . This stage can be seen in Plate (3) from 12 to 14. When the cylinder acquires a critical length it becomes unstable in its cylindrical form and tends to gain its stability by reducing its surface area. Therefore, it starts to form a neck in order to adjust its stability and eventually this neck detaches the drop from the cylinder. This process can be seen in Plate (3) from 14 to 18. The remaining liquid left behind on the nozzle relaxes to a spherical shape, acting as a seed for the next drop growth at the nozzle. Three different stages can be viewed as two separate time intervals. The time required for a drop to grow at the nozzle, t_1; and the time it takes to form a neck and detach from the nozzle, t_2.

Plate (4) shows the transition to jetting conditions as the velocity is increased. The velocity at which the drops no longer form at the nozzle tip but instead from

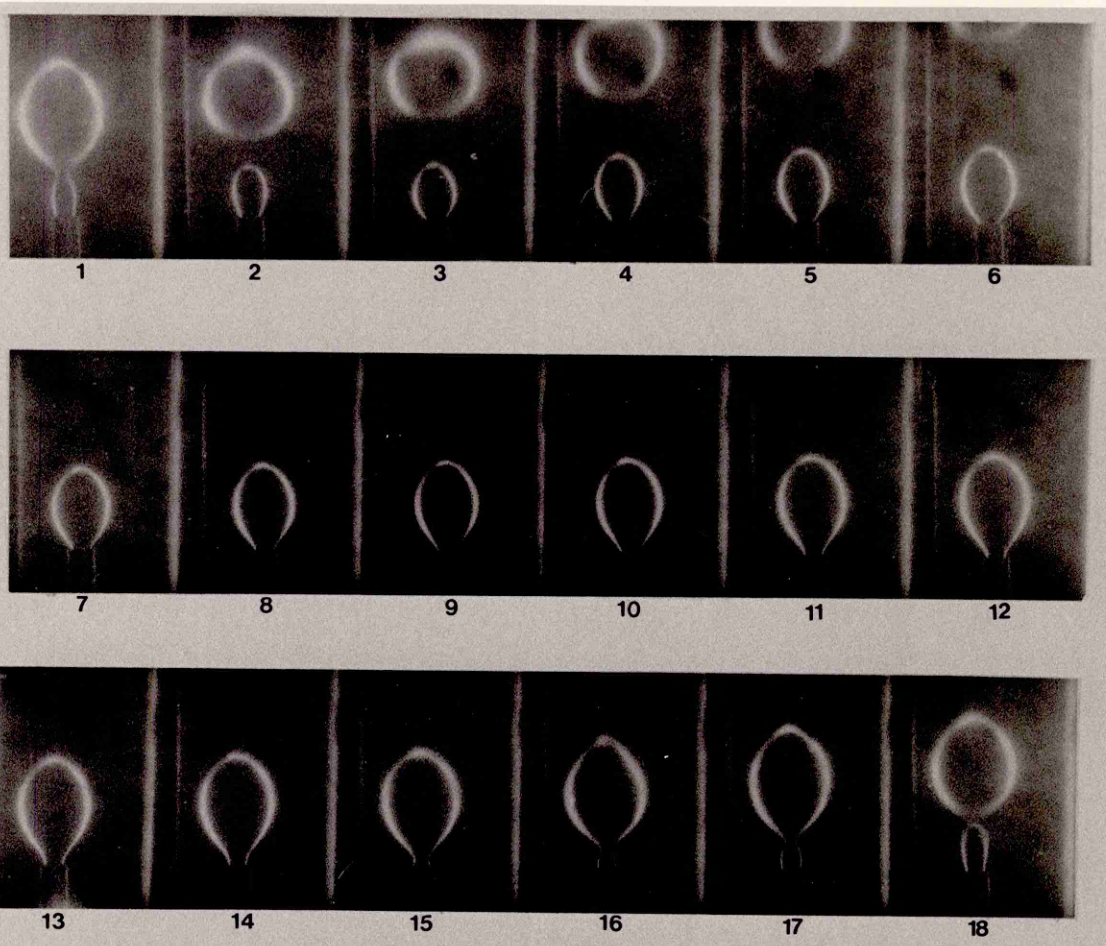

PLATE 3 HIGH SPEED CINE FILM SEQUENCE IN PREJETTING CONDITION

FLOWRATE - 0.68 cc/sec
FORMATIONTIME - 200 ms

the end of a short liquid jet is called the jetting velocity,Uj. At the jetting velocity it appears that after the detachment of the drop from the jet, the remaining liquid has no time to relax towards the nozzle before a new neck formation process starts. When the jetting occurs, there is generally a considerable decrease in the average drop size. At this point it is often reported that the mechanism of drop formation process changes, with the instability governing the breakup process. However, Plate (3) has shown that even before the jetting velocity, although the drop grows initially at the nozzle tip, the point of detachment is from the end of a definite, if short jet. Such observations suggest that the change from drop formation at the nozzle to the drop formation at end of the jet is not a sharp transition, but rather a progressive change depending on the relative magnitudes of various forces acting on the drop and the jet. Thus, it might be expected that the jet instability is an operating factor in determining the detachment time even in the prejetting condition. This observation forms the basis of subsequent development of the theory of drop formation in the prejetting regime to be discussed in chapter 6.

With a further increase in the nozzle velocity above the jetting velocity, the jet disintegrates to form various distinct families at regular intervals. These families contain drops of various sizes but the drop volumes appear to be related to one another as multiples

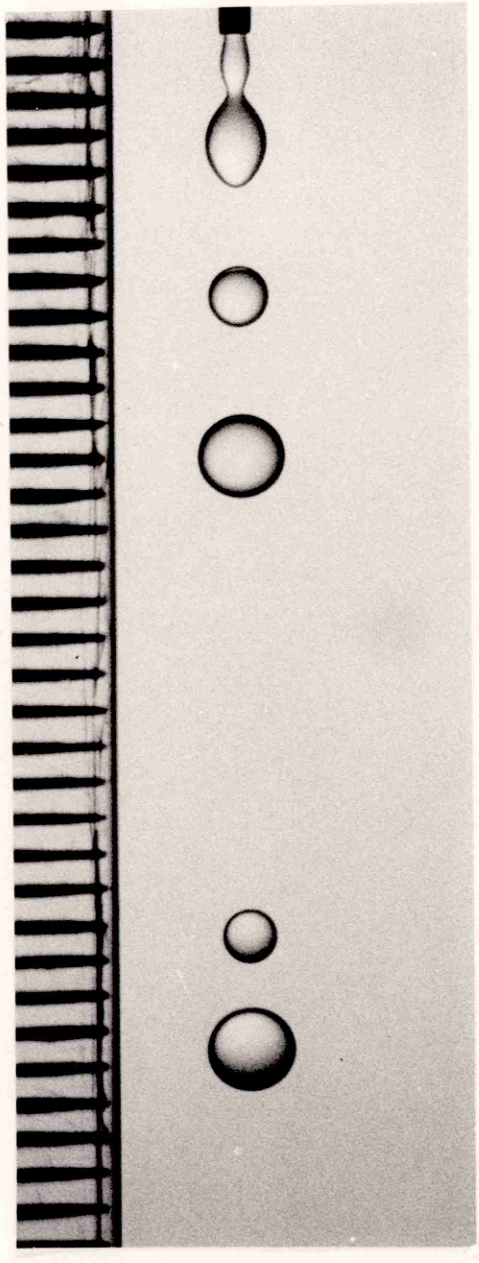

PLATE 4 JETTING CONDITION

FLOWRATE	-	0.90 cc/sec
VELOCITY	-	31.2 cm/sec
DROP DIAMETER	-	0.15 & 0.315 cm

of the fundamental (minimum) drop volume, which is equal to the volume of liquid contained within one wave length of the fastest growing wave on the jet. The large drops in the family grow by accumulating the jetting liquid over the successive waves on the jet. This process can very well be seen in the slow motion video pictures. These waves can be counted as they travel on the surface of the jet,accumulating their liquid in the drop until the drop detaches from the jet. For convenience, depending on the number of waves (or nodes) which are involved in the formation of the drop at the end of the liquid jet, the drop sizes can be referred to as 1-node(1N),2-node(2N), 3-node(3N) and 4-node(4N) etc.

The structure of these families varies with the velocity in the jetting regime. It has been observed that at low velocities the proportion of large to small drops in a family is higher and the ratio of the two reduces as the velocity increases; such variations can be seen in Plate (5).

Plate (5a) presents a monosized drop stream in the prejetting regime at a Weber number of 1.50 where the drop grows at the nozzle tip and detaches in close vicinity of the nozzle. As the flow rate increases, the point of detachment moves increasingly away from the nozzle tip until a small liquid jet is formed at the jetting velocity,Uj . Soon after the jetting starts (Plate (5b)) at a Weber number of 1.86 a mixture of large(10N) and small(1N) drops are formed. The size of the large drop is

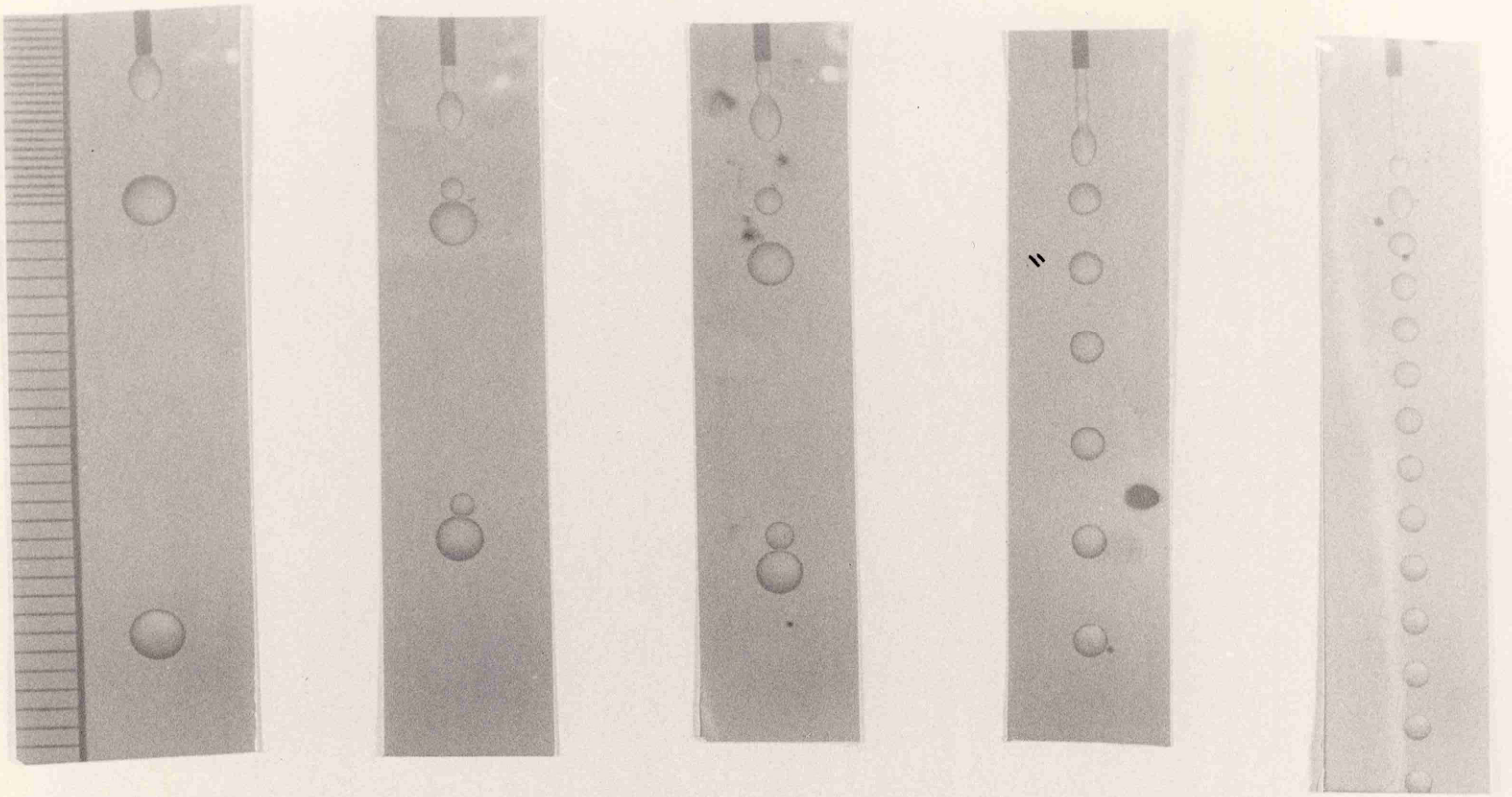

WE	1.50	1.86	1.90	2.73	4.19
Tg	300.0	128.0	128.0	38.5	15.5
Tf		11.63	11.61	9.6	7.75
GROUP	MONOSIZE	1ON1N	9N2N	4N	2N

PLATE 5 FORMATION OF DISTINCT FAMILIES IN THE EARLY JETTING CONDITION

of the same order of magnitude as the drop formed in the prejetting conditions at the tip of the nozzle. As the flow rate increases the size of these drops varies, as can be seen in Plate (5c) at Weber number of 1.90, where a large drop(9N) is actually smaller than the large drop at Weber number 1.86; the smaller drop(2N) is in fact larger than the small drop in Plate(5b). Experimentally it has been observed that this process continues until both the drops become the same size to produce a monosize stream as can be seen in Plate (5d), where 4N monosize drops are produced at a Weber number of 2.73. The stroboscopic measurements were used to measure the group, or family period Tg and the fundamental period Tf of the fastest growing wave on the surface of the jet. In all cases Tg was found to be an integer multiple of Tf. The formation time for a 4N monosize drop is exactly four times the fundamental period, that is Tg = 4Tf. At higher velocities, at a Weber number of 4.19 in Plate (5e), the 4N monosize drop stream changes to a 2N monosize drop stream, where the formation time is exactly twice the fundamental period, in other words Tg = 2Tf.

The transition of these drop families as described above, for example from 4N monosize to 2N monosize streams, is not a sudden change. The experimental observations suggest that these transitions are gradual and systematic; performed in a step by step manner. These reproducible and repeatable drop patterns also suggest the possibility of more than one wave being

present on the surface of the jet, interacting with each other to give a beat effect which which could be responsible for producing various distinct families of drops in a regular manner.

One way of characterizing these family groupings is in terms of a harmonic ratio which can be defined as;

$$H = \frac{\text{number of drops present in a family (ND)}}{\text{number of nodes present in a family (NN)}}$$

Thus the harmonic ratio H varies as the composition of the family changes with the velocity. This can be seen more clearly in Plate (6).

Plate (6a) shows a monosize stream of 2N drops at a Weber number of 4.19 where Tg = 2Tf, and hence NN = 2 and ND = 1. Therefore, the ratio of the number of nodes (NN) to the number of drops (ND) is H=ND/NN=1/2. Further, at higher velocities at a Weber number of 4.55 (Plate(6b) a family containing four 2N and one 1N (i.e 1N2N2N2N2N) have H=ND/NN = 5/9. At a Weber number of 4.85 a large family consisting of two groups which repeat alternatively was found as shown in Plate (6c). One group contains four 2N drops and one 1N drop, while the other contains three 2N drops and one 1N drop. Therefore the whole family can be represented as a string of 1N2N2N2N2N1N2N2N2N and the total number of drops (ND) in the family is 1+4+1+3 = 9 The total number of nodes (NN) 1(1x1)+4(2x1)+1(1x1)+3(2x1) = 16, which gives ND/NN 9/16. With a further increase in the jetting velocit

Weber number of 4.93 a family of three 2N drops and one 1N drop [Plate (6d)] have attained the ND/NN ratio equal to 4/7. At a Weber number of 5.29 a family containing two groups 1N2N2N2N and 1N2N2N (Plate (6c)) have acquired the ratio equal to 7/12. Finally, last in Plate (6f) corresponding to a Weber number of 5.75 a family of 1N2N2N has the ratio equal to 3/5. Therefore, the ratio increases as the proportion of smaller drops in the family increases.

It would be expected that the ND/NN would tend to unity with increasing velocity as the drop families include larger numbers of 1N drops until eventually a monosize stream of 1N drops would be produced. However, this ultimate condition could not be achieved experimentally in the present study.

As the harmonic ratio approaches unity it has been observed that there is a larger increase in the jet length and the rate of increase of the jet length with increasing velocity. The jet length depends on the growth rate of the surface disturbances. In the early part of the jetting regime, it appears that the jet breaks up earlier than expected from the growth of the single fastest growing wave, due to interactions with harmonics as described above. Later on in the jetting regime these harmonics have less effect and the jet achieves its natural length from the single wave controlling breakup into minimum size drops. Also, it has been noticed that as the minimum drop size condition is reached it was

difficult to isolate the fundamental period using the stroboscope, instead a band of the fundamental period was recorded. These subsidiary waves are not the harmonics but have their periods close to the fundamental wave. This was also reported by Bright(21). Since there is no longer one single fundamental wave responsible for the breakup, but rather a range of waves having very close wave frequencies,a stable monosize stream of 1N drops might not be achievable. In addition, an occasional appearance of multinode drops gave a flickering image on the TV monitor. As the number of drops in a family increases, the formation time of the family also increases, and hence to see these large families on the TV monitor the flash period must be large enough to freeze the family on the monitor. This is only possible if we use a very low flash frequency. There is an observational limit for the human eye therefore, if the stroboscopic flash frequency is lower than 10 Hz then the stroboscopic image becomes very difficult to retain on the retina for a fine adjustment. To investigate these large families having a large number of 1N drops, the stroboscope alone is not sufficient. Therefore, high speed photography was employed to follow these large family transitions and it was found that the harmonic ratio H still increases with increasing velocity, but a single monosize stream of 1N drops was never achieved.

The critical velocity U_m at which the jet length reaches its maximum value, marks the end of the regular

breakup of the liquid jet into drop families. Because of the large proportion of 1N drops in this region the mean drop size becomes equal to the minimum drop size produced from the fastest growing disturbance on the surface of the jet.

An additional increase in the flow rate above the critical value U_m produces conditions where the jet acquires a sinuous shape due to asymmetric waves being present on the surface of the jet. The transition between the early and late jetting regimes is shown in Plate (7a and 7b). At higher velocity, as shown in Plates (7c and 7d), the breakup pattern is highly irregular. The combination of symmetric and asymmetric waves produces a spread of drop sizes with mean drop size larger than the minimum drop size (Figure 7c). The jet length reduces quite rapidly. At very high flow rates small drops are sheared from the side of the jet (Figure 7d). The drop formation mechanism takes on the random aspect of atomization conditions.

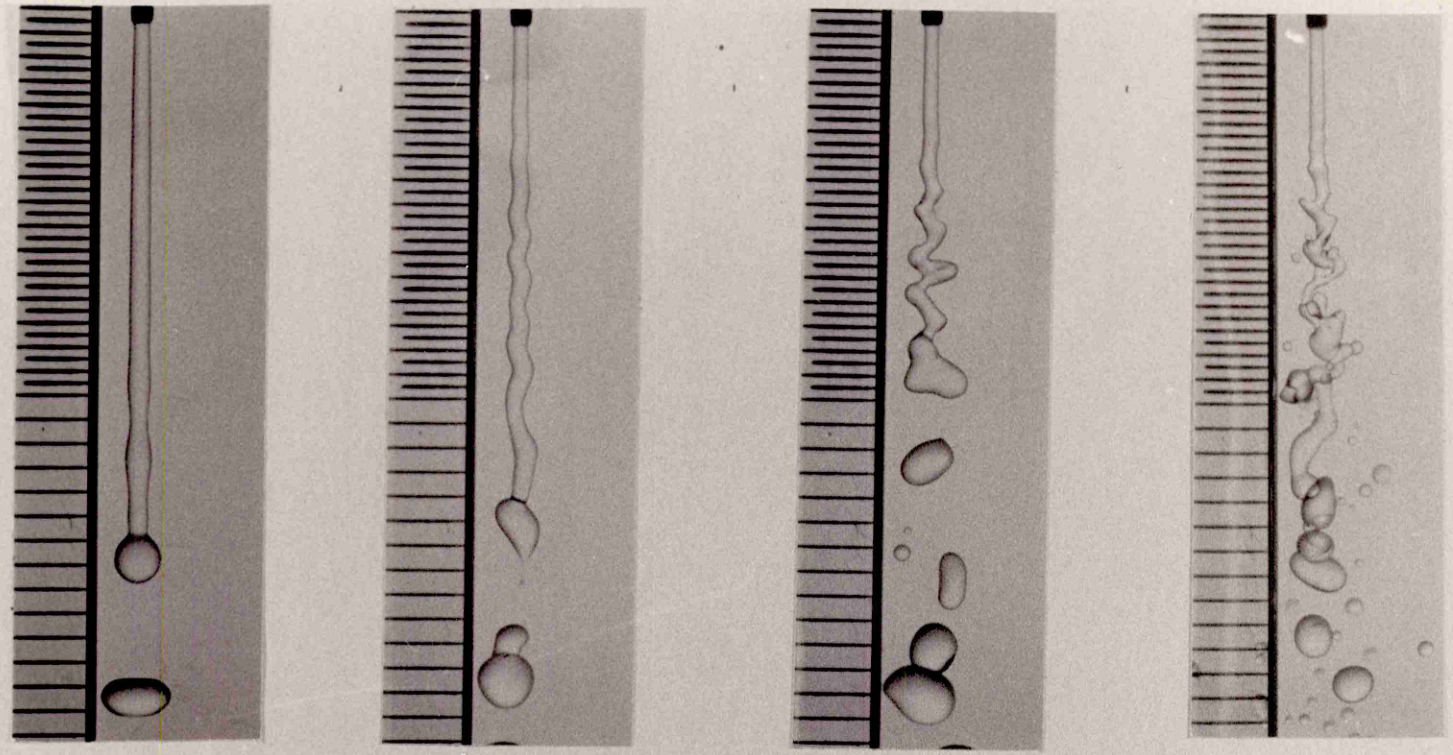

	8a	8b	8c	8d
WE	14.0	25.0	35.0	50.0
Un	84.5	112.0	133.0	159.0
Mean Drop Dia	1.011	1.132	1.200	1.250

PLATE 7 TRANSITION OF SYMMETRIC TO ASSYMETRIC JET

4.2 EXPERIMENTAL RESULTS

The experimental results for the present work are presented in two sections on the basis of two regimes of drop formation from the nozzle.

4.2.1 DROP FORMATION AT LOW VELOCITIES

Although there is a large volume of drop size data for the prejetting regime in the literature, there are only a few studies of the detailed behaviour of the drop during the time of its formation. It was felt that additional experiments were necessary to measure drop growth, velocity and formation time and to relate these primary quantities to existing theories. High speed cine measurements of drop and neck volumes, and velocities were made for water injected into decane system using a 0.0602 cm diameter nozzle at three different flowrates in the prejetting regime. The complete data set is presented in appendix A.

Figure 8 shows the experimental measurements of the volume of the drop and the volume of the neck during the time of formation at three different Weber numbers. Initially the total volume of the incoming liquid goes into a drop until a critical time t_1 where a fraction of the volume starts to go into the cylindrical neck. This critical time corresponds to the instant where the acted buoyancy and momentum forces due to the incoming liquid overcome the restraining surface tension force at the nozzle tip. The drop leaves the nozzle and grows on the

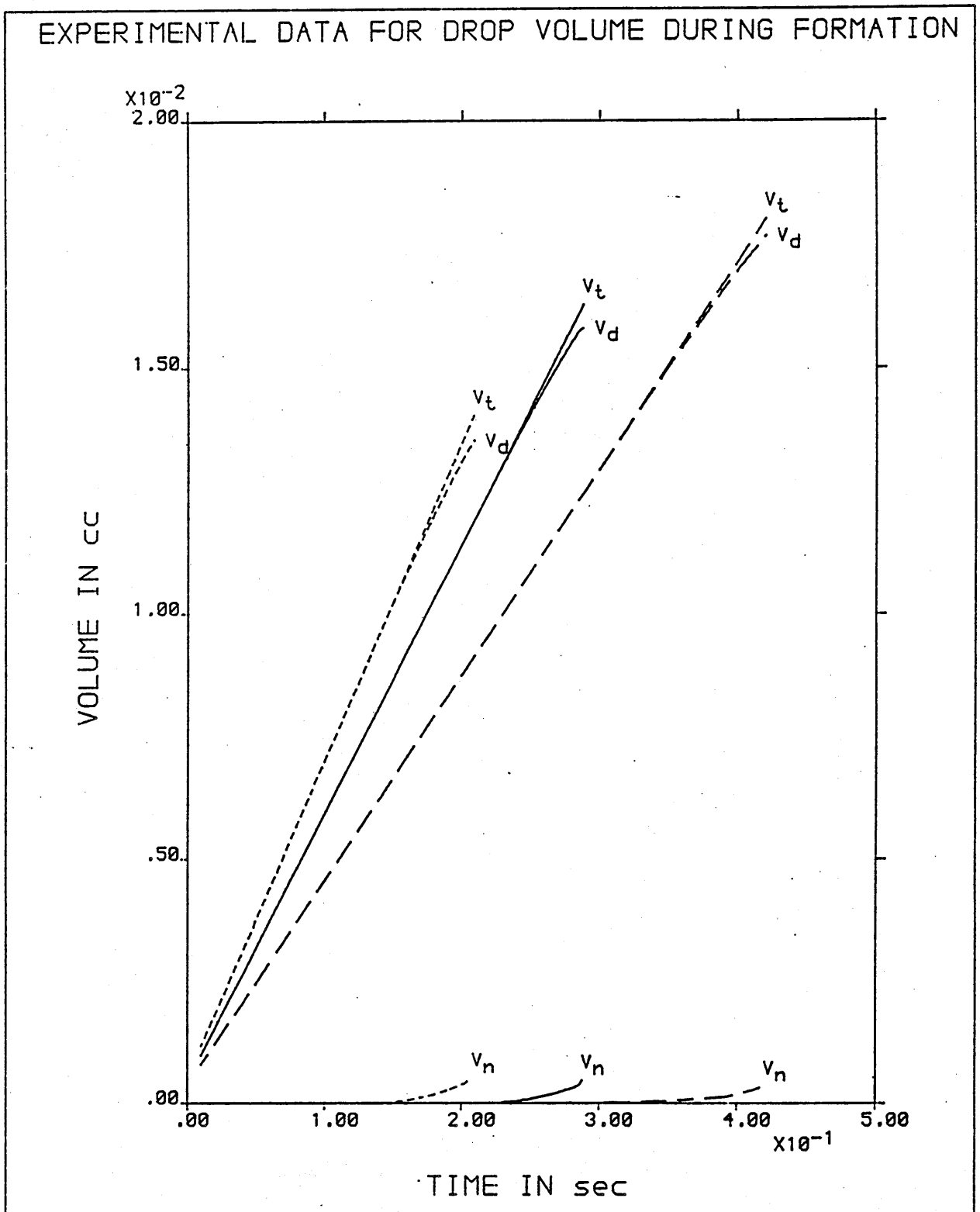

FIGURE 8 CHANGE OF DROP VOLUME DURING ITS FORMATION IN THE PREJETTING REGIME AT THREE DIFFERENT WEBER NUMBERS.

V_t = TOTAL VOLUME OF LIQUID
V_d = VOLUME OF DROP
V_n = VOLUME OF NECK

— — — AT WEBER NUMBER 0.59
——— AT WEBER NUMBER 1.07
------- AT WEBER NUMBER 1.48

top of the cylinder of the liquid. This process is called the 'take off' process. Further, it can be seen that this critical time t_1 reduces as the Weber number increases. This suggests that the take-off time for the drop from the nozzle, which marks the end of the first stage growth of the drop at the nozzle, reduces as the flow rate increases.

Figure 9 shows the distances travelled by the drop top edge, the drop centre and the neck as was measured from high speed cine film at a Weber number of 0.591 where the formation time of the drop was 420 ms. The two stage drop formation process can be seen in Figure 9. During the first stage of drop growth at the nozzle, the liquid cylinder left behind the drop at the time of the detachment of the previous drop, relaxes and goes back to the nozzle where it acquires a spherical shape. The spherical shaped drop grows at the nozzle with a constant rate until a critical time t_1 is reached, which marks the end of the first stage growth of the drop at the nozzle. In the second stage the drop rises on the top of a liquid cylinder where subsequent growth of the drop takes place. The length of the cylinder increases with time during the second stage. When the length of the liquid jet exceeds the circumference of the jet, it becomes unstable and forms a neck which eventually detaches the drop from the jet. The liquid left behind by the detached drop acts as a seed for the growth of the next drop at the nozzle and the process repeats itself.

EXP DATA FOR DISTANCES TRAVELLED DURING DROP GROWTH

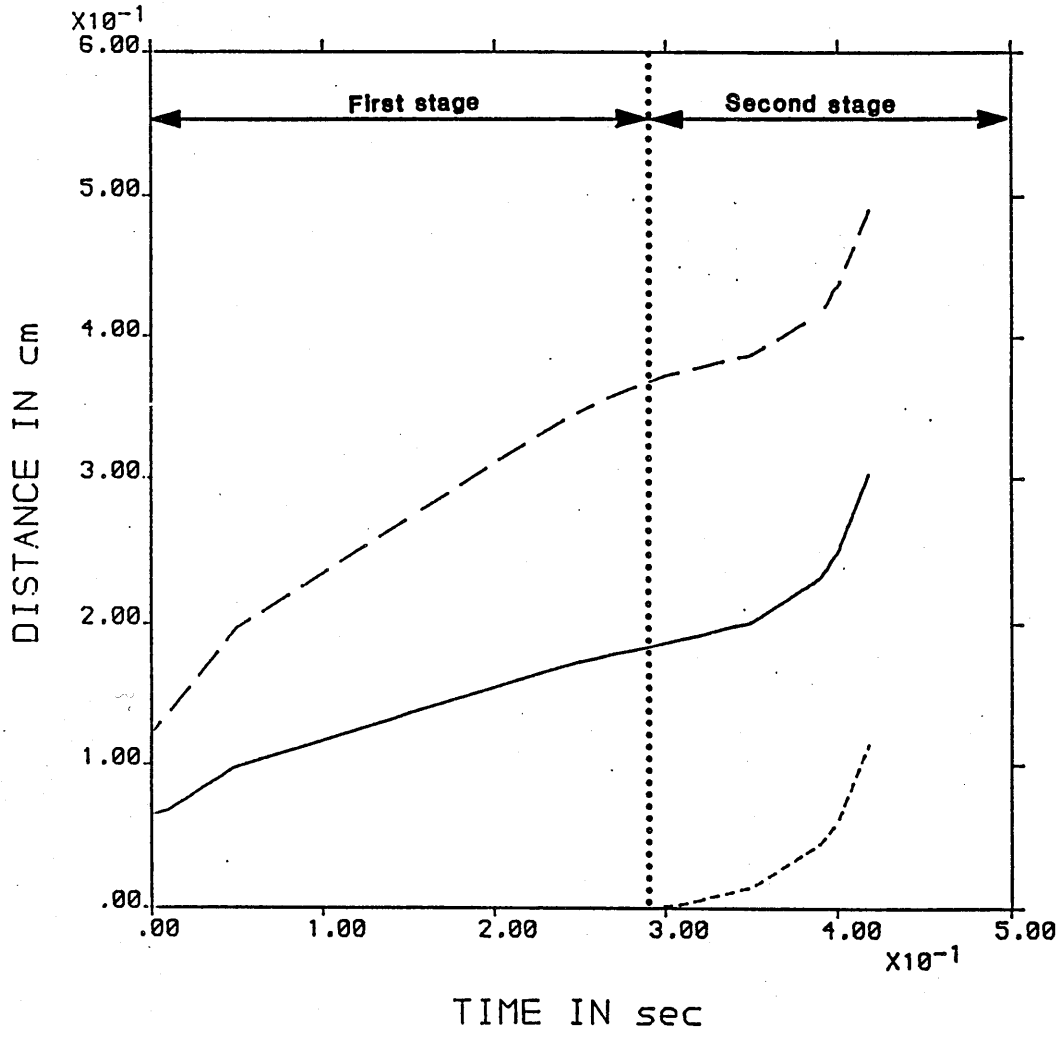

FIGURE 9 VARIATION OF DISTANCE WITH TIME IN THE PREJETTING REGIME

NOZZLE DIAMETER = 0.0602 cm
WEBER NUMBER = 0.59
TIME FOR 1st STAGE = 290 ms
TIME FOR 2nd STAGE = 130 ms
TOTAL TIME OF FORMATION = 420 ms

– — – DISTANCE TRAVELLED BY DROP TOP EDGE
——— DISTANCE TRAVELLED BY DROP CENTRE
------- DISTANCE TRAVELLED BY DROP NECK

Further, it can be seen from Figure 9 that the drop top edge travels more distance during the first stage, but in the second stage, after the neck is formed, the whole lot moves away from the nozzle with the same rate.

Figure 10 represents the velocity variation during the formation of a drop. It shows that the drop top edge velocity is higher than the drop centre velocity during the drop growth period at the nozzle. It can also be seen that the velocities are constant until the point where the drop takes off from the nozzle. After this point the cylindrical neck starts to form and the drop accelerates away from the nozzle.

The high speed cine film [as given in Plate(3)] shows that the drop shape is nonspherical during the growth period. Therefore, the rate of increase of the major and the minor axes of the drop were also measured. These rates are plotted in Figure 11. It can be seen that the rate of expansion of the major and the minor axes decreases near the point where the cylinder starts to grow and becomes zero. The figure shows that the drop top edge, centre and neck, all move with the same velocity during the second stage.

These observations suggest that the measured velocities in Figure 10 must be considered as relative to the natural expansion rate of the drop. Since the bottom edge of the drop is still attached with the nozzle and the top edge is travelling twice as fast as the drop centre. The velocity in the first stage reduces because

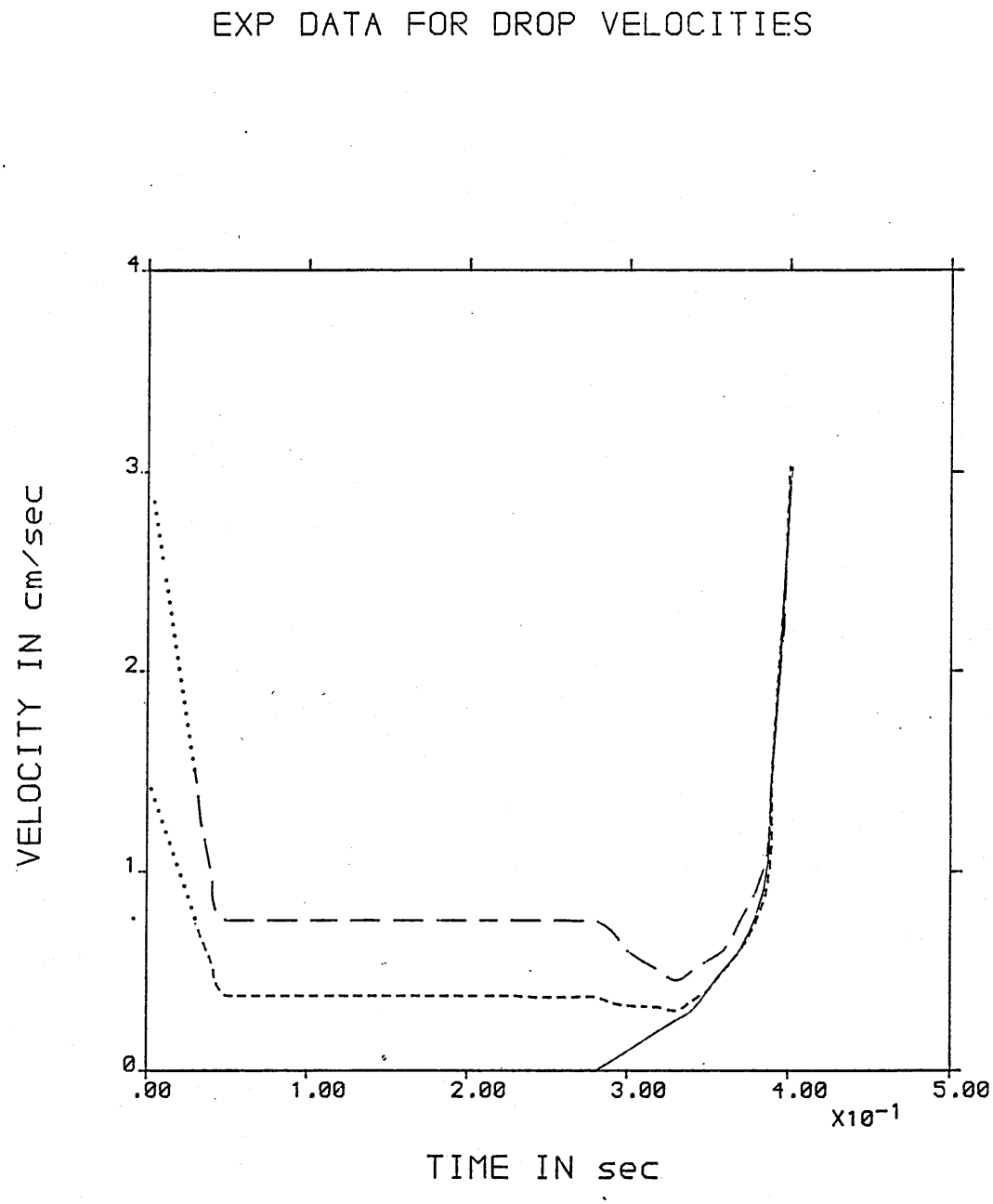

FIGURE 10 VARIATION OF THE DROP VELOCITIES WITH TIME IN THE PREJETTING REGIME

NOZZLE DIAMETER = 0.0602 cm
WEBER NUMBER = 0.59
TOTAL TIME OF FORMATION = 420 ms

– — – DROP TOP EDGE VELOCITY
——— DROP NECK VELOCITY
------- DROP CENTRE VELOCITY

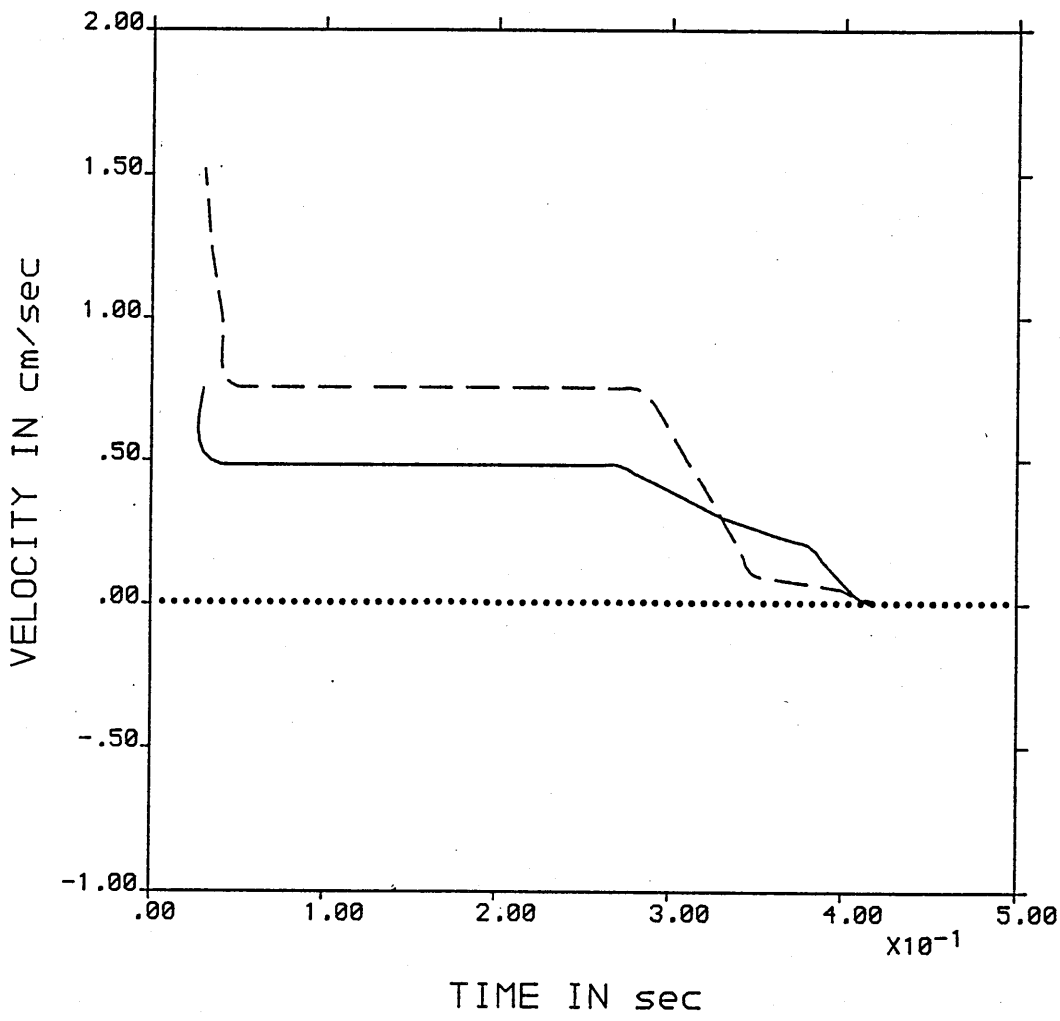

FIGURE 11 THE EXPANSION & ELONGATION VELOCITIES OF A DROP IN PREJETTING REGIME

NOZZLE DIAMETER = 0.0602 cm
WEBER NUMBER = 0.59
TOTAL TIME OF FORMATION = 420 ms

— — — MAJOR AXIS
——— MINOR AXIS

the expansion rate is inversely proportional to the drop surface area, and this leads to a decrease in the velocity. At the end of the growth stage where the buoyancy and momentum forces become equal to the maximum resisting force due to surface tension, the drop initially relaxes (Figure 10) with the relative velocity decreasing slightly as shown, but then accelerates because the increasing buoyancy force now exceeds the maximum constant surface tension resisting forces on the drop, as shown in Figure 10, until detachment occurs.

4.2.2 DROP FORMATION AT HIGHER VELOCITIES

At flow rates above the jetting velocity, a jet is formed which subsequently disintegrates to form drops. The prediction of the minimum drop size in the jetting region is based on the instability theory, whereas the drop size distribution is based on empirical correlations. Therefore, the present experimental results have been divided into two sections. The first section contains the experimental data which was collected for wave growth rate, wave length and wave velocity in order to test the various instability theories, and the second section presents the data for the distribution of drop size for the jetting regime.

4.2.2.1 WAVE PROPERTIES ON THE SURFACE OF THE JET

The variation of the displacement of the jet with time on the surface of the jet was measured at various distances from the nozzle for the six systems as described in chapter 3. A typical plot of time variation of the jet surface with distance from the nozzle for the decane into water system at three different Weber numbers,is shown in Figure 12. This figure suggests the presence of the fundamental wave which grows as the wave travels away from the nozzle. It can also be seen that near the jet breakup point there is a variation in the peak amplitude, suggesting interference of the fundamental with another disturbance on the jet near the breakup point. Because of this variation of the magnitude of the peaks at a

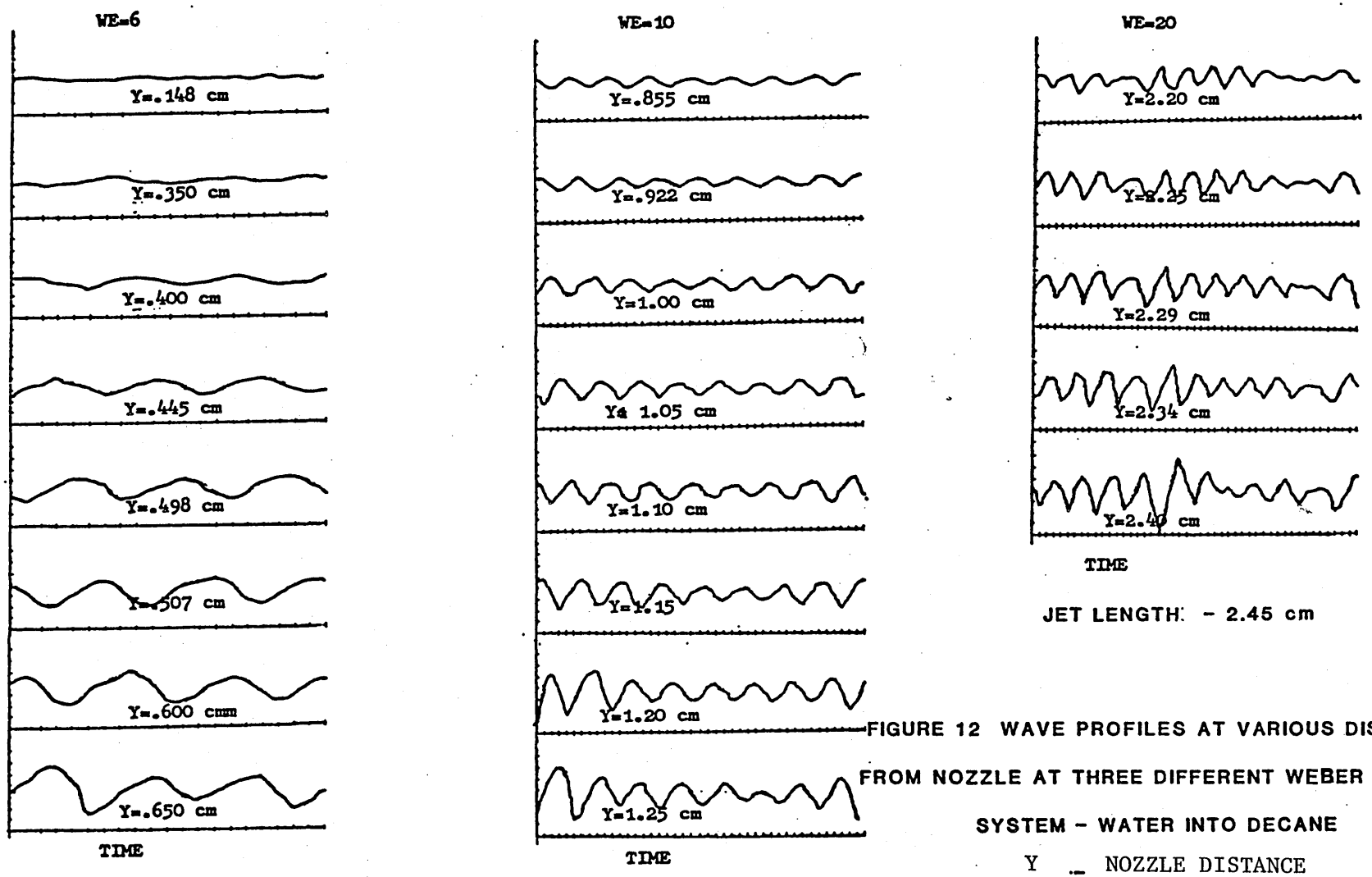

FIGURE 12 WAVE PROFILES AT VARIOUS DISTANCES FROM NOZZLE AT THREE DIFFERENT WEBER NUMBERS

SYSTEM - WATER INTO DECANE

Y _ NOZZLE DISTANCE

particular distance from the nozzle and lack of detailed knowledge of the wave interactions patterns, in the present work an average peak amplitude of the wave at a particular distance has been considered. This point will be discussed in detail in chapter 6. The variation of this average peak amplitude with distance from the nozzle at Weber numbers 6,10 and 20 for six different systems are plotted in Figures (13 to 18) and results are tabulated in appendix B.

These figures suggest that the rate of increase of average peak amplitude with distance depends on both the physical properties of the systems as well as on the velocity of the liquid through the nozzle. This variation can be seen in Figure 19 at two different constant Weber numbers for three different systems.This figure shows that at a constant Weber number, a high viscosity and low surface tension system (decanol into water) has a larger peak amplitude as compared to the system having a high surface tension and low viscosity (decane into water). The effect of the Weber number on the average peak amplitude in Figure 19 can be explained on the basis of the variation of the jet length with the nozzle velocity. The fundamental wave grows on the surface of the jet and when its amplitude becomes equal to, or greater than, the radius of the jet, the jet breaks up. For a particular system the jet breakup time is constant, but as the velocity increases through the nozzle the fundamental wave travels a longer distance during the same time, thus the jet length increases.

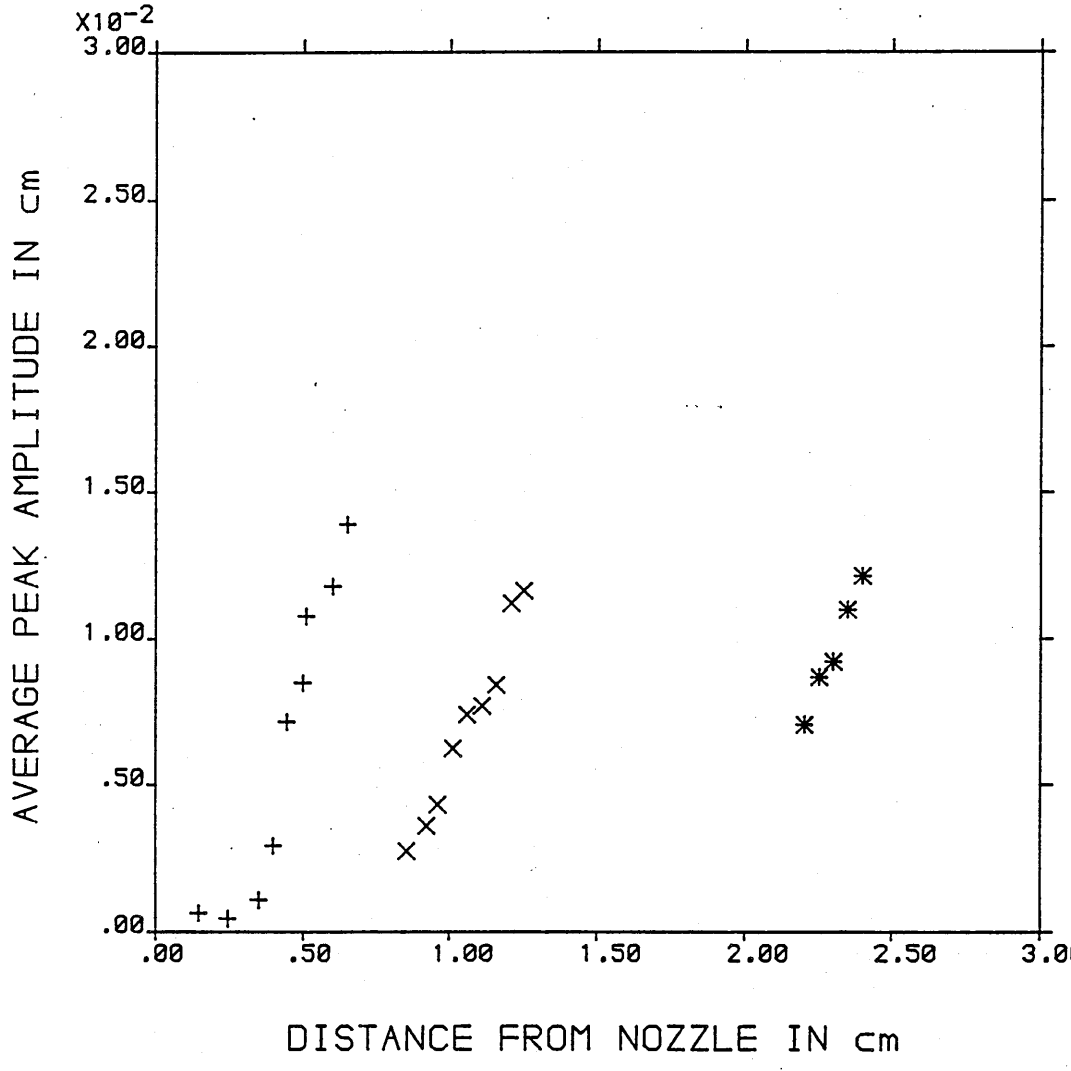

FIGURE 13 VARIATION OF THE AVERAGE PEAK AMPLITUDE WITH NOZZLE DISTANCE
SYSTEM - DECANE INTO WATER

\+ - AT WEBER NUMBER 6
× - AT WEBER NUMBER 10
* - AT WEBER NUMBER 20

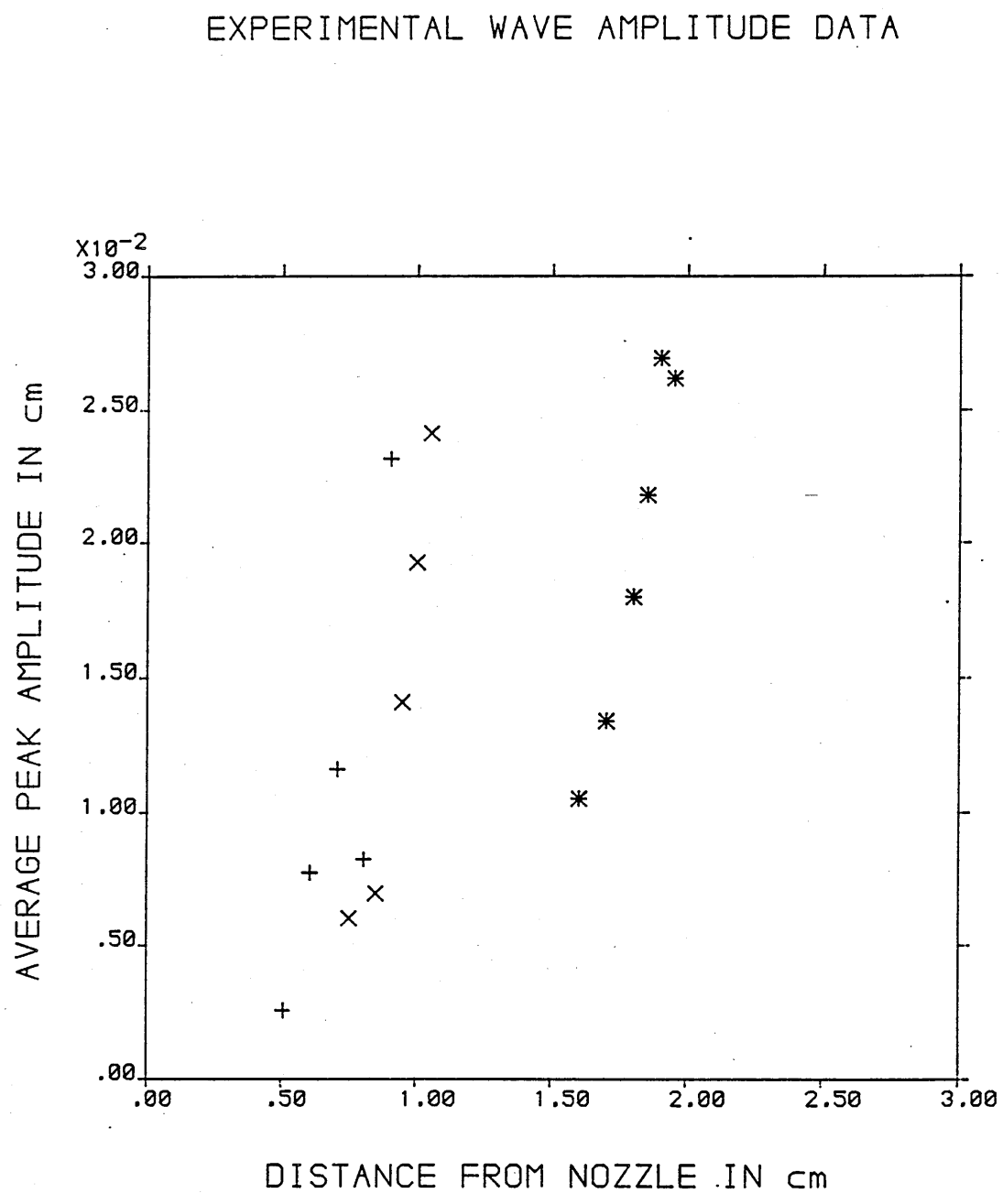

FIGURE 14 VARIATION OF THE AVERAGE PEAK AMPLITUDE WITH NOZZLE DISTANCE
SYSTEM - DECANOL INTO WATER

\+ - AT WEBER NUMBER 6
× - AT WEBER NUMBER 10
* - AT WEBER NUMBER 20

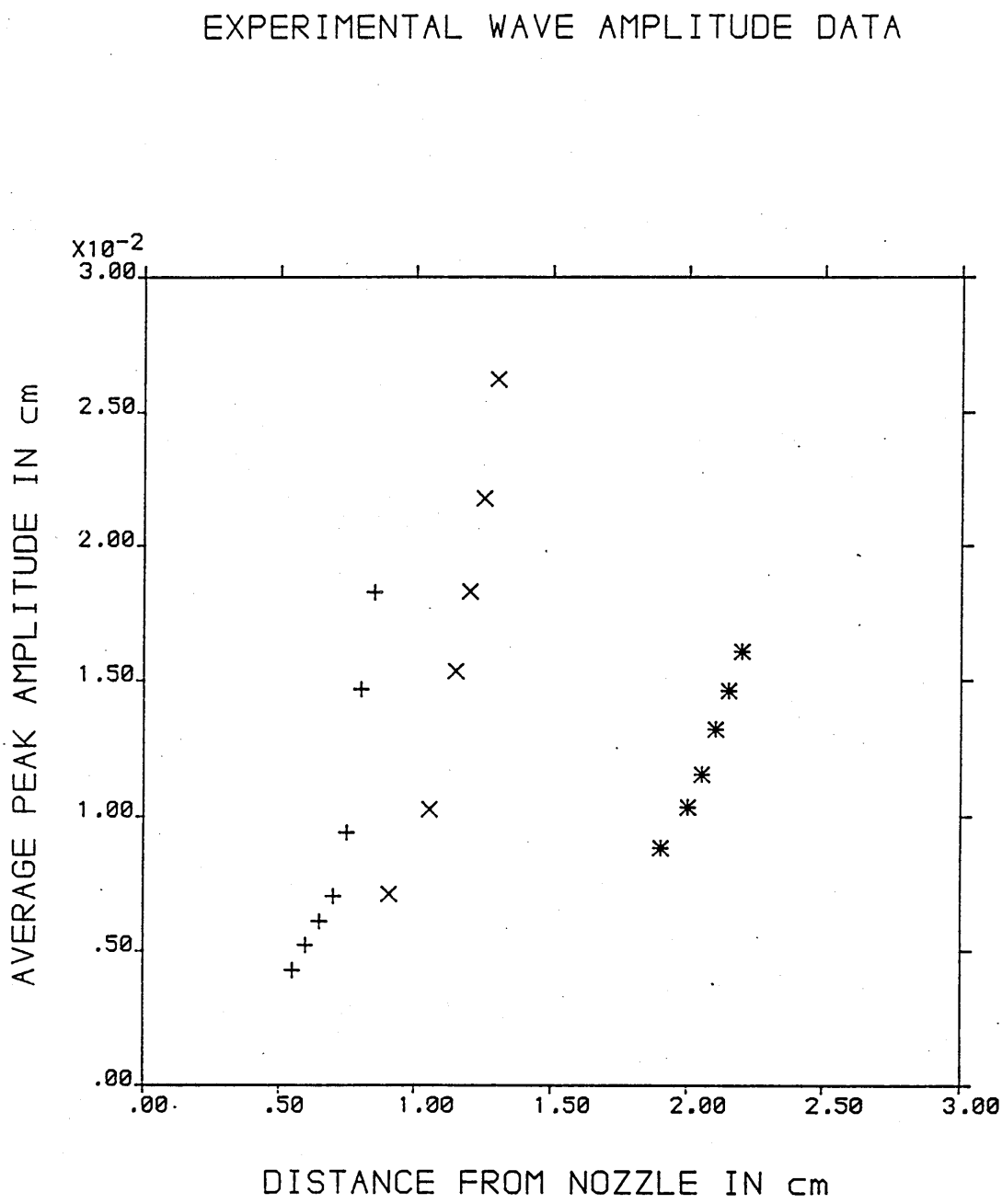

FIGURE 15 VARIATION OF THE AVERAGE PEAK AMPLITUDE WITH NOZZLE DISTANCE
SYSTEM - PARAFFIN INTO WATER

\+ - AT WEBER NUMBER 6
× - AT WEBER NUMBER 10
* - AT WEBER NUMBER 20

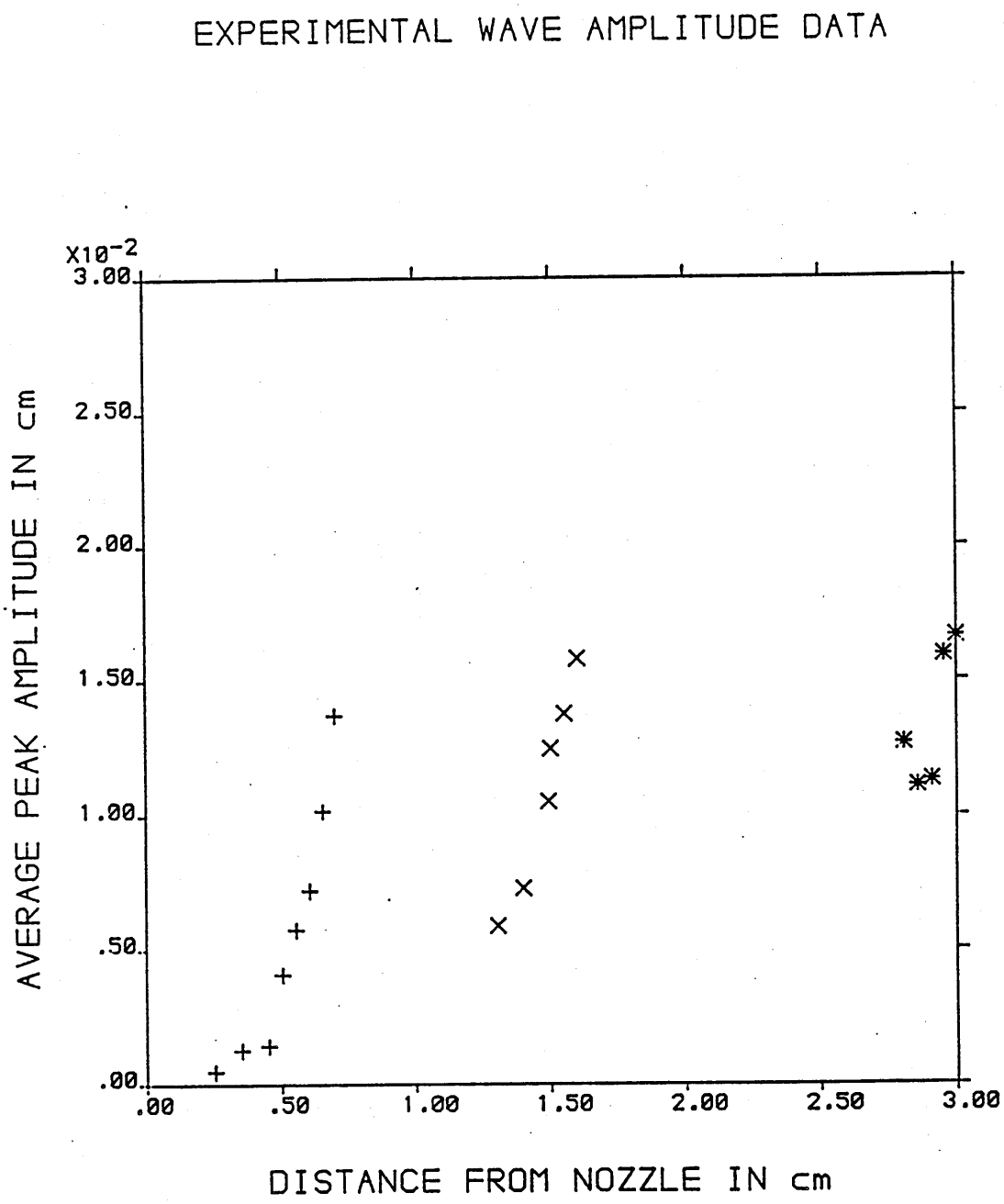

FIGURE 16 VARIATION OF THE AVERAGE PEAK AMPLITUDE WITH NOZZLE DISTANCE
SYSTEM - WATER INTO DECANE

\+ - AT WEBER NUMBER 6
× - AT WEBER NUMBER 10
* - AT WEBER NUMBER 20

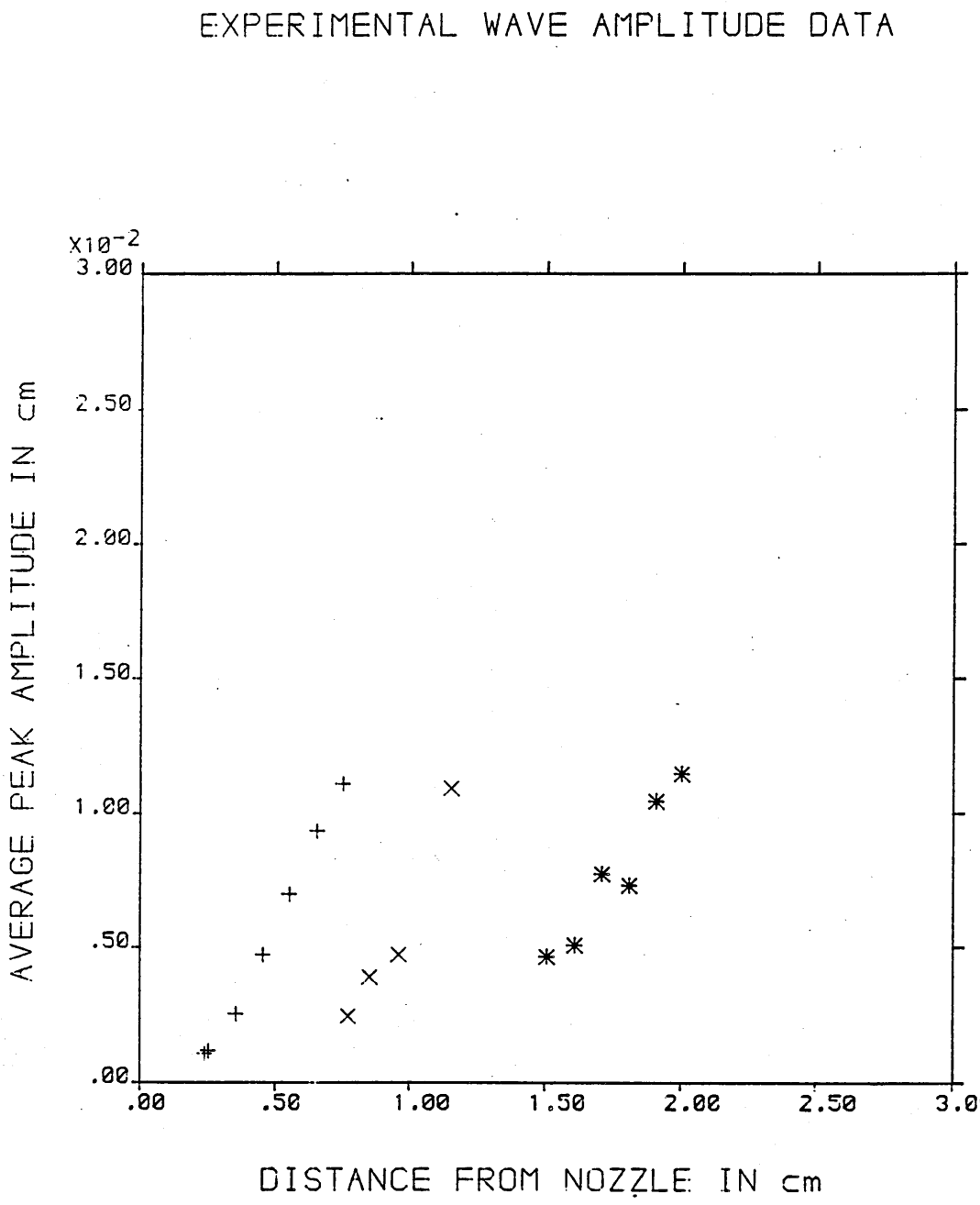

FIGURE 17 VARIATION OF THE AVERAGE PEAK AMPLITUDE WITH NOZZLE DISTANCE
SYSTEM - WATER INTO DECANOL

\+ - AT WEBER NUMBER 6
× - AT WEBER NUMBER 10
* - AT WEBER NUMBER 20

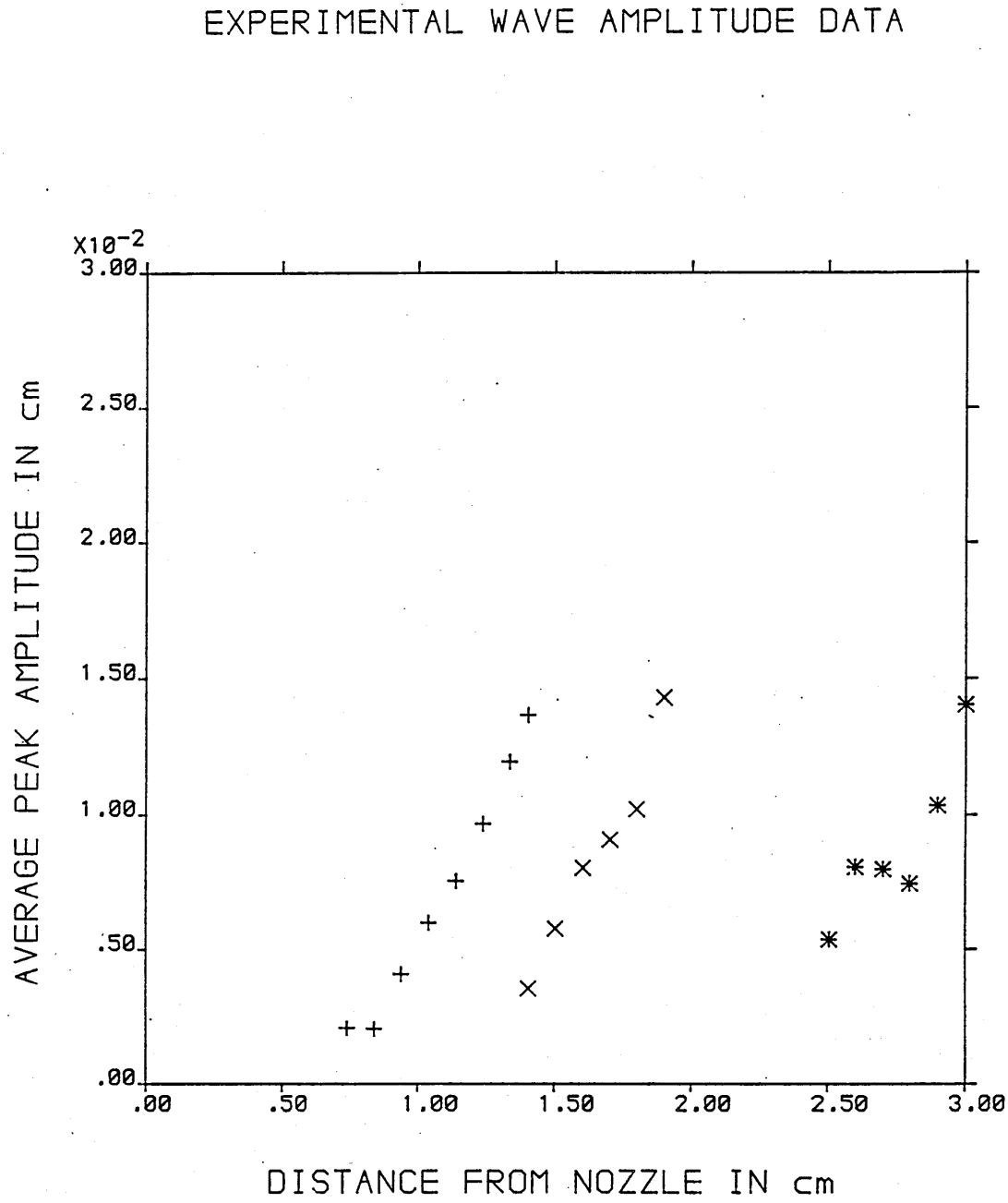

FIGURES 18 VARIATION OF THE AVERAGE PEAK AMPLITUDE WITH NOZZLE DISTANCE
SYSTEM - WATER INTO PARAFFIN

\+ - AT WEBER NUMBER 6

× - AT WEBER NUMBER 10

* - AT WEBER NUMBER 20

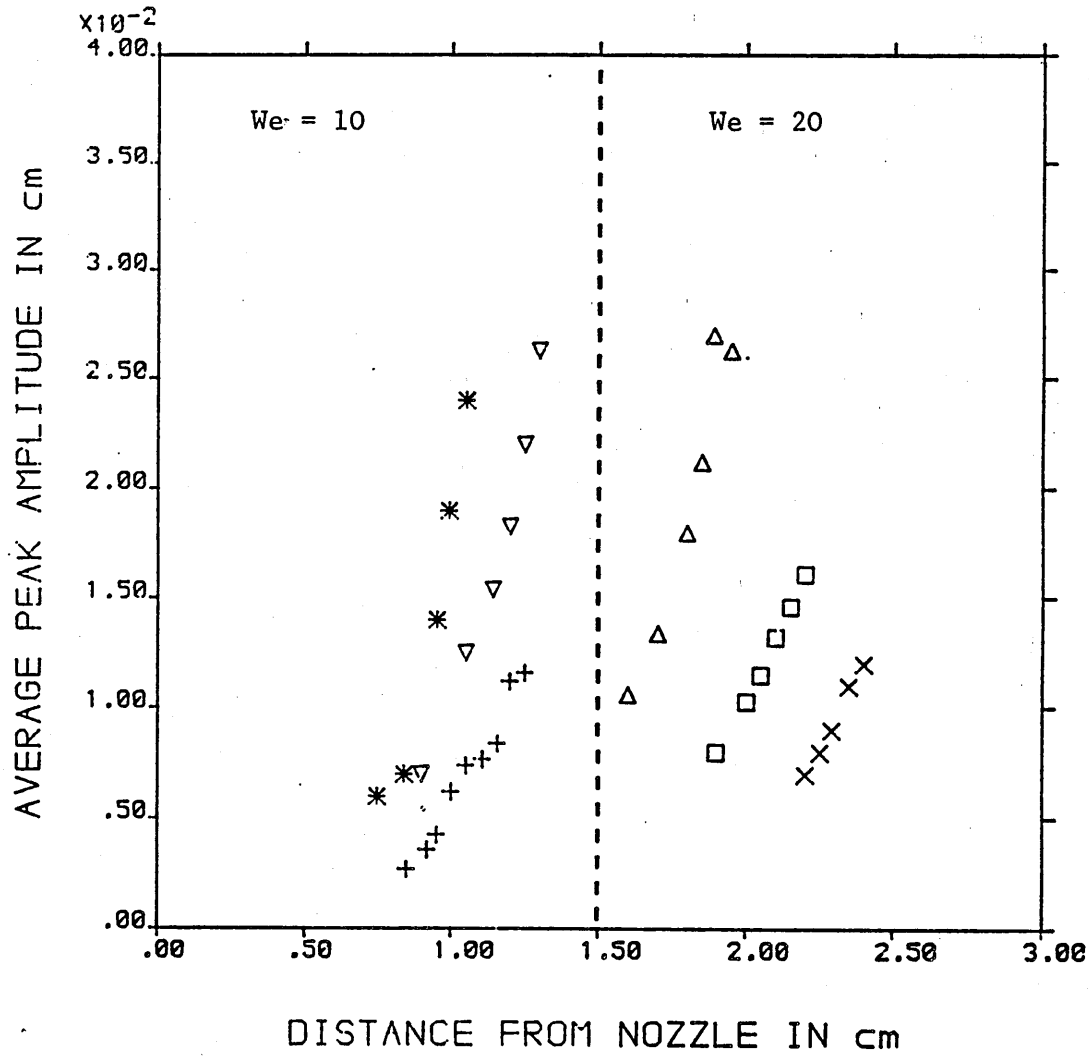

FIGURE 19 VARIATION OF THE AVERAGE PEAK AMPLITUDE WITH WEBER NUMBER AND THE PHYSICAL PROPERTIES OF THE SYSTEM

+ - DECANE INTO WATER AT WEBER NUMBER 10
× - DECANE INTO WATER AT WEBER NUMBER 20
✱ - DECANOL INTO WATER AT WEBER NUMBER 10
△ - DECANOL INTO WATER AT WEBER NUMBER 20
▽ - PARAFFIN INTO WATER AT WEBER NUMBER 10
□ - PARAFFIN INTO WATER AT WEBER NUMBER 20

The variation of the jet length with Weber number is presented in Figures (20,21 and 22). It can be seen that the viscosity, density and surface tension play an important role in controlling the jet length. Figure 20 shows that an increase in the dispersed phase viscosity reduces the jet length. Figure 21 indicates the same effect of continuous phase viscosity on the jet length. These results suggest that the viscosity of both the phases affect the growth rate of the wave on the surface of the jet. The effect of the interfacial tension can be seen in Figure 22 which shows that in viscous systems jet length increases with decrease in the interfacial tension.

In instability theory the dimensionless wave number is always given by 'ka' where a is the jet radius. Thus knowledge of the jet radius, or diameter, at the point of breakup is crucial for comparing experimental data with the theory. The variation of the jet diameter for different systems with distance from the nozzle is given in Figure 23, where it can be seen that in viscous systems the jet shows an appreciable increase in the jet diameter. A large error would be involved if the nozzle diameter were used in these systems to calculate the wave numbers. The jet diameter is an important parameter in order to calculate wave properties like wave lengths, wave velocity and wave frequency.

The experimentally measured wave velocity of the fundamental wave is plotted against the jet velocity in

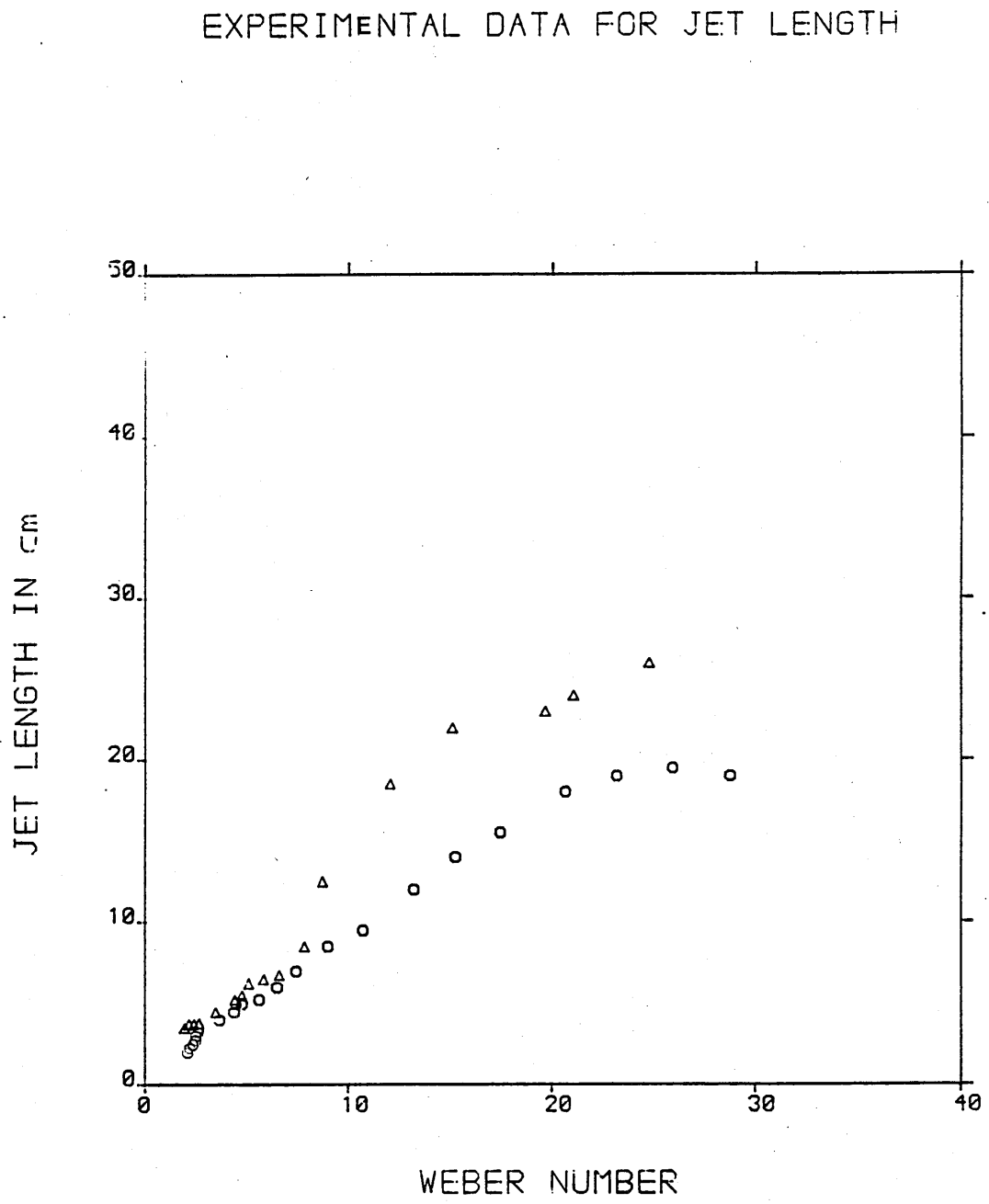

FIGURE 20 VARIATION OF THE JET LENGTH WITH WEBER NUMBER
NOZZLE DIAMETER = 0.0602 cm

△ - DECANE INTO WATER

o - PARAFFIN INTO WATER

EXPERIMENTAL DATA FOR JET LENGTH

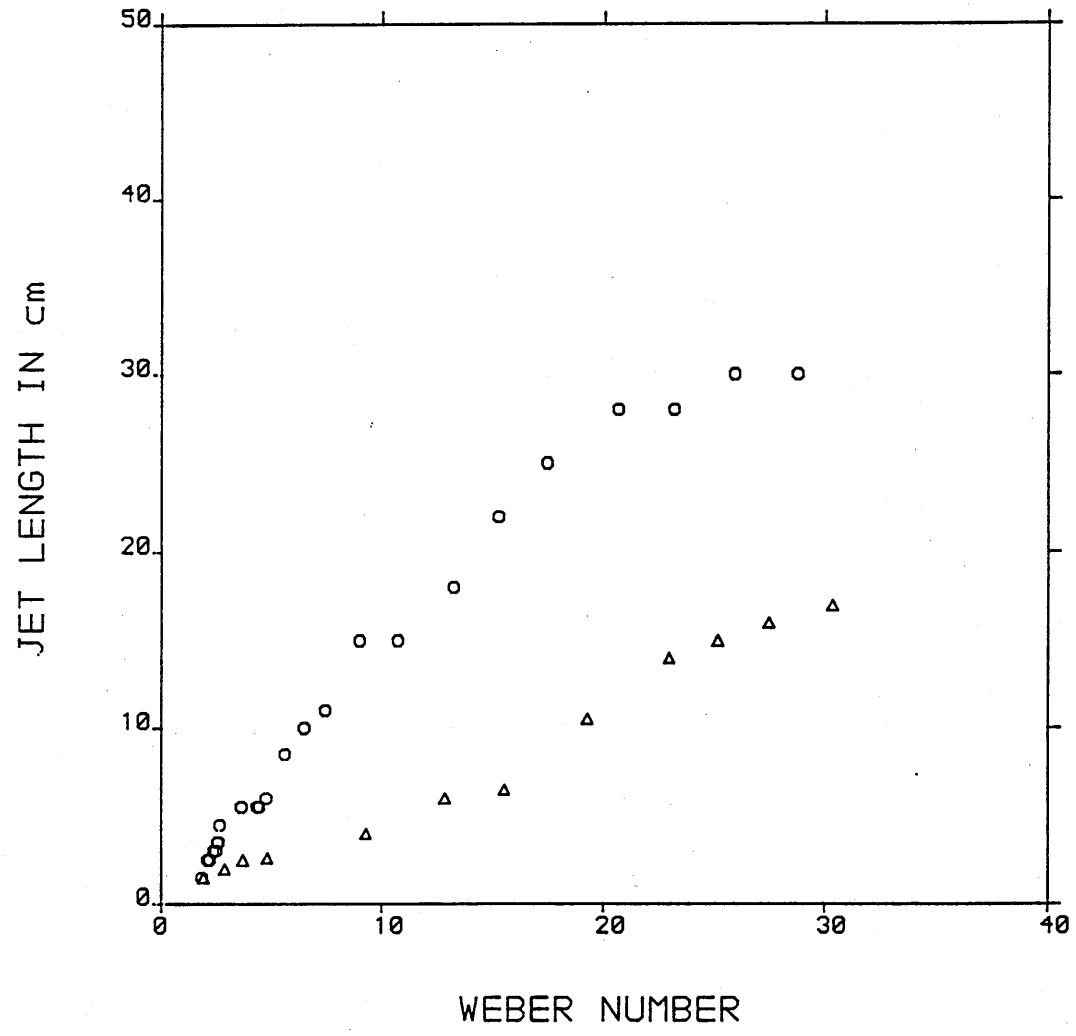

FIGURE 21 VARIATION OF THE JET LENGTH WITH WEBER NUMBER
NOZZLE DIAMETER = 0.0602 cm

△ - WATER INTO PARAFFIN

o - WATER INTO DECANE

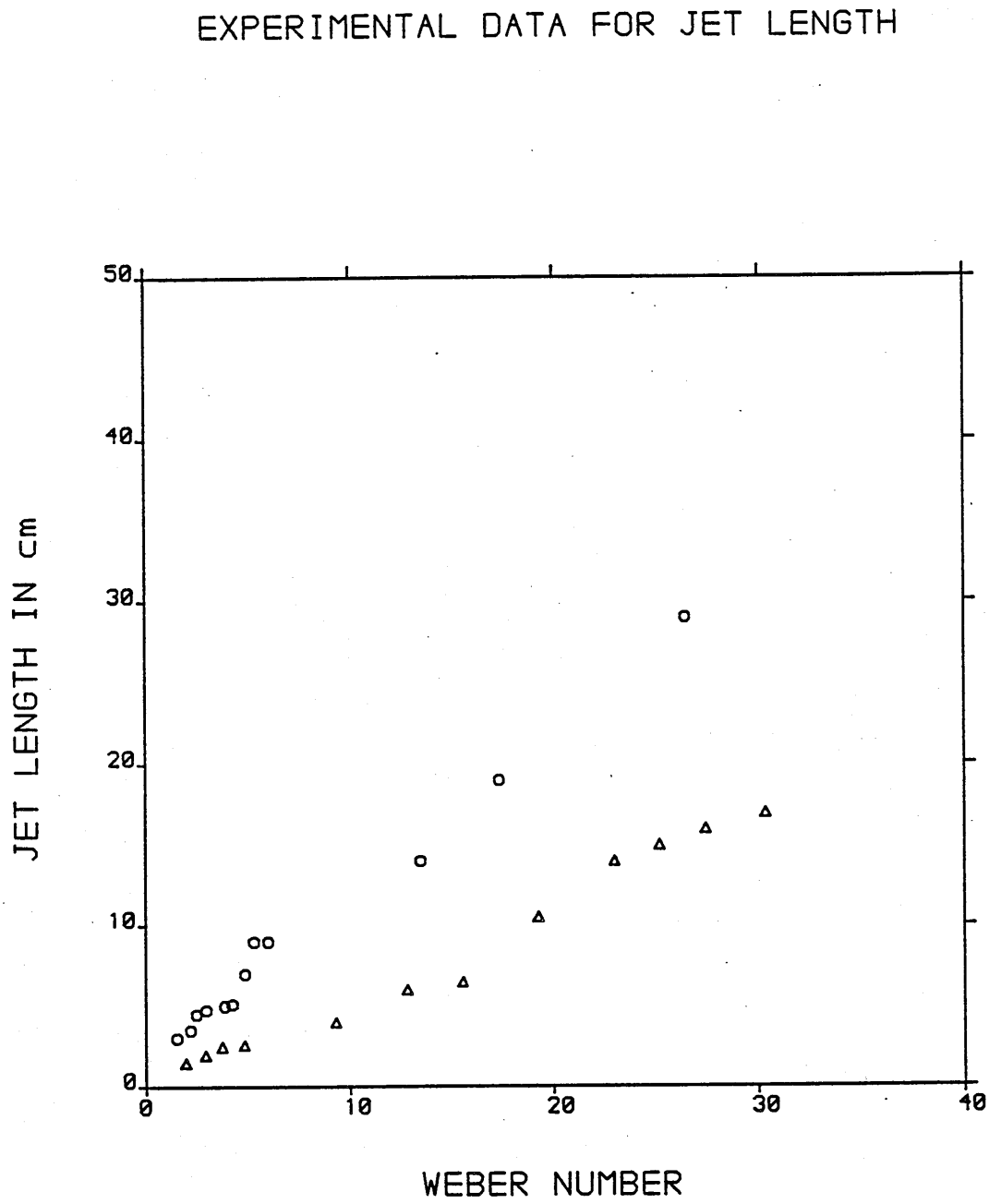

FIGURE 22 VARIATION OF THE JET LENGTH WITH WEBER NUMBER
NOZZLE DIAMETER = 0.0602 cm

△ - WATER INTO PARAFFIN

o - WATER INTO DECANOL

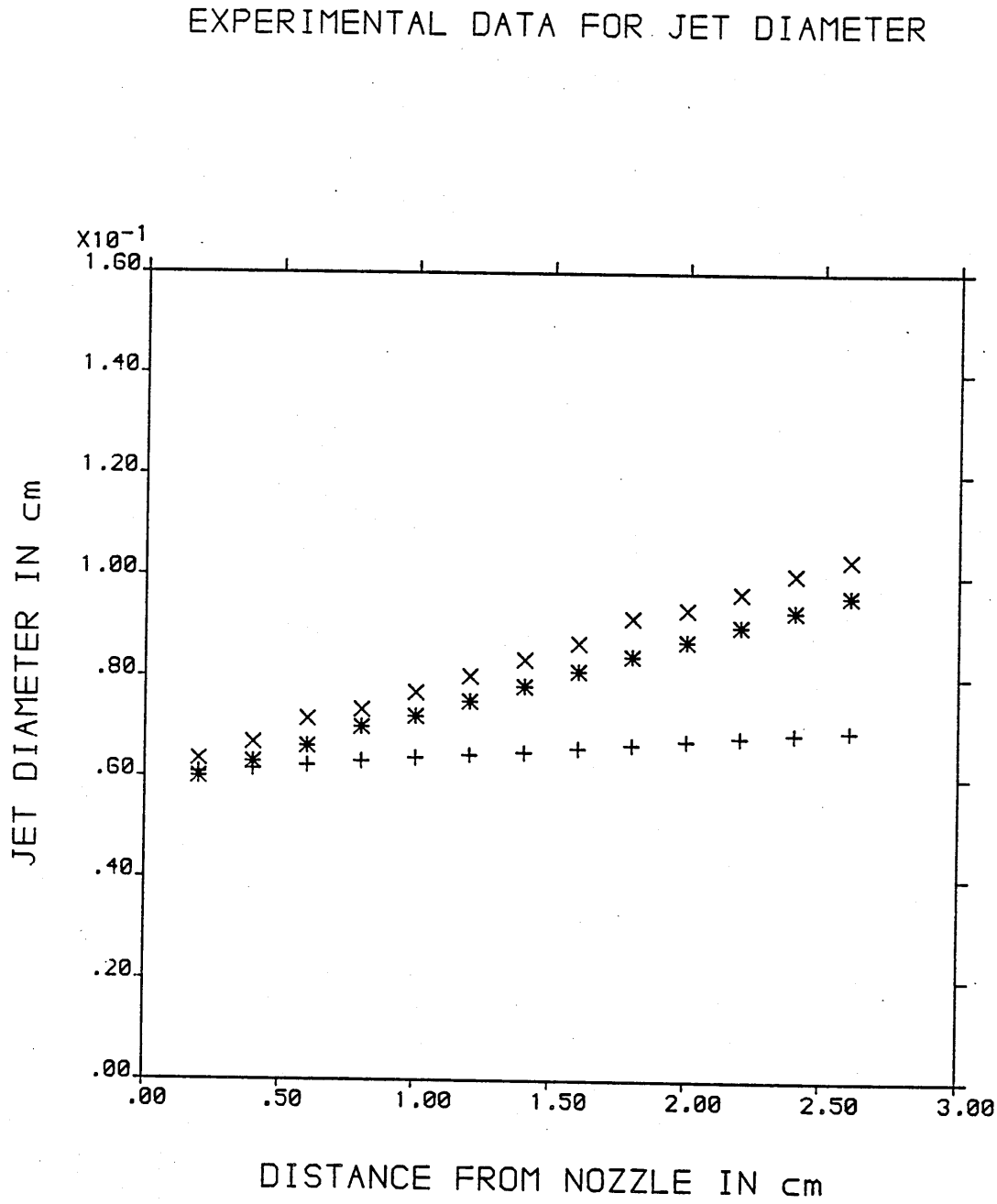

FIGURE 23 VARIATION OF THE JET DIAMETER WITH NOZZLE DISTANCE
NOZZLE DIAMETER = 0.0602 cm

\+ - DECANE INTO WATER
× - DECANOL INTO WATER
* - PARAFFIN INTO WATER

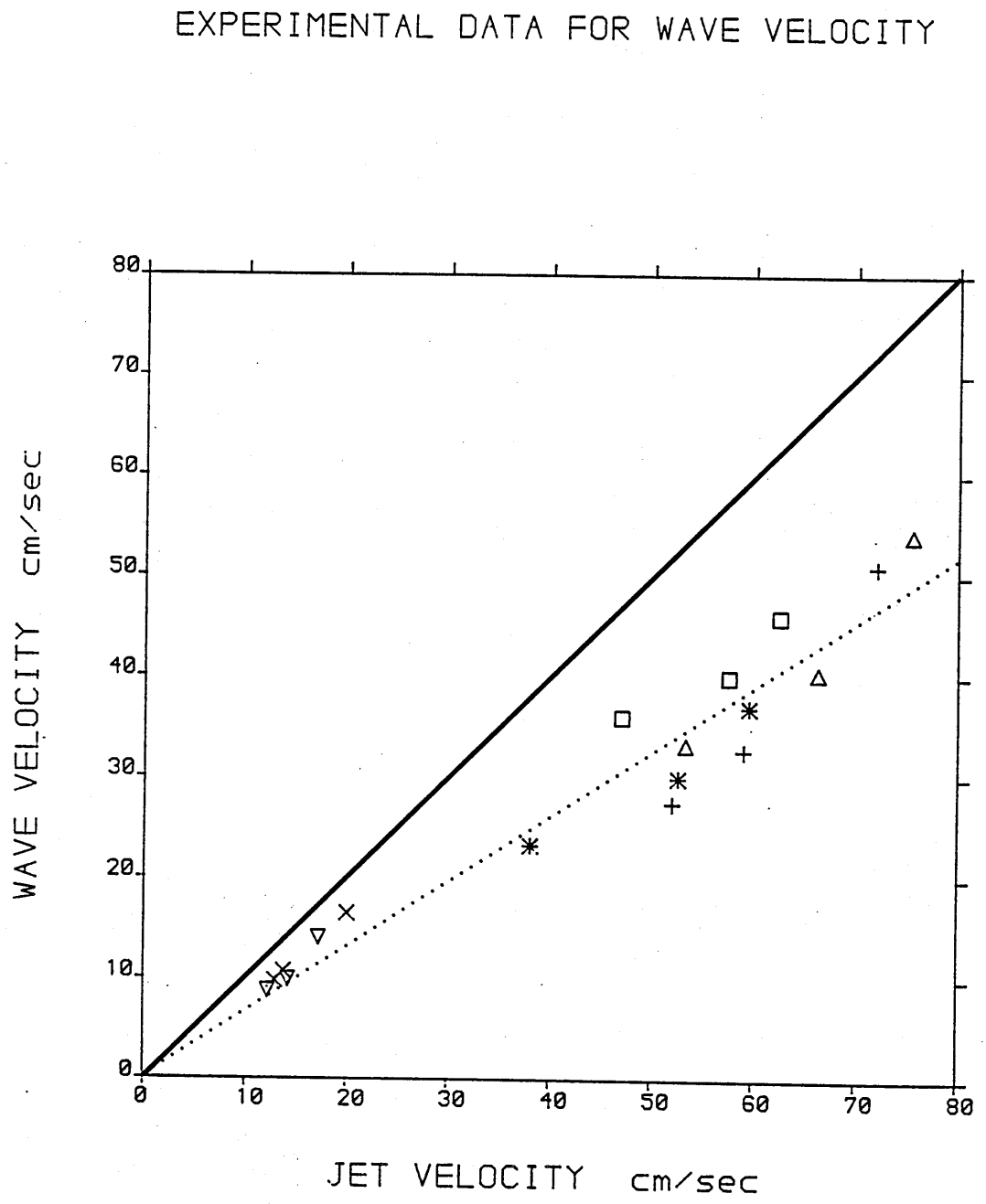

FIGURE 24 VARIATION OF THE WAVE VELOCITY WITH THE JET VELOCITY

+ - DECANE INTO WATER
× - DECANOL INTO WATER
✳ - PARAFFIN INTO WATER
△ - WATER INTO DECANE
▽ - WATER INTO DECANOL
□ - WATER INTO PARAFFIN

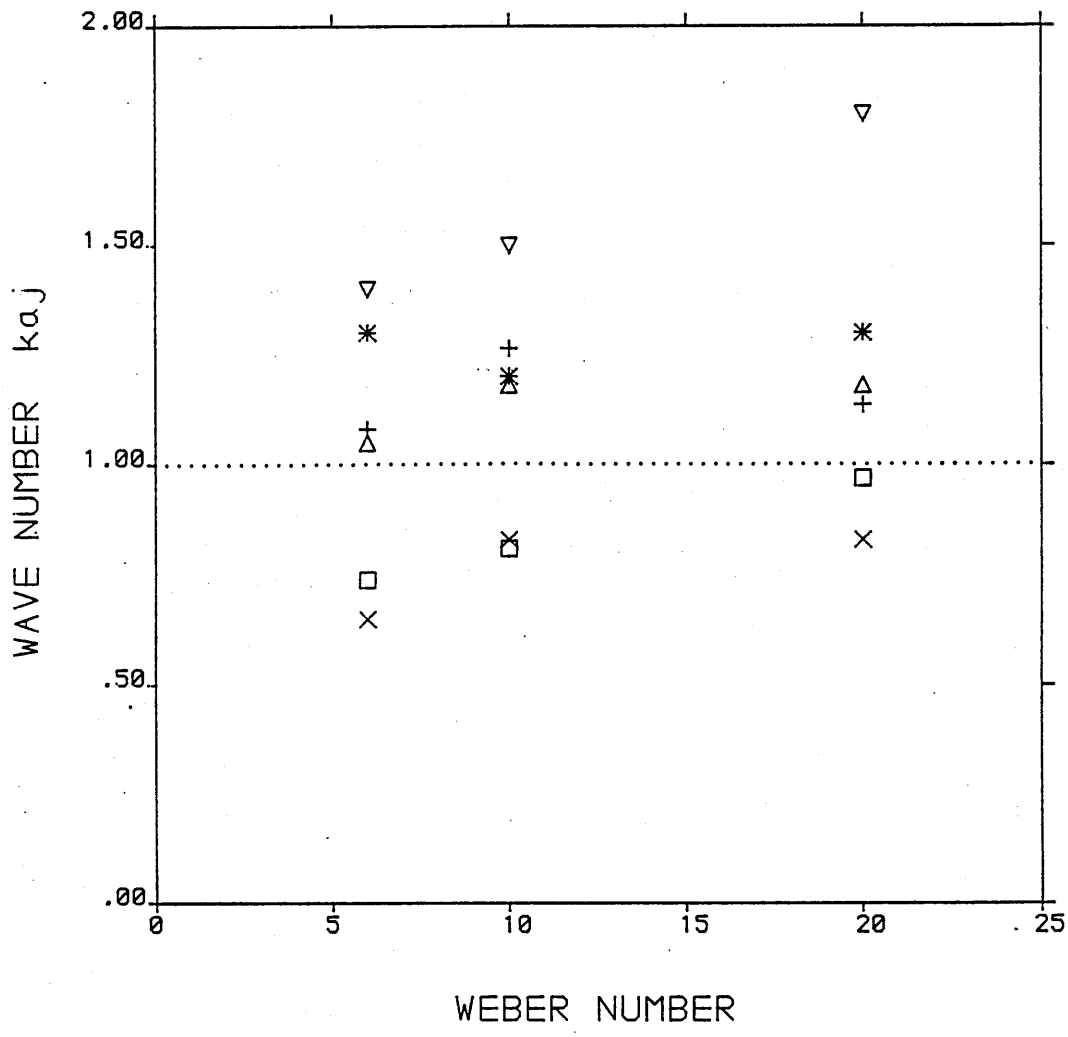

FIGURE 25 VARIATION OF THE WAVENUMBER WITH VELOCITY

+ - DECANE INTO WATER
× - DECANOL INTO WATER
✳ - PARAFFIN INTO WATER
△ - WATER INTO DECANE
▽ - WATER INTO DECANOL
□ - WATER INTO PARAFFIN

Figure 24. In most instability theories it has been assumed that the wave travels at the jet velocity. In all cases the wave velocity is smaller than the jet velocity.

Figure 25 shows the experimentally measured values of the wave number of the fundamental wave for six systems. It should be noted that the wave numbers span the region $0.60 < ka < 1.0$. In other words, in some cases wave numbers are outside the range of predictions from stationary instability theories ($ka > 1.0$)

The experimental observations and the data will be discussed in detail in chapter 6 where the effect of the wave velocity, wave length, jet length and jet diameter on the instability of the jet will be discussed thoroughly.

4.2.2.2 DROP SIZE IN THE JETTING REGIME

The formation of the drop families in the intermediate regime not only reveals that the mean drop size varies with the flow rate, but also suggests that there is a definite type of wave interaction on the surface of the jet. As we have discussed in the section 4.2.2.1 these interactions become more and more pronounced as the fundamental wave approaches the breakup point which can be seen in the wave profiles given in Figure 12. Measurements of the formation time of the group of drops, Tg, as well as the fundamental period, Tf, of the fundamental wave are given in Table (3). It can be seen that Tg is always an integer multiple of the fundamental period, Tf.

TABLE 3

EXPERIMENTALLY MEASURED GROUP PERIOD Tg AND FUNDAMENTAL PERIOD Tf FOR VARIOUS DROP FAMILIES FOUND IN WATER INTO DECANE SYSTEM

S.NO	WE	Tg ms	Tf ms	Tg/Tf	FAMILY
1.	1.86	203.0	18.5	11.0	10N/1N
2.	1.87	201.0	18.4	11.0	9N/2N
3.	2.73	55.3	13.6	4.0	4N monosize
4.	3.04	87.2	12.4	6.9	4N/3N
5.	3.25	105.0	11.8	9.0	4N/4N/1N
6.	3.57	186.2	10.9	17.7	3N/3N/1N/3N/3N/3N/1N
7.	4.19	19.0	9.6	2.0	2N monosize
8.	4.55	83.5	9.4	9.0	2N/2N/2N/2N/1N
9.	4.93	56.2	8.4	6.9	2N/2N/2N/1N
10.	5.78	35.4	7.4	4.9	2N/2N/1N

In the present work the relaxation process of the jet was considered at the point of breakup. It was observed from high speed cine films that soon after the detachment of the drop from the end of the jet, the jet relaxes and seems to generate a relaxing wave which travels backward on the surface of the jet. Simultaneously, the fundamental wave of the fastest growing disturbance travels forward with the wave velocity. The relaxation process of the jet can be seen very clearly in the slow motion video recordings.

The period of the relaxation wave, Tr, was measured from video recording and is presented in Table (4). Figure 26 shows that the fundamental period of the wave decreases with increasing Weber number, while the relaxation period stays constant. In other words, the relaxation period is independent of the flow rate or the jet velocity.

The experimental data gathered in this study have been used to support a number of theoretical approaches to predict drop size in liquid-liquid systems. These theories are outlined in the next chapter.

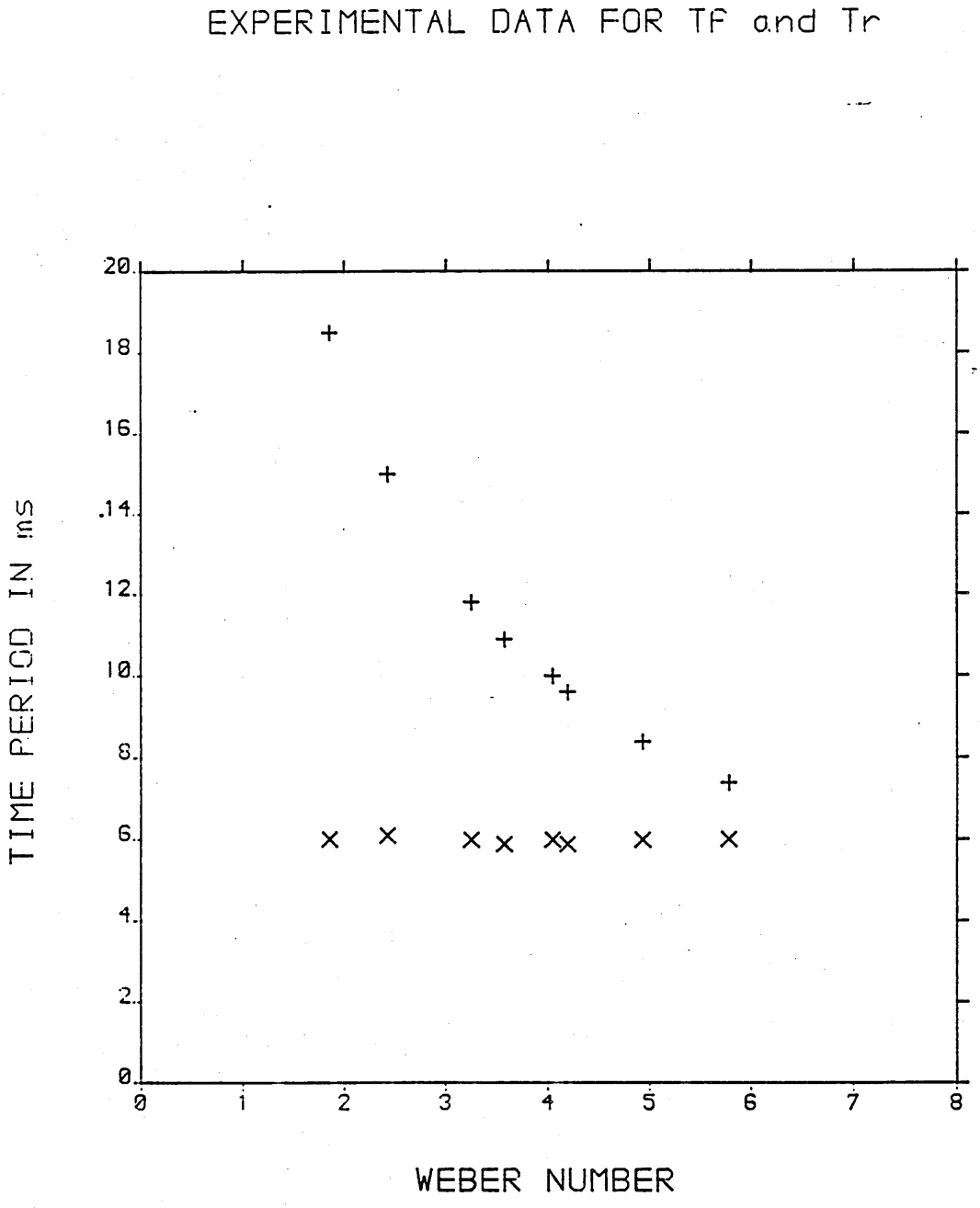

FIGURE 26 VARIATION OF FUNDAMENTAL AND RELAXATION TIME WITH WEBER NUMBER
SYSTEM - DECANE INTO WATER

+ - FUNDAMENTAL PERIOD

× - RELAXATION PERIOD

TABLE 4

EXPERIMENTALLY MEASURED FUNDAMENTAL AND RELAXATION TIME AT VARIOUS WEBER NUMBERS

S.NO	WE	FUNDAMENTAL TIME IN ms	RELAXATION TIME IN ms
1.	1.86	18.5	6.02
2.	2.42	15.0	6.1
3.	3.25	11.8	6.00
4.	3.57	10.9	5.90
5.	4.04	10.0	6.0
6.	4.19	9.6	5.90
7.	4.93	8.4	6.0
8.	5.78	7.4	6.01

CHAPTER 5

THEORETICAL DEVELOPMENTS

5.1 DROP FORMATION AT LOW VELOCITIES

The drop formation regime at low velocities is characterized by individually formed drops of uniform size growing at the nozzle tip. The regular pattern was shown in Plate (2).

There are four major forces which act on the drop during the process of its formation in liquid-liquid systems. The buoyancy force, F_b, due to the difference of the density between the two phases, and the momentum force, F_m, due to the momentum flow of liquid into the drop will tend to remove the drop from the nozzle. The interfacial tension force, F_s, will tend to retain the drop at the nozzle and the drag force, F_d, due to the continuous phase viscosity will act to reduce the motion of the drop during take-off from the nozzle. When the net force due to buoyancy and momentum, exceeds the net restraining force, due to surface tension and drag, the drop will accelerate away from the nozzle on a liquid cylindrical neck and finally detach when the neck becomes unstable.

The complete quantitative picture of the drop formation in the prejetting condition can be described under two distinct stages of its formation process, as was observed in chapter 4. In the present work a model has

been developed to explain a two stage drop formation process at the nozzle tip. The first stage of drop growth is based on a force balance while the second stage considers the instability of the neck behind the drop. The general equation for force balance can be written as;

$$\frac{d(\acute{\rho}VU)}{dt} = \Delta\rho gV + \frac{\rho Q^2}{A} - D_n\pi\sigma\cos\theta - 6\pi\mu D_n U \qquad [5.0]$$

where $\acute{\rho} = \rho + \frac{\hat{\rho}}{2}$ to account for added mass.

STAGE 1 DROP GROWTH AT THE NOZZLE

At this stage it is assumed that at all the time the forces are in balance with surface tension, adjusting with θ, increasing to exactly balance that is U = 0. The take off condition occurs when θ reaches a maximum value of $\pi/2$. At this stage, neglecting the drag force, we can express a force balance as;

Buoyancy force + Momentum force = surface tension force

$$\text{or} \quad V_1\Delta\rho g + \frac{\rho Q^2}{A} - D_n\pi\sigma = 0 \qquad [5.1]$$

where V_1 is the volume of the drop at the nozzle where surface tension force balances the buoyancy and momentum forces. This volume V_1 is equal to $[Qt_1 + V_0]$ where V_0 is the residual volume and t_1 is the time taken to increase the volume from V_0 to V_1.

Q - Volumetric flow rate.

A - Cross sectional area of the nozzle.

ρ - Density of the dispersed phase.

$\hat{\rho}$ - Density of the continuous phase.

$\Delta\rho$ - Density difference between the two phases.

upon re-arrangement, equation [5.1] can be written as;

$$V_1 = \frac{\pi D_n \sigma - \left[\frac{\rho Q^2}{A}\right]}{\Delta\rho g} \qquad [5.2]$$

Equation [5.2] can be written in a dimensionless form by using a fictitious static drop volume, V_s, which can be expressed as;

$$V_s = \left[\frac{\pi D_n \sigma}{\Delta\rho g}\right] \qquad [5.3]$$

or

$$\frac{V_s}{Q} = \left[\frac{\pi D_n \sigma}{\Delta\rho g}\right]\left[\frac{4}{U\pi D_n^2}\right] = \frac{4\sigma}{\Delta\rho g U D_n} \qquad [5.4]$$

Therefore, we can write equation [5.2] as;

$$\frac{V_1}{V_s} = \left[1 - \frac{\rho Q^2}{\pi A D_n \sigma}\right] \qquad [5.5]$$

or

$$\frac{V_1}{V_s} = \left[1 - \frac{We}{4}\right] \qquad [5.6]$$

The form of equation [5.6] is based on the assumption that the velocity profile is flat with momentum force $F_m = \rho D_n^2 U^2/4$. For a parabolic velocity profile momentum force can be expressed as $F_m = \rho D_n^2 U^2/3$, and then we can write equation [5.6] as;

$$\frac{V_1}{V_s} = [1 - \frac{We}{3}] \qquad [5.7]$$

Equations [5.6] and [5.7] suggest that the drop growth at the nozzle will not occur when the Weber number reaches 3 or 4, which might be used as a criterion for the jetting velocity. In addition we can calculate the time taken during the first stage of the drop growth, as we know;

$V_1 = Qt_1 + V_O$ (where V_O is the residual volume)

or

$$t_1 = [\frac{V_1 - V_O}{Q}] \qquad [5.8]$$

Equation [5.8] can be written in a dimensionless form as;

$$t_1 = \frac{V_s}{Q} [\frac{V_1}{V_s} - \frac{V_O}{V_s}]$$

Using equation [5.6] we can write

$$t_1 = \frac{V_s}{Q} [1 - \frac{We}{4} - \frac{V_O}{V_s}]$$

$$= \frac{V_s B}{Q} \qquad [5.9]$$

where $B = [1 - \frac{We}{4} - \frac{V_O}{V_s}]$

Since $V_s = \frac{\pi D_n \sigma}{\Delta \rho g}$ and $Q = \frac{\pi U D_n^2}{4}$, therefore

$$t_1 = B \left[\frac{4\sigma}{\Delta \rho g U D_n}\right] \qquad [5.10]$$

During this stage it is assumed that the centre and the top of the drop move acccording to an expansion process, that is

$$U_c = \frac{dL}{dt} = \frac{Q}{4\pi L^2} \text{ and } U_t = \frac{2dL}{dt} = \frac{2Q}{4\pi L^2}$$

where U_c and U_t are the drop centre and drop top edge velocities respectively and L is the position of the drop centre, thus

$$L = R = \left[\frac{6V}{\pi}\right]^{0.33} \text{ where } V = Qt + V_o$$

STAGE 2 TAKE OFF AND DETACHMENT

After the surface tension force has reached its maximum value the increased buoyancy will lead to the drop moving away from the nozzle on a jet of liquid. A force balance on the drop predicts an acceleration throughout this stage with the buoyancy increasing against a constant (maximum) surface tension force. Therefore, we can write, ignoring the drag term;

$$\frac{d\ (\dot{\rho}VU)}{dt} = \Delta\rho gV + \frac{\rho Q^2}{A} - \pi D_n \sigma \qquad [5.11]$$

At $t = 0$, $V = V_1$, $U = U_1$. The volume in this stage can be represented by $V = V_1 + Qt$ where V_1 is the volume of the drop at the end of the first stage.

$$\dot{\rho}VU = \int_0^{t_2} Qt\Delta\rho dt = Q\Delta\rho g \frac{t^2}{2} \qquad [5.12]$$

$$U = \frac{\Delta\rho g}{2\dot{\rho}} \left[\frac{t^2}{t+t_1^*}\right] + U_1 \qquad [5.13]$$

where $t_1^* = V_1/Q$.

Assuming $U = dL/dt$ and $U_1 = 0$ we can solve equation [5.13] in terms of L as

$$L - L_1 = \frac{\Delta\rho g}{2\dot{\rho}} \int_0^{t_2} \left[\frac{t^2 dt}{t+t_1}\right]$$

$$= \frac{\Delta\rho g}{2\dot{\rho}} \left[\left(\frac{t^2 - 2t_1 t}{2}\right) + t_1^2 \ln\left(\frac{t + t_1}{t_1}\right)\right]_0^{t_2} \qquad [5.14]$$

where L_1 is the centre position of the drop at the end of the first stage.

Let $\tau = \frac{t_2}{t_1}$ and $L - L_1 = \hat{L}$

We can write equation [5.14] as;

$$\frac{\tau^2}{2} - 2\tau + 1n(1 + \tau) = \frac{2\hat{L}\rho'}{t^2\Delta\rho g} \qquad [5.15]$$

Using equations [5.9] and [5.4] we can write equation [5.15] as

$$\frac{\tau^2}{2} - 2\tau + 1n(1 + \tau) = \frac{1}{8}\frac{\hat{L}}{D_n}\left[\frac{\rho'}{\rho}\right]\frac{WeEo}{B^2} \qquad [5.16]$$

Equation [5.16] was solved using graphical solution for the left hand side of the equation. This is shown in Figure 27, and then equation [5.16] can be expressed as power series

$$\tau = 1.86\left[\frac{1}{8}\frac{\hat{L}}{D_n}\left[\frac{\rho'}{\rho}\right]\frac{WeEo}{B^2}\right]^{0.375} \qquad [5.17]$$

Now we can calculate the total volume of the drop at the end of the second stage to be

$$V_t = Q(t_1 + t_2)$$

GRAPHICAL SOLUTION FOR EQUATION [5.16]

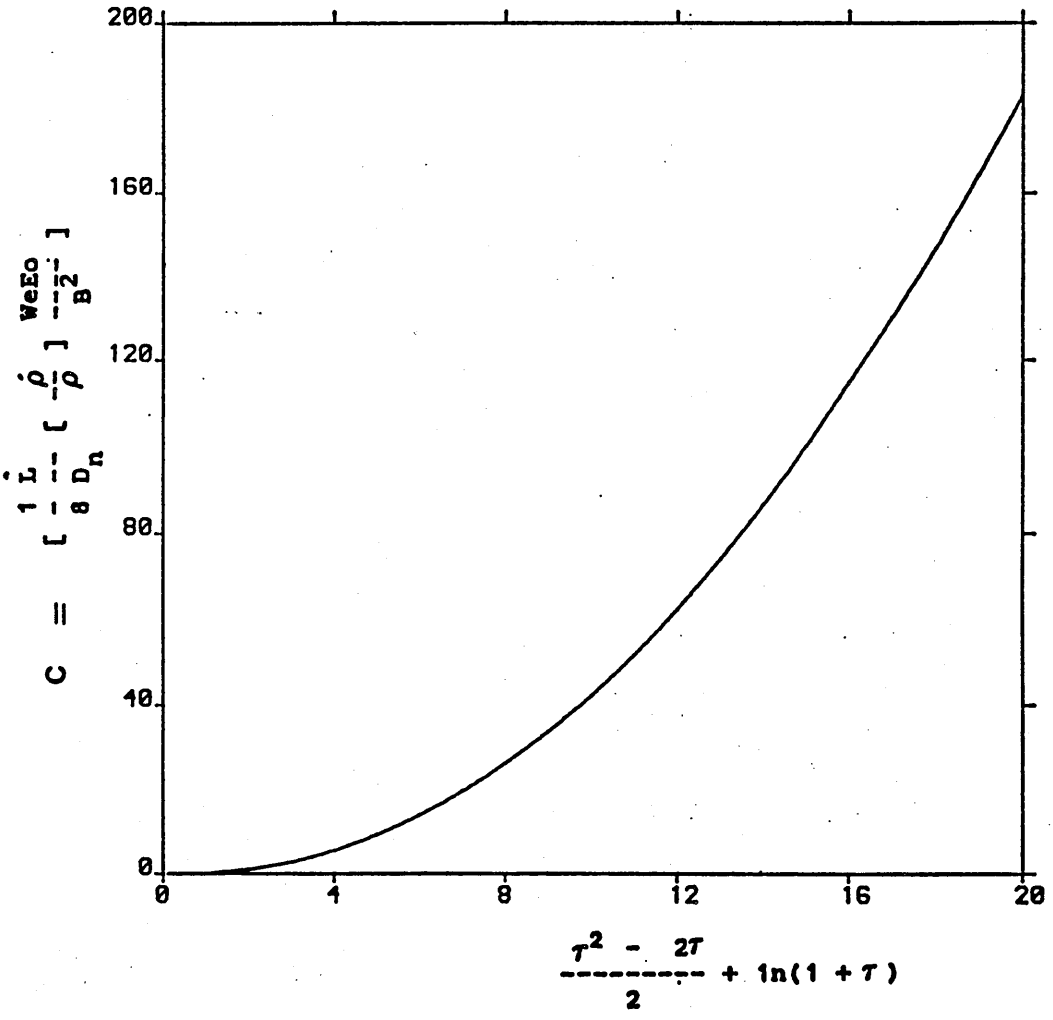

FIGURE 27 GRAPHICAL SOLUTION OF MODEL EQUATION [5.16]

$$V_t = Qt_1\left(1 + \frac{t_2}{t_1}\right) = Qt_1\left(1 + \frac{\tau}{\left[1 + \frac{V_O}{V_s}\right]}\right)$$

$$= Qt_1\left(1 + \frac{\tau\left[1 + \frac{We}{4}\right]}{B}\right)$$

$$\frac{V_t}{V_s} = \frac{Qt_1}{V_s}(1 + \tau)$$

$$= B\left[1 + \left[\frac{\tau\left[1 + \frac{We}{4}\right]}{B}\right]\left[\Delta\rho g\left(\frac{D_n^3}{\pi D_n \sigma}\right)\right]\right]$$

$$\frac{V_t}{V_s} = \left[\frac{D_d^3}{6D_n^3}\right]\left[\frac{\Delta\rho g D_n^2}{\sigma}\right] = \frac{D_d^3}{D_n^3}\left(\frac{E_O}{6}\right)$$

In terms of drop diameter this equation can be written as

$$\frac{D_d}{D_n} = \left[\frac{6B}{Eo}(1 + \tau)\right]^{0.33} \qquad [5.18]$$

In order to use equations [5.17] and [5.18] to predict the drop diameter, D_d, some estimate of L and V_O must be made.

JET STABILITY CRITERION

To calculate the point of detachment of the drop at the end of the second stage, it will be assumed that the jet behind the drop becomes unstable to surface tension forces. This will occur when the surface area of the jet increases to a point where it exceeds the surface area of a sphere of equal volume. In the present model it has been assumed that the neck behind the drop acquires the geometry of a cone as was observed experimentally.

Considering Figure 28 the volume and the surface area of the cone and the sphere of the same volume can be written as

for a cone

$$V = \frac{\pi}{3} L (r^2 + r_0^2 + r_0 r) \qquad [5.19]$$

$$A = \pi L(r + r_0) \qquad [5.20]$$

For the equivalent sphere

$$V = \frac{4\pi R^2}{3} \qquad [5.21]$$

$$A = 4\pi R^2 \qquad [5.22]$$

Using equation [5.19] we can rearrange equation [5.21] as

$$R = \frac{L}{4} (r^2 + r_0^2 + r_0 r)^{1/3} \qquad [5.23]$$

Assuming that the cone has an equal surface area as that of the sphere of the same volume then we can write:

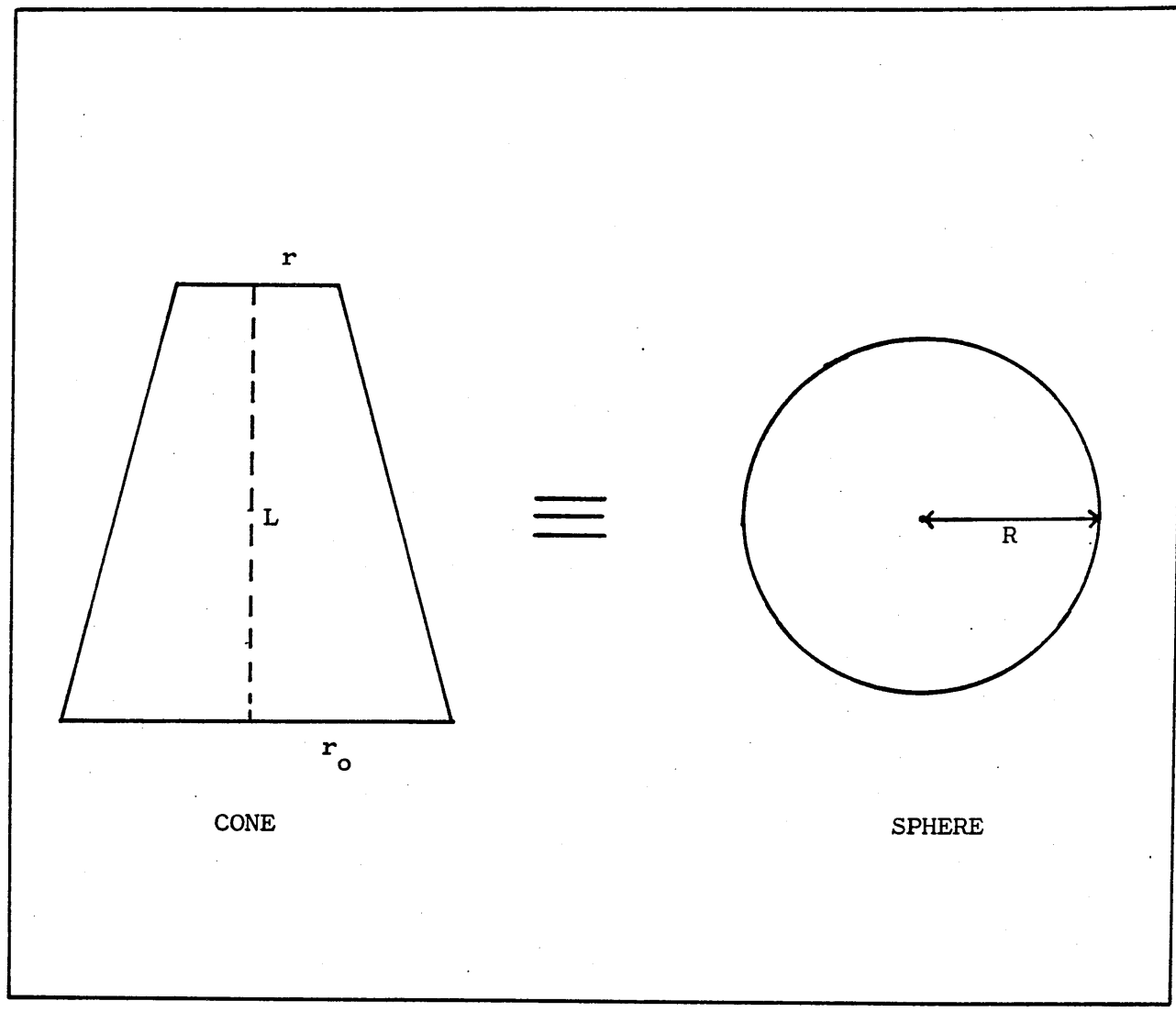

FIGURE 28 Stability criterion for predicting residual volume in prejetting condition

$$\pi L(r_o + r) = 4\pi R^2$$

using equation [5.23] we obtained

$$L(r_o + r) = 4\left[\frac{L\,(r^2 + r_o^2 + r_o^2)}{4}\right]^{2/3}$$

or

$$L = 4\left[\frac{(r^2 + r_o^2 + r_o r)^2}{(r_o + r)^3}\right] \qquad [5.24]$$

If we put $f = \frac{r}{r_o}$ then $r = r_o f$

Equation [5.24] can now be written as

$$L = 4r_o\left[\frac{(f^2 + 1 + f)^2}{(1 + f)^3}\right] \qquad [5.25]$$

Since $D_n = 2\,r_o$, therefore

$$\frac{L}{D_n} = 2\left[\frac{(1 + f + f^2)^2}{(1 + f)^3}\right] \qquad [5.26]$$

From equation [5.19]

$$V = \frac{\pi L r_o^2\,(1 + f + f^2)}{3} \qquad [5.27]$$

Using a static drop volume $V_s = \pi D_n \sigma / \Delta\rho g$ and rearranging equation [5.27] we get

$$\frac{V}{V_s} = \frac{4}{3}\,r_o^3\left[\frac{1 + f + f^2}{1 + f}\right]^3\left[\frac{\Delta\rho g}{\pi D_n \sigma}\right] \qquad [5.28]$$

$$= \frac{E_o}{6}\left[1 + \frac{f^2}{1+f}\right]^3 \qquad [5.29]$$

FORCE BALANCE ON THE JET

We can now write a force balance equation for the geometry of the jet as

buoyancy force+momentum force-surface tension force = 0

$$\Delta\rho gV + \frac{\rho Q^2}{\pi}\left[\frac{1}{r_o^2} - \frac{1}{r^2}\right] - 2\pi\sigma(r_o - r) = 0 \qquad [5.30]$$

or

$$\rho\pi r_o^4 U^2 \left[\frac{r_o^2 - r^2}{r_o^2 r^2}\right] = \Delta\rho gV - 2\pi\sigma(r_o - r) \qquad [5.31]$$

Rearranging equation [5.31]

$$(r_o - r)\left[\rho\pi r_o^2 U^2 \left[\frac{r_o + r}{r^2}\right] + 2\pi\sigma\right] = \Delta\rho gV \qquad [5.32]$$

Putting a value for V from equation [5.28]

$$(r^o - r)\left[\rho\pi r_o^2 U^2 \left[\frac{r_o + r}{r^2}\right] + 2\pi\sigma\right] =$$

$$\frac{4}{3} r_o^3 \left[1 + \frac{f^2}{1+f}\right]^3 \Delta\rho g \qquad [5.33]$$

since $We = \rho\pi D_n U^2/\sigma$ therefore

$$\rho U^2 r_o^2 (1 + f)\left[\frac{1 + f}{f^2} + \frac{4}{We}\right] = \frac{4}{3} r_o^3 \left[1 + \frac{f^2}{1+f}\right]^3 \Delta\rho g \qquad [5.34]$$

or

$$(1 + f)\left[\frac{1+f}{f^2} + \frac{4}{We}\right] = \frac{4}{3}\left[\frac{\Delta\rho g r_o}{\rho U^2}\right]\left[1 + \frac{f^2}{1+f}\right]^3 \qquad [5.35]$$

Replacing $2r_o = D_n$ and $Eo = \Delta\rho g D_n/\sigma$ in equation [5.35]

$$(1 + f)\left[\frac{1 + f}{f^2} + \frac{4}{We}\right] = \frac{2}{3}\frac{Eo}{We}\left[1 + \frac{f^2}{1+f}\right]^3 \qquad [5.36]$$

Now comparing equations [5.35] and [5.36] we can write

$$Eo = \frac{\frac{6\,(1-f)}{f^2}\left[1+\frac{(1+f)We}{4f}\right]}{\left[1+\frac{f}{1+f}\right]^3} \qquad [5.37]$$

Equation [5.37] suggests that Eo = f(f,We)

Using equation [5.29] we can write

$$\frac{V_o}{V_s} = (1+f)\left[1+\frac{(1+f)We}{4f^2}\right] \qquad [5.38]$$

Equation [5.38] suggests that $\frac{V_o}{V_s}$ = f(f,We)

Using equation [5.38] in equation [5.9] we can write

$$B=1-\frac{We}{4}-(1-f)-\frac{(1-f^2)We}{4f^2}=f-\frac{We}{4}\left[1+\frac{1+f^2}{f^2}\right]$$

$$B = f-\frac{We}{4f^2}=\frac{4f^3-We}{4f^2} \qquad [5.39]$$

Equation [5.39] suggests that B = f(f,We)

From equations [5.26] and [5.39] we can write

$$\frac{1}{8}\frac{L}{D_n B^2}=\frac{4F^2(1+f+f^2)^2}{(1+f)^3[4f^3-We]^2}=D=f(f,We)$$

From equation [5.26]

$$\frac{L}{D_n}=\frac{2\,(1+f+f^2)}{(1+f)^3} \text{ which suggests that } \frac{L}{D_n}=f(f)$$

Therefore, having thus calculated L/D_n it can be used in equation [5.17] to estimate τ, and this information can be used to predict the drop diameter using equation [5.18]

5.2 INSTABILITY ANALYSIS

The instability analysis considers the pressure and velocity fields as made up of a sum of large and small motions, which can be represented by;

$$P_T = P + P^0 \qquad [5.40]$$

$$u_T = u + u^0 \qquad [5.41]$$

where P and u are pressure and velocity terms associated with the large motion of the jet and surrounding continuous phase; P^0 and u^0 are fluctuations about P and u respectively.

Ignoring the terms involving the viscosity and product of the fluctuating quantities in the linear analysis an equation of small motion can be written as;

Equation of continuity

$$\nabla . u^0 = 0 \qquad [5.42]$$

Equation of motion

$$\frac{\partial u^0}{\partial t} = (u.\nabla)u^0 = -\frac{\nabla P^0}{\varrho} \qquad [5.43]$$

The linear equation [5.42] and [5.43] can be reduced to ordinary differential equations by a transformation involving terms of complex functions. Therefore, the solutions were obtained by assuming;

$$\begin{aligned} P^0 &= P^0(r)e^{\alpha t+i(kz+h\theta)} \\ u^0 &= u^0(r)e^{\alpha t+i(kz+h\theta)} \\ \eta &= \eta_0 e^{\alpha t+i(kz+h\theta)} \end{aligned} \qquad [5.44]$$

where η is the wave amplitude at position (z,θ) after time t

α-is the wave growth rate which may be complex

k-is the wave number which is real positive

h-is the wave oscillation mode, which is 0 for symmetric oscillations and 1 for assymetric oscillation.

Considering the geometry of the wave motion, as indicated in Figure 29 and substituting equation [5.47] into [4.43] for cylindrical coordinates gives the following sets of Navier Stokes equations

$$\begin{aligned} [NSz] \quad & (\alpha + ikU)u + ik\pi = 0 \\ [NSr] \quad & (\alpha + ikU)v + \pi' = 0 \\ [NS\theta] \quad & (\alpha + ikU)w + ih\pi/r = 0 \end{aligned} \qquad [5.45]$$

where $u = u_z^0; v = u_r^0; w = u_\theta^0; \pi = P^0/\varrho;$ $U = u_z$ and the prime (′) indicates the derivative with respect to r.

The fluctuating pressure field can be obtained by considering the divergence of the component equations of motion [5.45] and combining with the equation of continuity [5.42] to obtain

$$r^2\pi'' + r\pi' - (k^2r^2 + h^2)\pi = 0 \qquad [5.46]$$

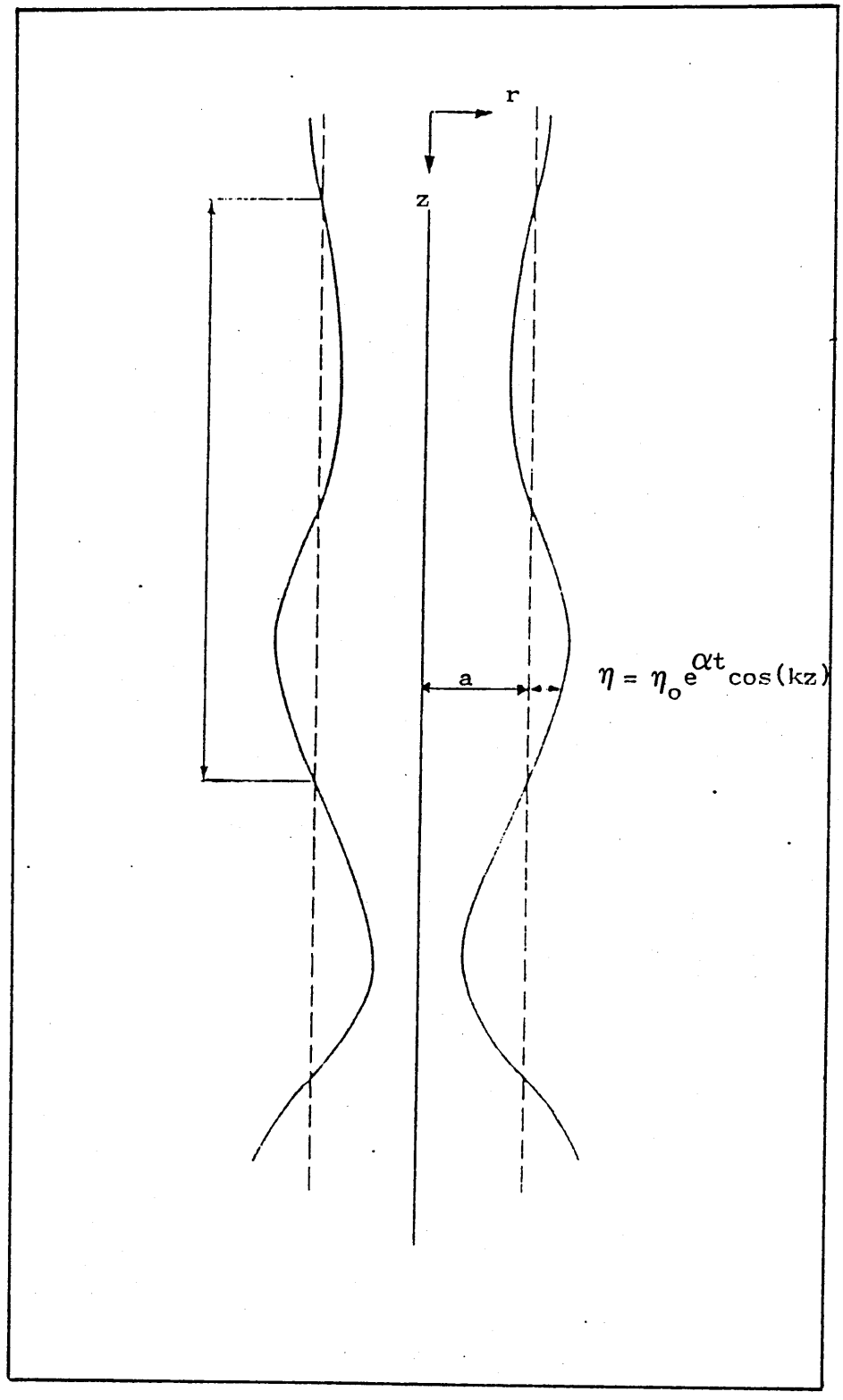

FIGURE 29 SYMMETRICAL WAVE PROFILE ON THE SURFACE OF THE JET

$$\frac{r^2 d^2\pi}{dr^2} + \frac{r d\pi}{dr} - (k^2 r^2 + h)\pi = 0 \qquad [5.47]$$

The general solution of equation [5.47] involves a linear super position of Bessel functions

$$\pi = AI_h(kr) + BK_h(kr) \qquad [5.48]$$

Considering the boundary conditions, equation [5.48] can be solved for both jet and continuous phases as;

For the jet phase where r = 0 and π is finite therefore

$$\pi = AI_h(kr) \qquad [5.49]$$

For the continuous phase where r = ∞ and π = 0 therefore

$$\pi = BK_h(kr) \qquad [5.50]$$

The constants A and B are found from the kinematics of the interface. At r≃a where

$$v = \frac{d\eta}{dt} = \frac{\partial\eta}{\partial t} + U\left[\frac{\partial\eta}{\partial z}\right] = (\alpha + ikU) \qquad [5.51]$$

$$\hat{v} = \frac{d\eta}{dt} = \frac{\partial\eta}{\partial t} + \hat{U}\left[\frac{\partial\eta}{\partial z}\right] = (\alpha + ik\hat{U}) \qquad [5.52]$$

It is assumed that the radial velocity fluctuation at the interface is;

$$v = -\frac{\pi'}{(\alpha + ikU)} \qquad [5.53]$$

Using equation [5.53] and substituting values from equations [5.19] to [5.52], we can calculate the value of the constants A and B at the the interface as

$$A = -\frac{(\alpha + ikU)^2\eta}{I_h'(ka)} \qquad [5.54]$$

$$B = \frac{(\alpha + ik\hat{U})^2 \eta}{K_h'(ka)} \qquad [5.55]$$

The solution of the jet and the continuous phase can now be matched at the interface between the two phases. At the interface there is a continuity of tangential and normal velocity as well as a continuity of tangential and normal stresses. Considering the continuity of longitudinal stress we can relate the pressure on either side of the interface as follows;

$$\tau_n = \hat{\tau}_n + P\sigma \qquad [5.56]$$

where $\tau_n = p - 2\mu \frac{\partial u_r}{\partial r}$

$$\hat{\tau}_n = \hat{p} - 2\mu \frac{\partial \hat{u}_r}{\partial r}$$

and

$$P\sigma = \frac{\sigma}{a}\eta - \left(\frac{\sigma}{a^2}\right)\left[\eta + a^2 \frac{\partial^2 \eta}{\partial z^2} + \frac{\partial^2 \eta}{\partial \theta^2}\right]$$

Separating out the small scale motion, equation [5.56] can be written in terms of a complex function as;

$$-\pi + s\pi + 2\nu(v' - m\hat{v}') = \left(-\frac{\sigma}{\rho a^2}\right)[1 - \tilde{k}^2]\eta \qquad [5.57]$$

where $s = \frac{\hat{\rho}}{\rho}$; $m = \frac{\hat{\mu}}{\mu}$ and $\nu = \frac{\mu}{\sigma}$

If we assume that at the interface $U_I = U = \hat{U}$, then using equation [5.57] we can derive a characteristic equation as

$$(\alpha + ikU_I)^2 [I^* + sk^*] + (\frac{2\nu k}{a^2}) [\alpha + ikU_I] [I^o + mK^o] = (\frac{\sigma}{\varrho a^3}) [1 - \tilde{k}] \tilde{k} \qquad [5.58]$$

where $I^* = I_0(ka)/I_1(ka)$

$K^* = K_0(ka)/K_1(ka)$

$I^o = \tilde{k}I^* - 1$

$K^o = \tilde{k}K^* - 1$

The growth rate in equation [5.57] is complex in form consisting of a real (growth rate) part and an imaginary (wave frequency) component. Putting $\alpha = \beta + i\omega$, the real part (growth rate) of equation [5.58] can be expressed as

$$\beta = (\sigma/\varrho a^3)C / [A + 2qB] \qquad [5.59]$$

where $A = I^* + sK^*$

$B = I^o + mK^o$

$C = \tilde{k}(\tilde{k} - \tilde{k}^2)$

$q = \nu\tilde{k}/a\beta$

The imaginary part, wave frequency can be given as $\omega = kU_I$ where U_I is the wave velocity at the interface and equal to $\tilde{c}$ where

$$\tilde{c} = \tilde{\omega}/\tilde{k}$$

The equation [5.59] indicates a progressive wave with a velocity $\tilde{c}$ and growth rate, β. The principal forces involved in the individual terms can account for the propagation of the disturbance wave on the surface of the jet.

Surface tension forces are associated with the term

$$C = \tilde{k}(1 - h^2 - \tilde{k}^2)$$

For a symmetrical wave h=0, it follows that c will be positive (destabilising) when $\tilde{k} > 1$ and negative (stabilising) when $\tilde{k} < 1$, as was described by Rayleigh. For an asymmetric wave h=1 and C will always be negative (stabilising).

The viscous forces are associated with the damping coefficient qB. An increase in the damping coefficient reduces the growth rate as indicated in equation [5.59].

The combined effect of the principal forces on the wave motion will depend on the type of the wave (symmetric or asymmetric), the wave number and the relative magnitude of the forces. The equation [5.59] can be written in dimensionless form as

$$\tilde{\beta}^2 = \beta^2 \left(\frac{\rho a^3}{\sigma}\right) = \left[\frac{C}{A + 2qB}\right]$$

with $q = \sqrt{\frac{2\tilde{k}z}{\tilde{\beta}}}$

These growth rate equations differ from previously proposed growth rate equations. Most of the previous workers assume that the wave travels on the surface of the jet with the jet velocity. But in the present work it is assumed that the wave travels with an interfacial velocity which is always less than the average jet velocity. This point will be discussed in detail in the next chapter.

The equation [5.59] can be reduced to Weber's equation [2.31] if we assume a stationary continuous phase with $U = 0$, $C = \hat{U}$ and s, m are very small. Further ignoring the effect of viscosity this equation can be reduced to Christiansen and Hixson equation [2.23].

NUMERICAL SOLUTIONS

The values of the dimensionless growth have been calculated as a function of the wave number for a symmetrical wave. The base values were chosen to show the effect of different parameters like s,m and z individually and separately on the growth rate.

In general the characteristic growth rate curves pass through a single maximum at an optimum wave number representing the fastest growing wave.

Figure 30 shows the damping effect of the increased continuous phase viscosity on the wave growth. Figure 31 shows a similar effect for increased jet phase viscosity or Ohnesorge number, Z. It is indicated that the increase in the viscosity suppresses the growth rate of the wave.

Figure 32 shows the effect of the density ratio s on the growth rate. As indicated the increased s reduces the growth rate, but the effect is not as pronounced as in the case of m or z. There is generally a good agreement between the theory and experiment in the present study for the prediction of the growth rate, wave number and wave velocity. The discrepancy will be discussed in chapter 6.

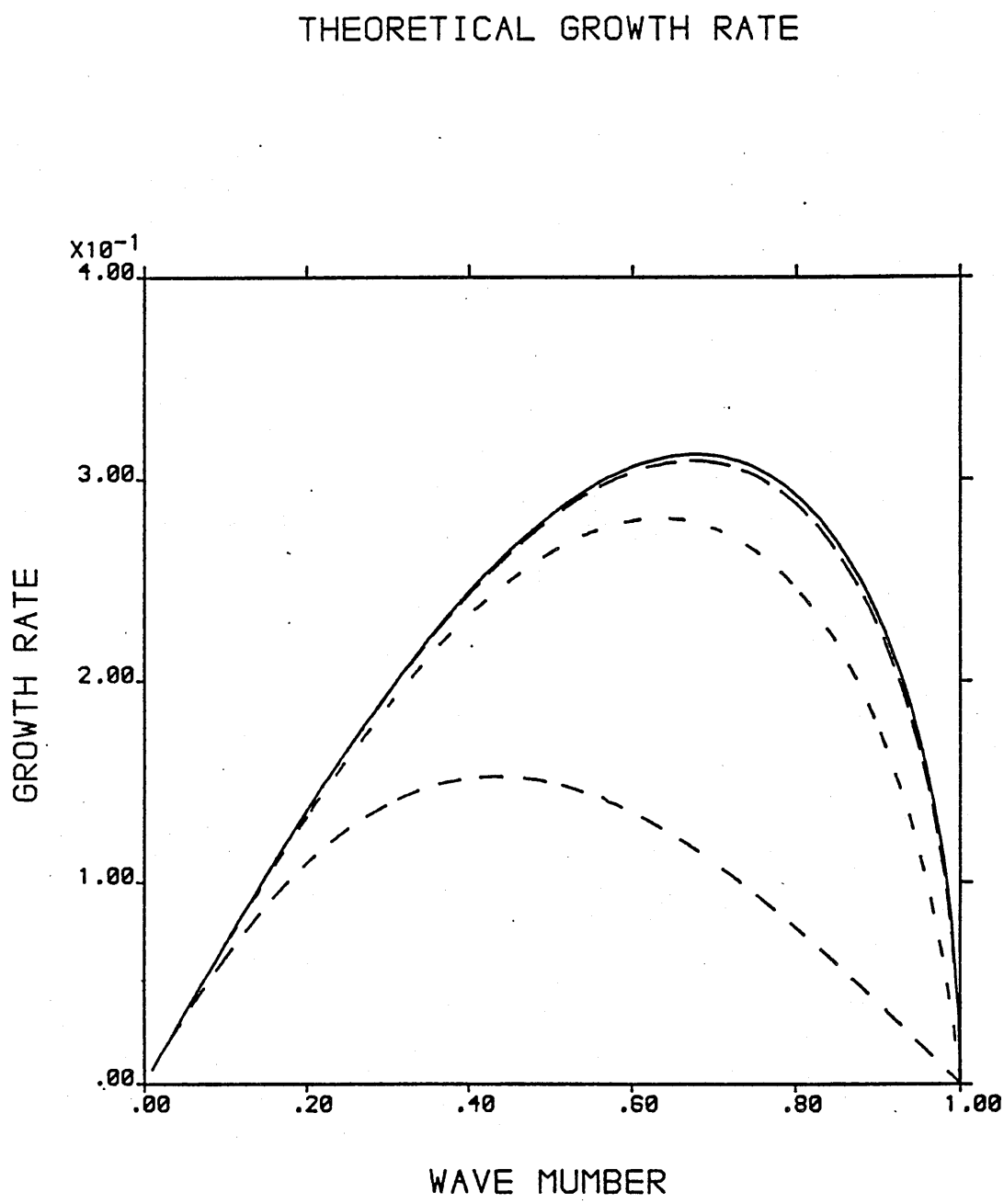

FIGURE 30 THEORETICAL PREDICTION OF THE GROWTH RATE OF SYMMETRIC WAVES
INFLUENCE OF THE CONTINUOUS PHASE VISCOSITY
BASE LINE VALUES

——— AT M = 0.10, Z = 0.001, S = 1
– — – AT M = 1.00, Z = 0.001, S = 1
- – - AT M = 10.0, Z = 0.001, S = 1
– — – AT M = 100.0, Z = 0.001, S = 1

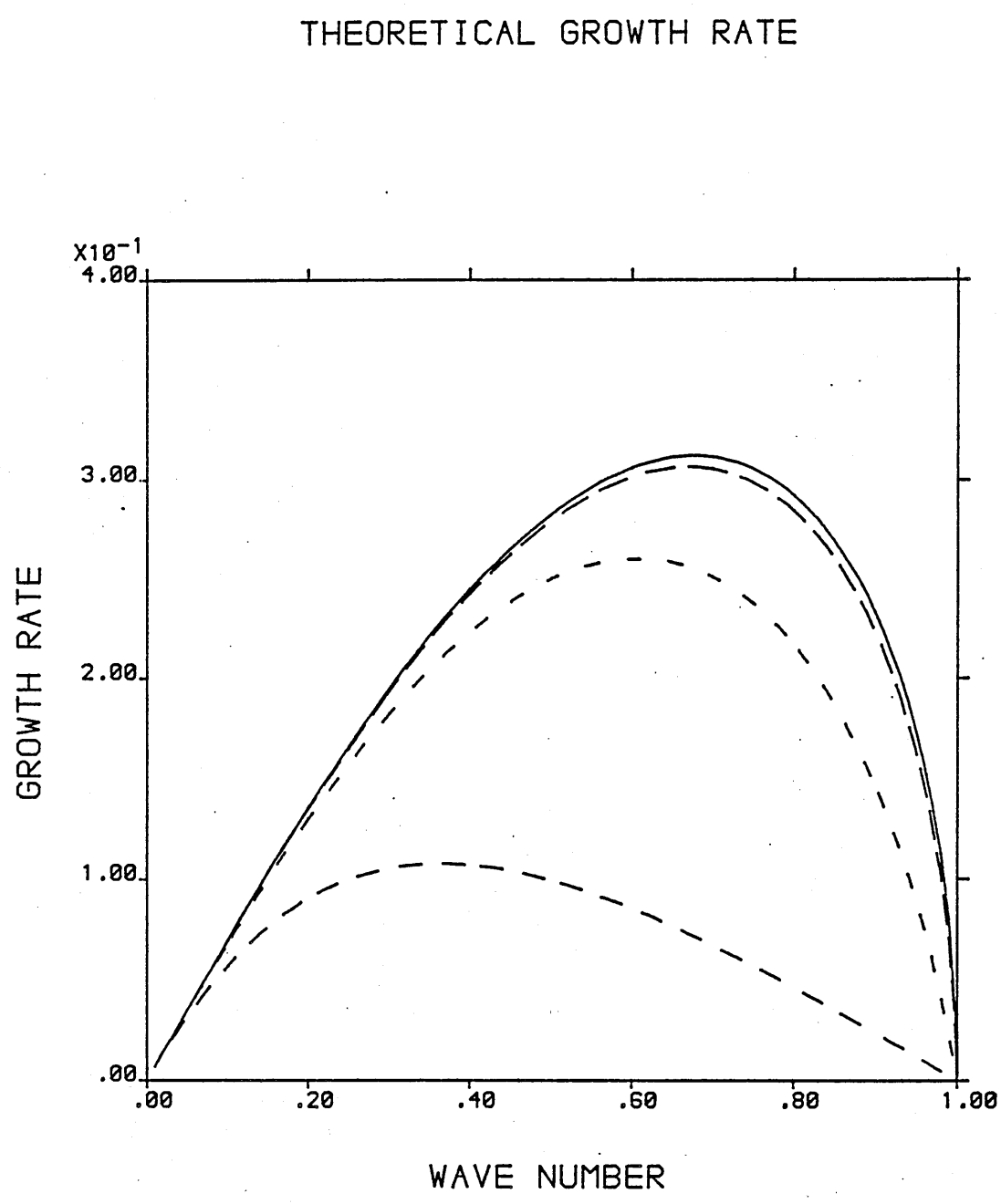

FIGUE 31 THEORETICAL PREDICTION OF THE GROWTH RATE OF SYMMETRIC WAVES
INFLUENCE OF THE JET PHASE VISCOSITY
BASE LINE VALUES

——— AT Z = 0.001, S = 1.0, M = 1.0
– — – AT Z = 0.01, S = 1.0, M = 1.0
- – - AT Z = 0.1, S = 1.0, M = 1.0
– — – AT Z = 1.0, S = 1.0 M = 1.0

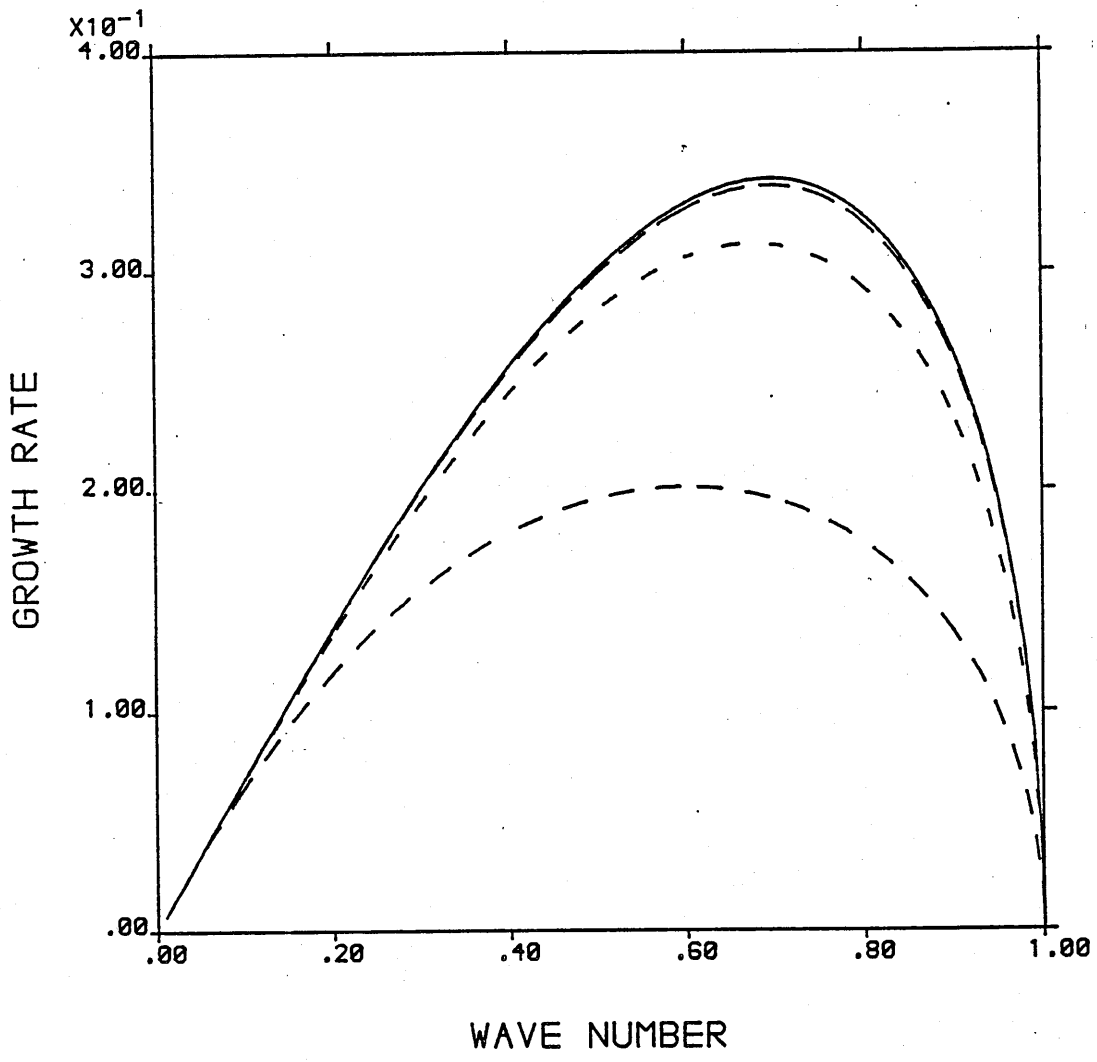

FIGURE 32 THEORETICAL PREDICTION OF THE GROWTH RATE OF SYMMETRIC WAVES
INFLUENCE OF THE DENSITY
BASE LINE VALUES

——— AT S = 0.01, M = 1.0, Z = 0.001
– — – AT S = 0.10, M = 1.0, Z = 0.001
- — - AT S = 1.00, M = 1.0, Z = 0.001
– — – AT S = 10.00, M = 1.0, Z = 0.001

5.3 DROP SIZE IN THE JETTING REGIME

It is not possible to be able to explain the drop size variation in the jetting regime on the basis of the instability theory alone. As already discussed, it is based on the assumption that there is only one wave present on the surface of the jet which grows fastest and breaks the jet into drops. If this were true then we should expect only monosize drops of one node at every flow rate in the jetting regime, because only the fundamental wave would break the jet to form drops of the fundamental volume. Since the drop size varies in the jetting regime, additional assumptions are needed to account for the formation of multinode drops from the liquid jet.

Using the instability theory one can consider the growth of the fundamental wave on the jet surface. This takes a time Tf to grow enough to pinch the jet at the ultimate antinode of the wave to form a one node drop. The fundamental period of the wave can be written as

$$Tf = \frac{\pi D_n}{\tilde{k}c} \qquad [5.60]$$

where $\tilde{k}$ is the dimensionless wave number of the fastest growing wave on the surface of the jet which can be predicted from instability theory. D_n is the nozzle diameter and c is the wave velocity.

As the drop detaches, the jet initially relaxes as observed experimentally. Due to this relaxation process, it appears that a relaxing wave generates from the end of

the jet and propagates backward with a constant relaxation period Tr.

Considering the vibration mode on the jet surface as described by Lamb (26), the period of relaxing vibration Tr can be calculated from

$$\frac{1}{\frac{1}{2}}_{Tr} = ka\left[\frac{I_s'(ka)}{I_s(ka)}\right](k^2a^2 + S - 1)\frac{\sigma}{\rho D_n}$$

where ka is dimensionless wave number, S is the mode of vibrations which is 0 or 1 for either the symmetric or asymmetric waves respectively and is the interfacial tension.

For the symmetric mode of oscillation this equation can be written as

$$\frac{1}{\frac{1}{2}}_{Tr} = \left[\frac{I_o'(\tilde{k})}{I_o(\tilde{k})}\right][\tilde{k}^2 - 1]\frac{\sigma}{\rho D_n} \qquad [5.61]$$

where the dimensionless wave number $\tilde{k}$ = ka. Equation [5.61] can further be simplified to yield

$$Tr = \sqrt{K\frac{\rho D_n^3}{\tilde{k}\sigma}} \qquad [5.62]$$

where a dimensionless constant K is defined to be

$$K = \frac{1}{\left[\frac{I_o'(\tilde{k})}{I_o(\tilde{k})}\right][\tilde{k}-1]}$$

The relaxation period Tr of the wave can be predicted if the value of dimensionless constant K is known. The

experimental value, using Figure 26, shows that the relaxation period of the wave is constant at around a value of 6ms. For water into decane system the experimental value of K was estimated to be 3.714.

CHAPTER 6

DISCUSSION

6.1 DROP FORMATION AT LOW VELOCITIES

The model developed in chapter 5 was used to predict the experimental drop size data for water into decane system. The predicted values of the present model were compared with Meister & Sheele, Hayworth & Treybal and Kumar & Hartland. A full comparison is given in Table(5).

The mean percentage deviation for all data in the prejetting regime using equation [5.18] was 3.04%. For the same data Hayworth & Treybal [equation 2.3] and Kumar & Hartland (equation [2.11]) predicted a mean percentage deviation of 26.0% and 24.4% respectively. The prediction of Meister & Sheele was found to be the closest to the present model with a mean percentage deviation of 8.5%.

As we have discussed in chapter 2 Kumar & Hartland derived their equation [2.11] purely on the basis of a data fitting exercise. They did not consider the drop formation mechanism or the factors which could affect the final volume of the forming drop such as formation time, the volume of liquid which goes into the drop and the residual volume during the second stage of the formation. Therefore, a big variation in the prediction using their equation is not an unexpected result.

TABLE 5

COMPARISON OF THE PREDICTED AND EXPERIMENTAL DATA FOR DROP DIAMETER IN LOW FLOW RATE REGIME

S. No	WE No	EXP DATA	COMPARISON EQ [5.18]	EQ [2.9]	EQ [2.3]	EQ [2.11]	ERROR ESTIMATION EQ [5.18]	EQ [2.9]	EQ [2.3]	EQ [2.11]
1.	0.638	0.332	0.3319	0.3008	0.2739	0.4368	0.03%	10.3%	21.2%	23.9%
2.	1.072	0.319	0.3278	0.2960	0.2510	0.4164	2.60%	7.70%	27.0%	23.4%
3.	1.481	0.302	0.3231	0.2809	0.2325	0.4080	6.50%	7.51%	29.8%	25.9%
Mean Percentage Error							3.04%	8.50%	26.0%	24.4%

EQUATION [5.18] - Present Model
EQUATION [2.9] - Meister and Scheele
EQUATION [2.3] - Hayworth and Treybal
EQUATION [2.11] - Kumar and Hartland

In the case of Hayworth & Treybal, there are a number of reasons why their equation [2.3] could not predict good results for the present data. Hayworth & Traybal used a surfactant Alketrage C to vary the surface tension in order to study the effect of the interfacial tension on the forming drop. The effective interfacial tension increases as the velocity through the nozzle increases due to diffusion of the surfactant to the interface. This causes a much greater increase in the drop volume with increasing velocity than observed in pure systems. Thus Hayworth & Treybal's interfacial dependency is not generally applicable and causes error in pure systems. Secondly, Hayworth & Treybal did not consider the possibility of volume flow into the drop during the process of break off. Further, Harkins-Brown the correction factor was used to account for the residual volume which is an errorful estimation of the residual volume as will be discussed subsequently.

It has been pointed out in chapter 2 that both Kumar & Hartland and Hayworth & Treybal did not consider a two stage formation process of drop in the prejetting condition. They based their prediction predominantly on the empirical data fitting exercise. Therefore, a direct comparison of their predictions is not really applicable for the present study.

Meister & Scheele's equation produced a close prediction for the drop size as shown in Table (5). They have also considered a two stage drop formation process in

their theoretical analysis. Therefore, equation [2.9] can be used to compare the prediction of drop volumes in individual stages separately, much of the following discussion will be discussed in the light of Meister & Sheele´ equation [2.9].

Figure 33 shows the prediction of the drop volume during the first stage of its formation using the present model [5.18] and equation [2.9] proposed by Meister & Sheele. It can be seen that the experimental data is well predicted by the present model. However, the discrepancy with Meister & Sheele possibly lies with the term predicting the momentum force during this stage. Meister & Sheele assumed a parabolic velocity profile to derive their equation. This assumption overestimates the momentum force during this stage and therefore, the time to ´take off´ was underestimated. In the present model the assumption of the flat velocity profile allowed a longer time for a drop to take off from the nozzle. Further, it should be noted that Meister & Sheele included a drag term to account for the effect of viscosity, but in the present model this term was neglected. Since in the present work only one system, water into decane, was investigated the viscosity was very low, and hence the drag forces were negligible as can be seen in Table (6) where the relative magnitude of various forces are presented.

Figure 34 is plotted to calculate the drop volume in the second stage of its formation using equation [5.16].

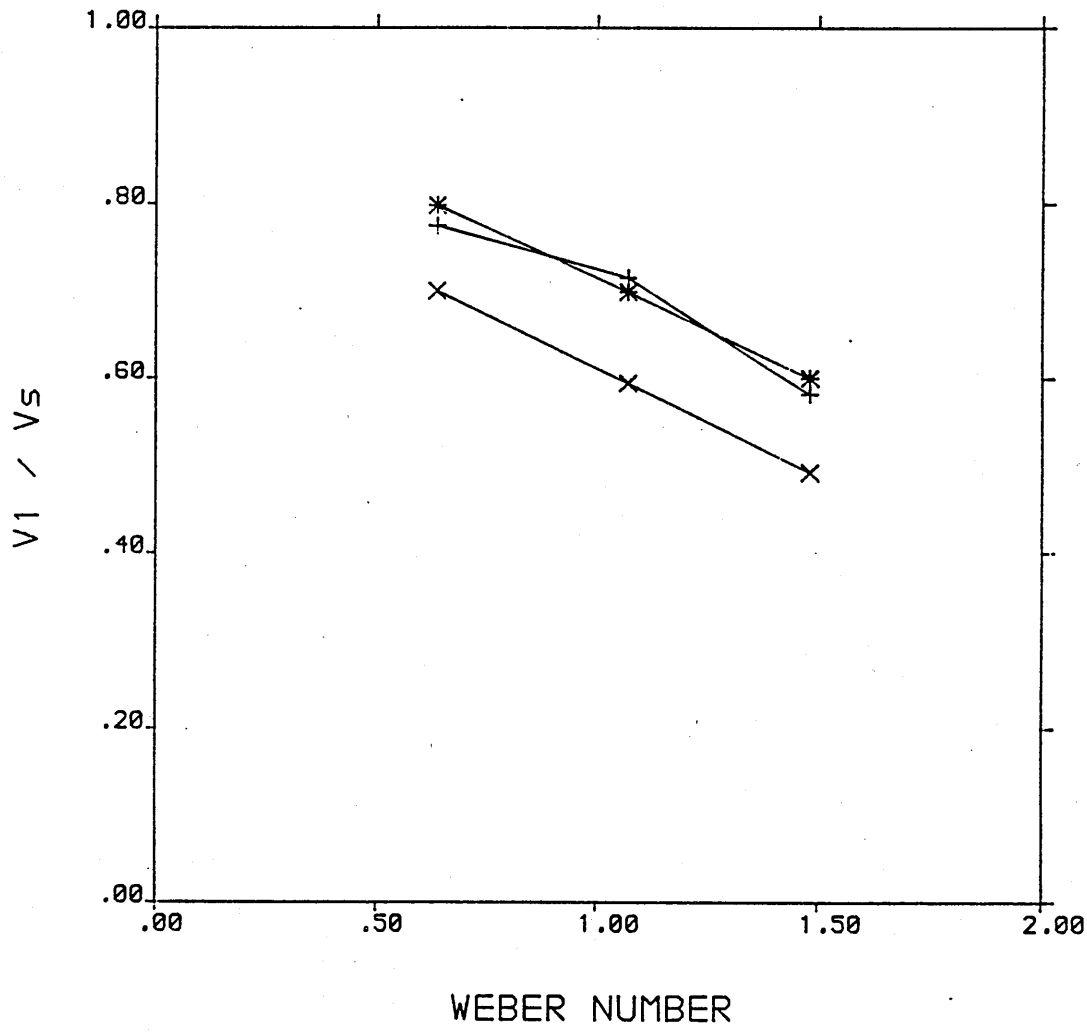

FIGURE 33 COMPARISON OF THE PREDICTED DROP VOLUME

\+ - EXPERIMENTAL VALUES
× - MEISTER AND SHEELE
* - PRESENT MODEL

TABLE 6

SYSTEM WATER INTO DECANE

RELATIVE MAGNITUDE OF VARIOUS FORCES ON THE DROP DURING TIME OF FORMATION

S.NO	FLOW RATE ml/sec	BUOYANCY FORCE N	MOMENTUM FORCE N	S.TENSION FORCE N	DRAG FORCE N
1.	0.000	0.00	0.00	4.255	0.000
2.	0.001	0.3	0.00	4.255	0.001
3.	0.002	0.5	0.01	4.255	0.002
4.	0.003	0.8	0.03	4.255	0.004
5.	0.004	1.0	0.05	4.255	0.005
6.	0.005	1.3	0.08	4.255	0.006
7.	0.006	1.6	0.12	4.255	0.007
8.	0.007	1.8	0.17	4.255	0.008
9.	0.008	2.1	0.22	4.255	0.010
10.	0.009	2.4	0.27	4.255	0.011
11.	0.010	2.6	0.34	4.255	0.012
13.	0.011	2.9	0.41	4.255	0.013
14.	0.012	3.1	0.49	4.255	0.014
15.	0.013	3.4	0.57	4.255	0.015
16.	0.014	3.7	0.66	4.255	0.017
17.	0.015	3.9	0.76	4.255	0.018
18.	0.016	4.2	0.87	4.255	0.019
19.	0.017	4.5	0.98	4.255	0.020
20.	0.018	4.7	1.10	4.255	0.021
21.	0.019	5.0	1.22	4.255	0.023
22.	0.020	5.2	1.35	4.255	0.024
23.	0.021	5.5	1.49	4.255	0.025
24.	0.022	5.8	1.64	4.255	0.026
25.	0.023	6.0	1.79	4.255	0.027
26.	0.024	6.3	1.95	4.255	0.029
27.	0.025	6.5	2.12	4.255	0.030

Though the present model predicts higher values than the experimentally measured drop volume for this stage, the differences can be explained if we consider the drop detachment process in detail.

A small portion of liquid is left behind the drop at the nozzle during the process of its detachment, as can be seen in the high speed sequence given in Plate (4).This residual volume increases at higher flowrates through the nozzle. Figure 35 shows the plot for the present set of experiments. The experimental values for this volume are far higher than predicted by Meister & Scheele, because they have used the Harkins-Brown correction factor to account for the residual volume. The Harkins-Brown correction factor is only valid for a static drop formation process and should not be included in the dynamic processes. Therefore, instead of considering this correction factor in the present model, a new approach of instability mechanism was used to calculate the residual volume as described in chapter 5.

The inclusion of the jet instability to predict this residual volume also supports the experimental observation made in chapter4, where it has been observed as shown in high speed sequence of Plate(4), that even in the prejetting conditions the drop breaks off from the end of a definite transitory jet and the point of detachment moves increasingly away from the nozzle as the flow rate increases. As we can see in Figure 35 the predicted value of the residual volume follows the same pattern as its

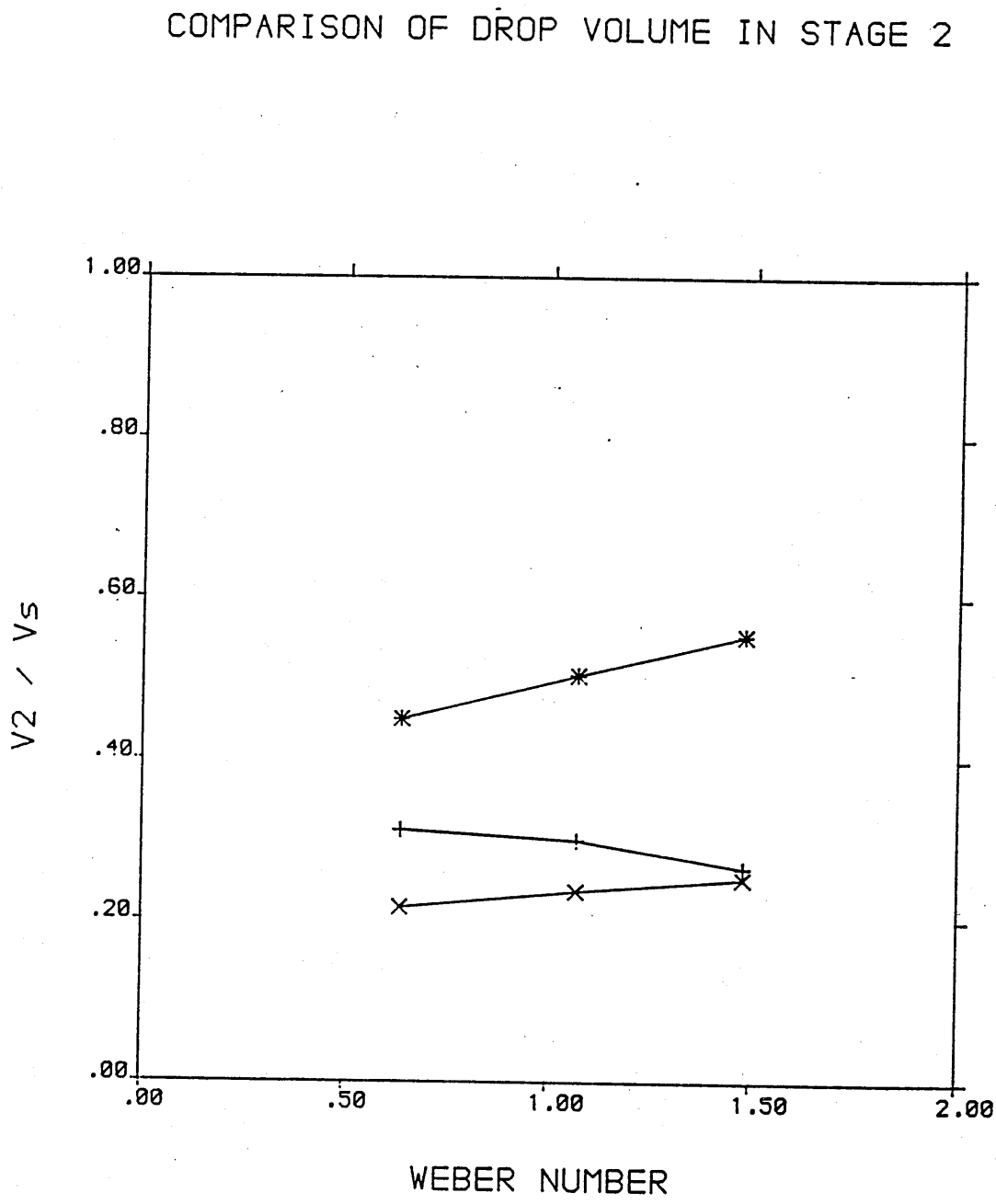

FIGURE 34 COMPARISON OF THE PREDICTED DROP VOLUME

\+ - EXPERIMENTAL VALUES
× - MEISTER AND SHEELE
* - PRESENT MODEL

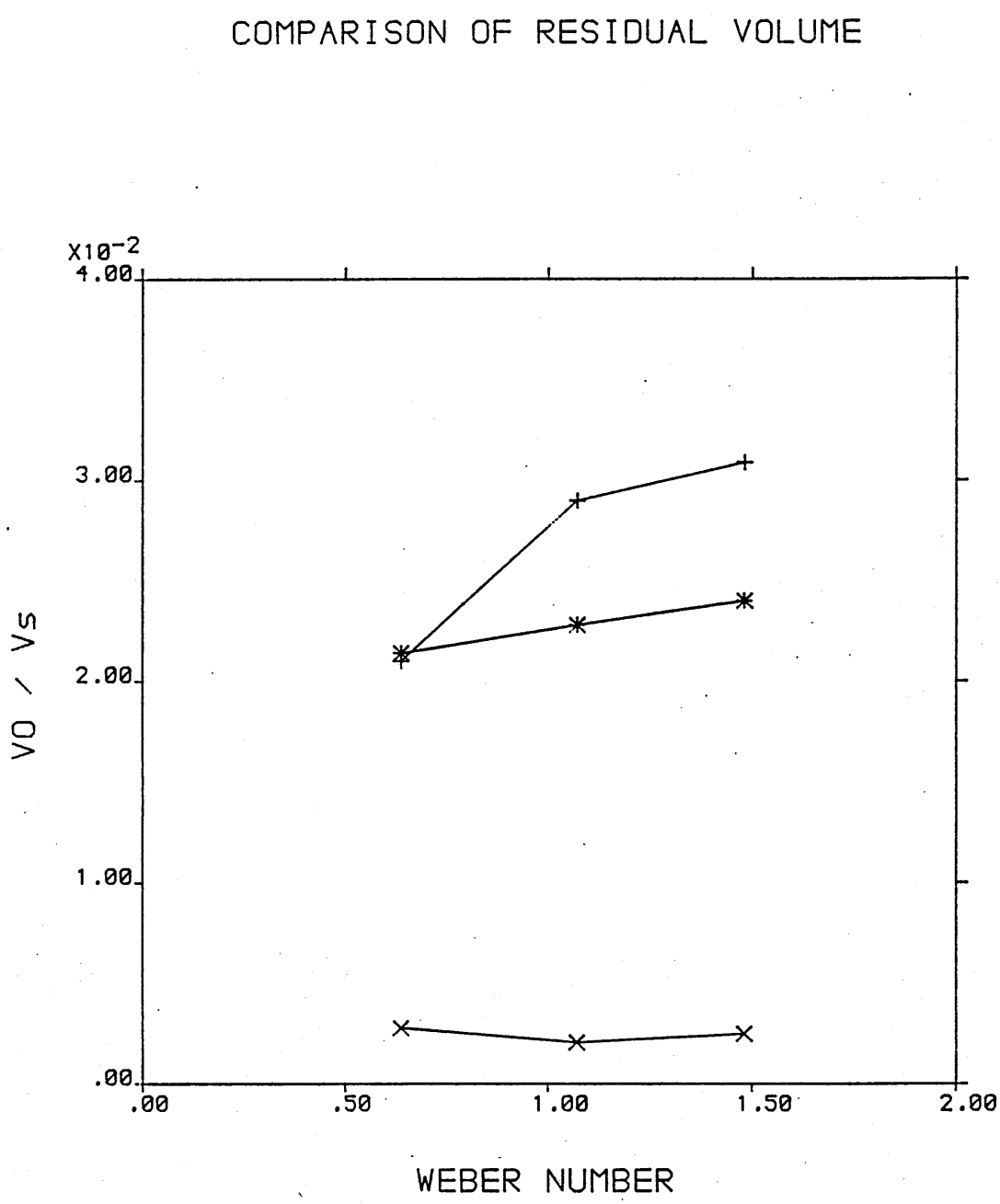

FIGURE 35 COMPARISON OF THE PREDICTED DROP VOLUME

\+ - EXPERIMENTAL VALUES
× - MEISTER AND SHEELE
* - PRESENT MODEL

experimentally calculated counter part that is the residual volume increases with the flow rate. In other words, the inclusion of the instability theory shows that the length of the transitory jet increases, or the point of the detachment of the drop moves away from the nozzle as the flow rate increases. Further, as shown in Figure 8 the time of growth t_1 at the nozzle decreases as the flow increases. At a critical flow rate where t_1 becomes zero, and the residual volume (or jet) is left behind, the detached drop does not get time to relax towards the nozzle before the new neck starts to form. Therefore, as the system evolves beyond this state the instability alone governs the drop formation process. This follows along the same lines as discussed above: the effect of the jet instability on the final drop volume becomes more and more pronounced as the flow rate increases until the jetting starts, where the instability of the jet governs the drop sizes. This supports the observations made in chapter 4, that the transition of the drop formation mechanism at the nozzle (prejetting regime) to the drop formation mechanism at the end of the jet is not a sharp transition. It further suggests that the net increase in the drop volume in the second stage depends on both the volume of the drop in the second stage and the residual volume of liquid which is left behind the drop.

Figure 36 is plotted for the final drop diameter using equation (5.18) and the results are tabulated in Table (7). As can be seen the present model predicts

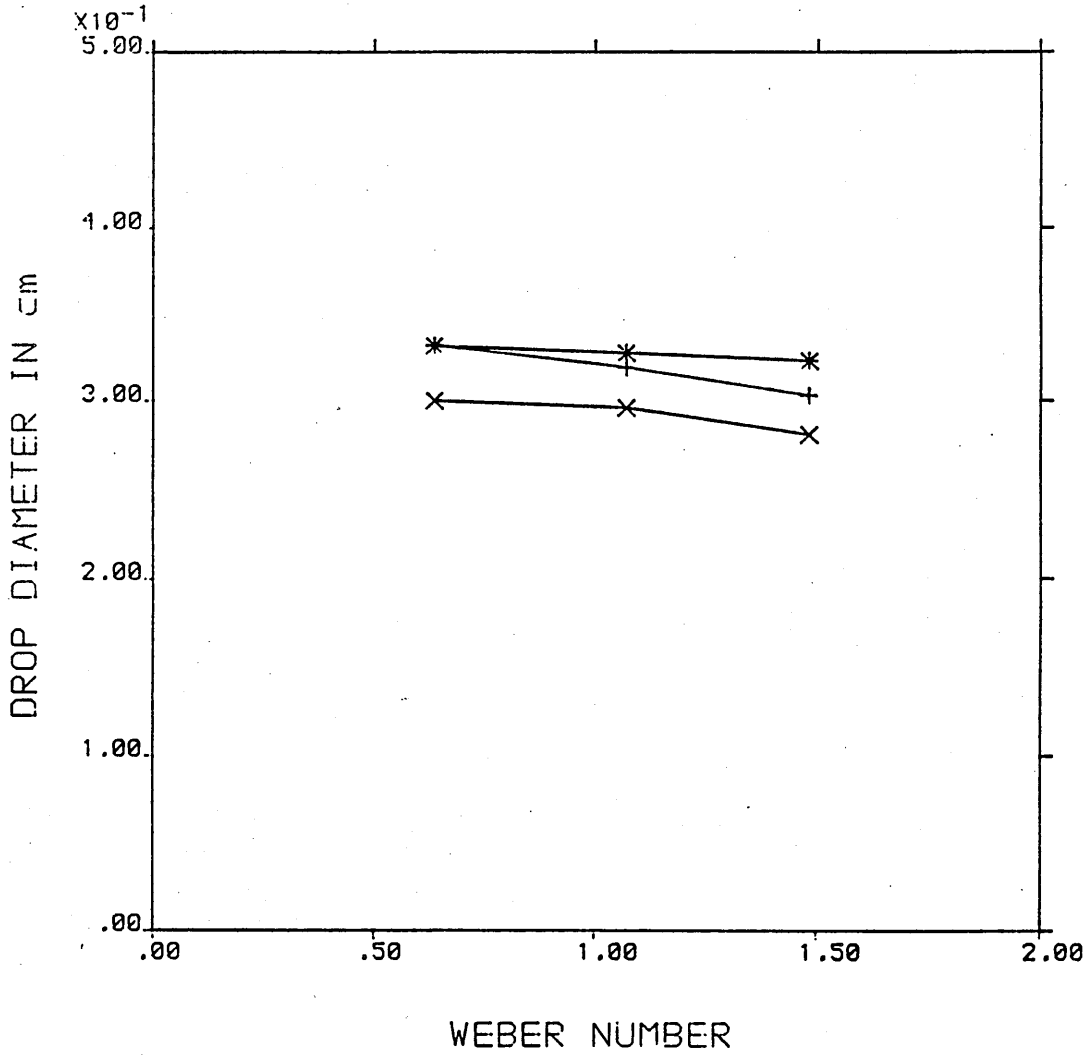

FIGURE 36 COMPARISON OF THE PREDICTED DROP DIAMETER

\+ - EXPERIMENTAL VALUES
× - MEISTER AND SHEELE
* - PRESENT MODEL

TABLE 7

COMPARISON OF EXPERIMENTAL AND PREDICTED DROP VOLUMES IN DIFFERENT STAGES OF ITS FORMATION AT VARIOUS WEBER NUMBERS

Formation Stages	We No	Drop volume in cc		
		Experimental results	EQ NO [2.9]	EQ NO [5.18]
in first stage V1/Vs	0.63	0.779	0.70005	0.7995
	1.07	0.706	0.59456	0.7002
	1.48	0.601	0.49242	0.6003
in second stage V2/Vs	0.63	0.311	0.21481	0.4502
	1.07	0.299	0.23614	0.5050
	1.48	0.265	0.25198	0.5537
residual volume VO/Vs	0.63	0.021	0.00279	0.0213
	1.07	0.029	0.00267	0.0218
	1.48	0.030	0.00251	0.0220
total volume Vt	0.63	1.089	0.91207	1.1223
	1.07	0.976	0.86790	1.1828
	1.48	0.835	0.74103	1.1310
drop diameter	0.63	0.332	0.30985	0.3319
	1.07	0.319	0.29600	0.3278
	1.48	0.302	0.28094	0.3231

slightly higher values than the experimentally measured ones. However, the overall prediction using equation [5.18] is much better than the predicted values of Meister & Sheele. The discrepancy suggests that Meister & Sheele's equation also suffers from empiricism. The weak point of their analysis is the term for predicting the flow into the drop during the necking process. This term was empirically correlated for a very limited number of data points for the heptane water system only. Therefore, their equation is not generally applicable. The present model has not only predicted a good agreement for the present experimental data, but is theoretically based and does not depend on experimental data fitting.

The quantitative prediction of the final drop volume can be improved if the jet geometry after the drop detachment is fully understood. The present model assumed a conical geometry of the jet soon after the drop detachment. This assumption might not be true, therefore more experimental information is needed to consider the right geometry of the jet to improve the prediction of the residual volume. This residual volume plays an important role in the determination of the final drop volume as can be seen in equation [5.18], which suggests that if this volume is lower, then the predicted final drop volume would be higher.

6.2 WAVE PROPERTIES

As described in chapter 2 the wave properties on the surface of the jet have been studied by many previous workers. Most of them based their theoretical analysis on the original instability theory proposed by Rayleigh(9) and extended it to calculate the wave length, wave velocity and wave frequency of the fastest growing wave on the surface of the jet.This information was used to predict the drop size in the jetting region.

According to instability theory, the amplitude of the fastest growing disturbance wave grows exponentially on the surface of the jet as the wave travels away from the nozzle. When this amplitude becomes equal to the radius of the jet, the jet breaks up into drops. The size of these drops depends on the wave length of the fastest growing disturbances. As has been pointed out in chapter 2 very little experimental data on wave properties are available to test the various instability theories.

The growth rate of the wave on the surface of the jet has been calculated from the measurement of the wave amplitude using the following equation:

$$\eta = \eta_0 e^{\alpha t} \qquad [6.1]$$

where η_0 is the initial amplitude of the wave, n is the amplitude at time t and α is the growth factor. Rearranging equation [6.1] in terms of distance along the jet we can write

$$t = Y/c \qquad [6.2]$$

Where Y is the distance from the nozzle and c is the velocity of the wave on the surface of the jet. Thus equation [6.1] can be written as;

$$\log\eta = \alpha Y/c + \log\eta_0 \qquad [6.3]$$

A plot of $\log\eta$ against the distance Y should give a straight line having a slope equal to α/c and an intercept of $\log\eta_0$. These plots are presented in Figure 37 to 42 , and the results are tabulated in appendix B

It can be seen that the intercept $\log\eta_0$ is equal to a constant, -9.0 for all the systems. This confirmed the assumption made by previous workers that the initial amplitude is a function of the particular nozzle used and independent of the liquid properties. Meister & Scheele found a constant value of 5.8 for log (a/η_0) which matches very well with the present finding of log (a/η_0) equal to 6.

To calculate the growth rate from such plots experimentally measured wave velocities were used. As shown in Figure 24 the wave velocity always travels slower than the jet velocity. The results of Figure 24 have shown that the assumption made by most of the previous workers that the wave travels with the jet velocity on the surface of the jet is not valid. The experimentally calculated growth rate for six systems are presented in Table (8) along with the predictions of Rayleigh equation [2.20] and Bright, equation [2.38].

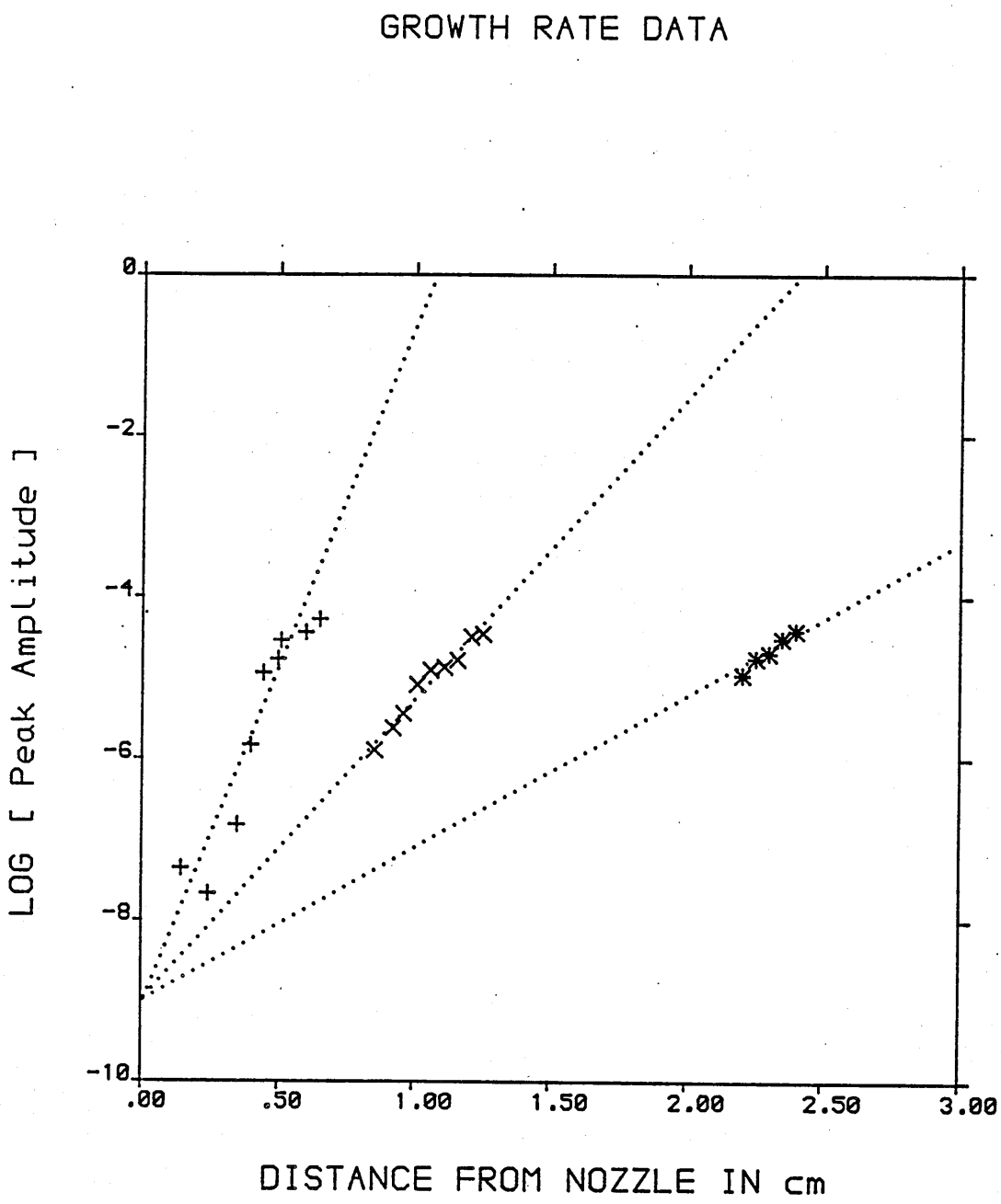

FIGURE 37 VARIATION OF THE GROWTH RATE WITH WEBER NUMBER
SYSTEM - DECANE INTO WATER

\+ - AT WEBER NUMBER 6
× - AT WEBER NUMBER 10
* - AT WEBER NUMBER 20

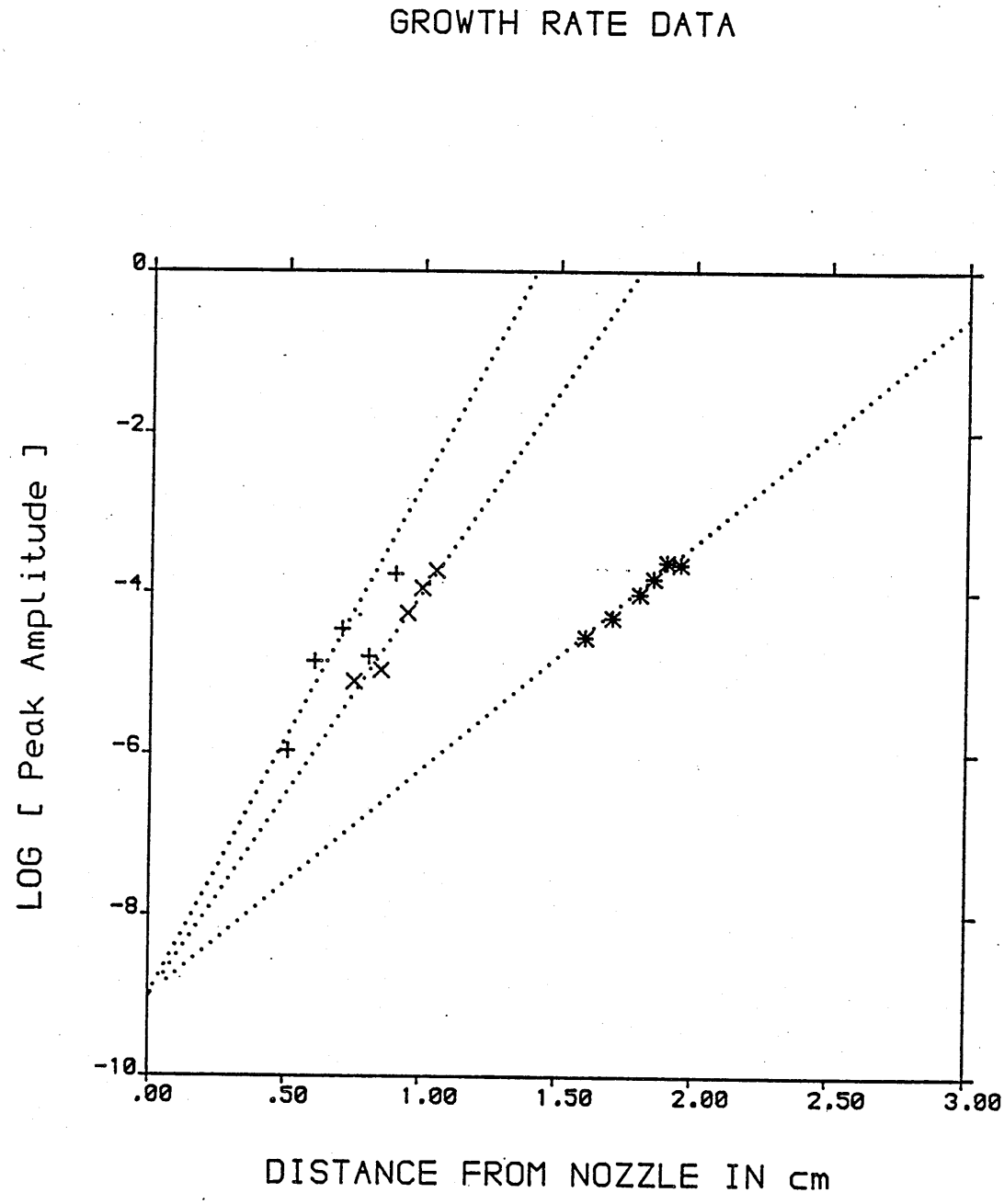

FIGURE 38 VARIATION OF THE GROWTH RATE WITH THE WEBER NUMBER
SYSTEM - DECANOL INTO WATER

\+ - AT WEBER NUMBER 6
× - AT WEBER NUMBER 10
* - AT WEBER NUMBER 20

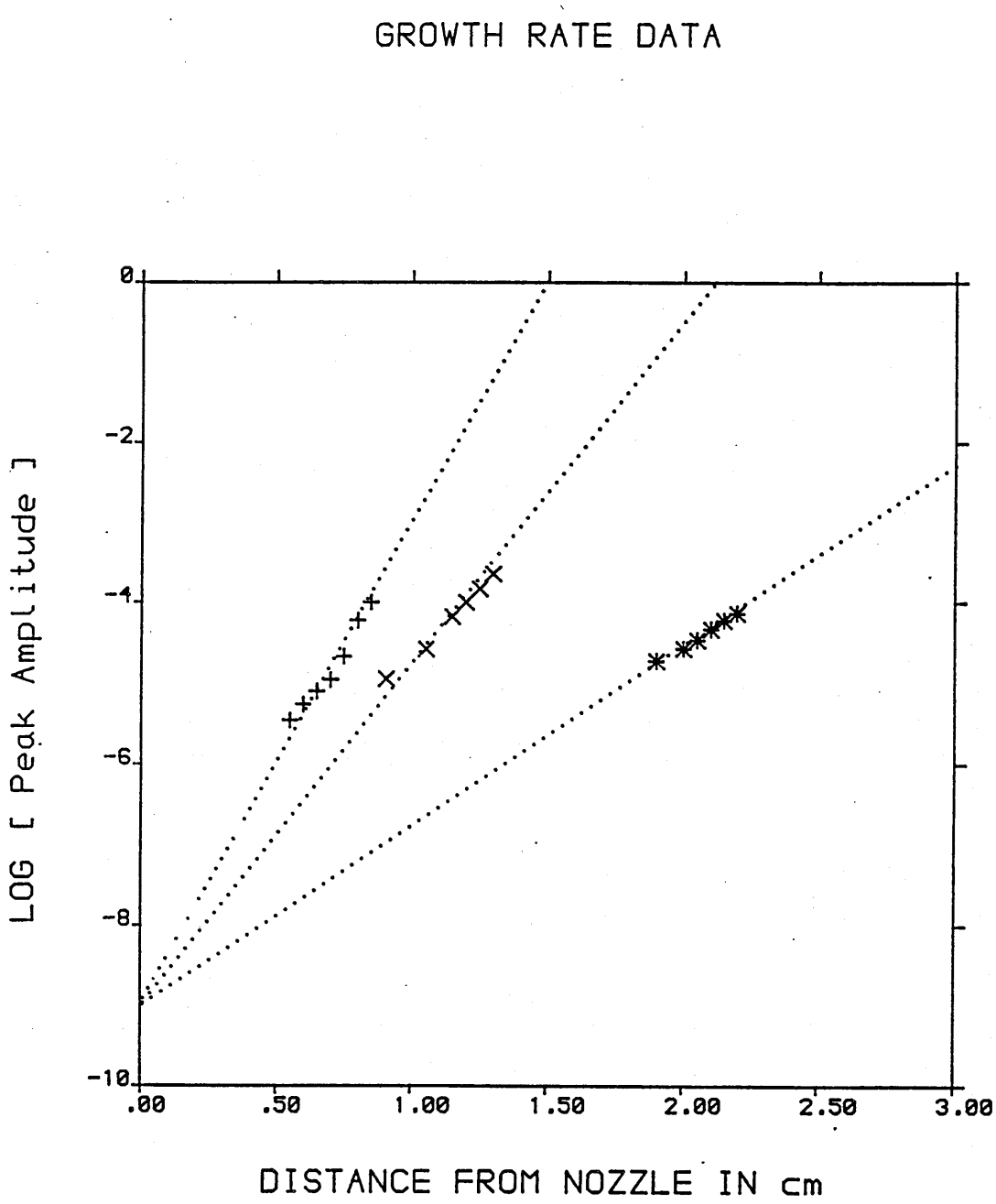

FIGURE 39 VARIATION OF THE GROWTH RATE WITH WEBER NUMBER
SYSTEM - PARAFFIN INTO WATER

\+ - AT WEBER NUMBER 6

× - AT WEBER NUMBER 10

* - AT WEBER NUMBER 20

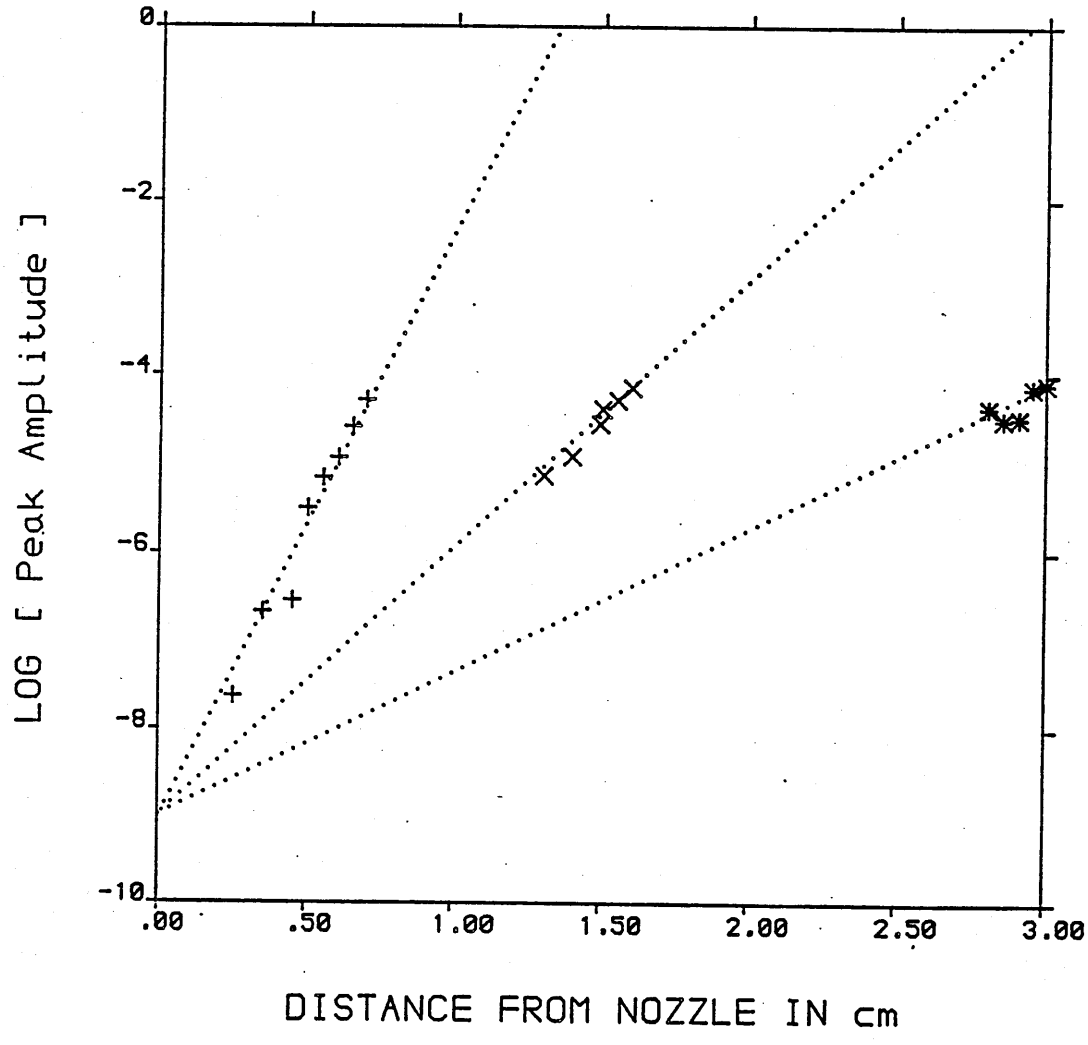

FIGURE 40 VARIATION OF THE GROWTH RATE WITH WEBER NUMBER
SYSTEM - WATER INTO DECANE

\+ - AT WEBER NUMBER 6

× - AT WEBER NUMBER 10

* - AT WEBER NUMBER 20

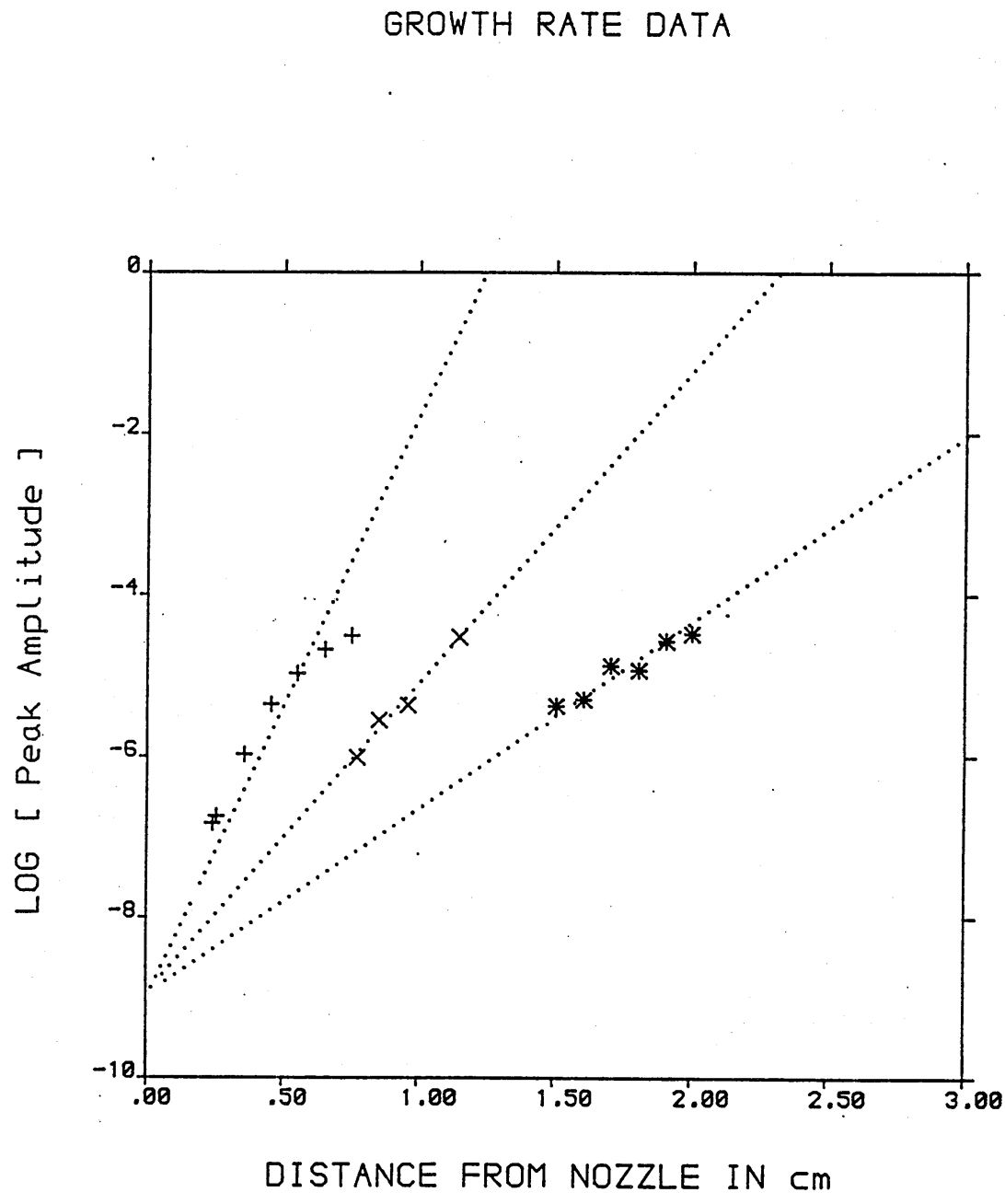

FIGURE 41 VARIATION OF THE GROWTH RATE WITH WEBER NUMBER
SYSTEM - WATER INTO DECANOL

\+ - AT WEBER NUMBER 6
× - AT WEBER NUMBER 10
* - AT WEBER NUMBER 20

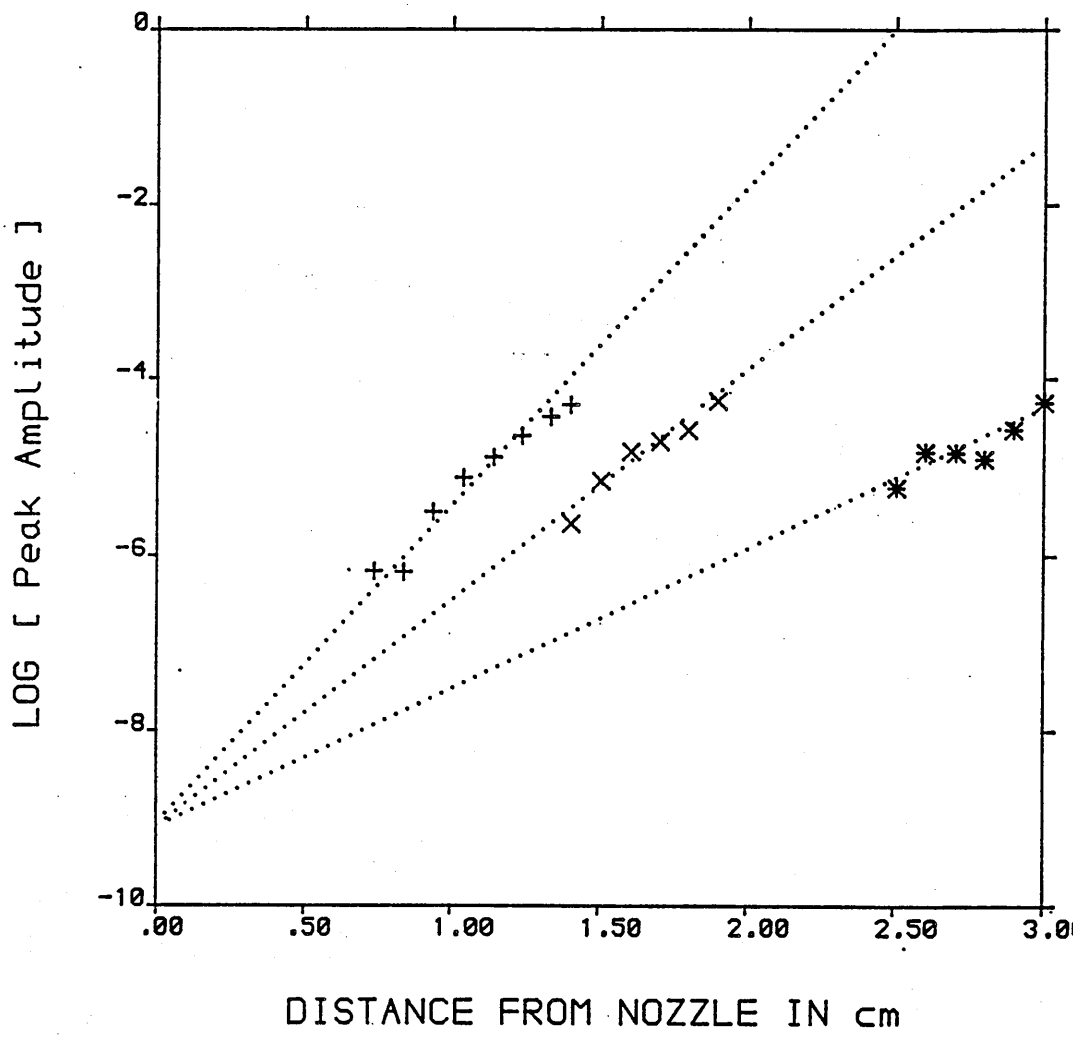

FIGURE 42 VARIATION OF THE GROWTH RATE WITH WEBER NUMBER
SYSTEM - WATER INTO PARAFFIN

\+ - AT WEBER NUMBER 6

× - AT WEBER NUMBER 10

* - AT WEBER NUMBER 20

Table (8) shows that the growth rate is well predicted in the present study using equation [5.59]. The discrepancy of the results with the stationary instability theory equation [2.20] and inertial instability theory equation [2.38], can be explained if we compare the present results individually and separately with these equations.

The equation [2.20], as proposed by Rayleigh(9), is based on two major assumptions. Primarily, he considered a stationary liquid jet, therefore the effect of the relative velocity of the two phase was ignored completely; this assumption could produce good results for the liquid/air system where the continuous phase density and viscosity are negligible. Secondly, he assumed that only one single wave of the fastest growing disturbance travels with the nozzle velocity on the surface of the jet. The present experimental data as given in Figure 24 suggest that the wave always travel slower than the jet velocity. Further equation [2.20] predicts that the wave possessing a wave number equal to 0.696 will grow faster on the jet surface and cause the jet to break into drops. But experimentally measured values of the wave numbers span the range $0.6<ka<1.8$ as shown in Figure 25.

On the other hand, the experimentally calculated values of the growth rate can also be compared using equation [2.38],proposed by Bright(24). He considered the effect of the relative velocity and the viscosities of the two phases. He suggested that the viscous forces are

TABLE 8

COMPARISON OF EXPERIMENTAL AND PREDICTED DIMENSIONLESS GROWTH RATE

SYSTEM	WE	EXP VALUES	EQ [5.59]	EQ [2.20]	EQ [2.38]
Decane / Water	6.0	0.2262	0.2303	0.2537	0.4000
	10.0	0.2259	0.2303	0.2537	0.4684
	20.0	0.2241	0.2303	0.2537	0.5890
Decanol / Water	6.0	0.1777	0.1123	0.2557	0.2464
	10.0	0.1822	0.1123	0.2557	0.2843
	20.0	0.1796	0.1123	0.2557	0.3558
Paraffin / Water	6.0	0.1780	0.1850	0.2418	0.4608
	10.0	0.1773	0.1850	0.2418	0.7143
	20.0	0.1733	0.1850	0.2418	0.9409
Water / Decane	6.0	0.2753	0.2335	0.2536	0.4172
	10.0	0.2704	0.2335	0.2536	0.5222
	20.0	0.2487	0.2335	0.2536	0.6709
Water / Decanol	6.0	0.1689	0.1115	0.2550	0.2418
	10.0	0.1739	0.1115	0.2550	0.2676
	20.0	0.1628	0.1115	0.2550	0.3125
Water / Paraffin	6.0	0.1630	0.1923	0.2538	0.3107
	10.0	0.1619	0.1923	0.2538	0.3275
	20.0	0.1628	0.1923	0.2538	0.3566

associated with the damping coefficient, and an increase in the damping coefficient will reduce the growth rate of the wave. He also considered the inertial forces due to relative motion on either side of the interface.

The combined effect of the viscous and inertial forces on the wave motion on the surface of the jet depends on the relative magnitudes of the forces. In the derivation of equation [2.38] he considered a shear velocity gradient at the interface, which has the effect of reducing the magnitude of the inertial term in the equation. Although equation [2.38] is based on the wave velocity and predicts the wave numbers to be of the same order as were measured experimentally, it has been found that the calculated growth rates were far higher than the measured growth rates. Further as can be seen in Table (8) the predicted growth rate using equation [2.38] increases with the Weber number.

If the experimental growth rates are compared with the corresponding theoretical values obtained from equations [2.20] and [2.38] the following picture can emerge: the experimental results show the same trend as one would have expected from using a stationary theory, that is to say, a constant growth rate independent of the Weber number (equation [2.20]). The experimental data indicates that the wave velocity is always lower than that of the jet velocity, and the wave number has a value around 1. These two findings alone suggested that for liquid liquid systems the wave velocity and the effect of

the physical properties of both the phases should have been included in the stationary theory in order to improve the prediction of the wave number. These two parameter were included in the present study to derive equation [5.59]. The prediction of the growth rate is given in Table (8)

The prediction of the growth rate using equation [5.59] has confirmed that the viscosity of both the phases affects the growth rate of the growing wave on the surface of the jet. The effect of the dispersed phase viscosity can be seen in the decanol/water and paraffin/water systems in Table (8). The effect of the continuous phase viscosity on the growth rate of the wave can be seen in Table (8) for the water/decanol and water/paraffin systems. In both the cases the predicted growth rates are lower than the non viscous systems and match the experimental findings. This explains the damping effect of the wave on the surface of the jet due to viscosity as we have discussed in chapter 5. Since Rayleigh only considered the physical properties of the dispersed phase his equation could not account for such variations.

Further, Rayleigh's theory predicts values of the wave number around a value of 0.696 which is lower than the experimentally measured values. The discrepancy however, should be explained. The stationary theory considered that the wave travels with the jet velocity, but Figure 24 has shown that the wave velocity is always slower than the nozzle velocity. Therefore, in the

present work the prediction of the wave number was corrected to account for the difference between the actual wave and nozzle velocities.

Hence,

$$ka_{mean} = (U/c)\, ka_{predicted} \qquad [6.4]$$

where U is the nozzle velocity and c is the wave velocity. The corrected wave numbers are presented in Table (9) where it can be seen that the experimental values are in good agreement.

The present study suggests that the wave growth rate does not depend on the jet velocity and the wave velocity is always slower than the nozzle velocity. These facts are important for predicting a fundamental drop size in the jetting regime, since the fundamental drop volume depends on the wave length of the fastest growing disturbances on the surface of the jet.

TABLE 9

COMPARISON OF EXPERIMENTAL AND PREDICTED DIMENSIONLESS WAVE NUMBER

SYSTEM	WE	EXP ka value	EQ [6.4]	EQ [2.20]	EQ [2.38]
Decane/ Water	6.0	1.05	1.160	0.696	0.91
	10.0	1.18	1.165	0.696	1.05
	20.0	1.18	1.136	0.696	1.20
Decanol /Water	6.0	0.65	1.030	0.696	0.71
	10.0	0.83	1.125	0.696	0.81
	20.0	0.86	1.262	0.696	0.93
Paraffin /Water	6.0	1.30	1.570	0.696	0.93
	10.0	1.20	1.710	0.696	1.23
	20.0	1.30	1.620	0.696	1.42
Water / Decane	6.0	1.06	0.990	0.696	0.71
	10.0	1.18	1.004	0.696	0.82
	20.0	1.20	1.312	0.696	0.96
Water / Decanol	6.0	1.41	1.360	0.696	0.61
	10.0	1.50	1.560	0.696	0.80
	20.0	1.80	1.541	0.696	1.30
Water /Paraffin	6.0	0.74	1.011	0.696	0.61
	10.0	0.80	1.130	0.696	0.73
	20.0	0.97	1.323	0.696	0.83

6.3 DROP SIZE IN THE JETTING REGIME

It is not possible to be able to explain the drop size variation on the basis of the instability theory alone, since it assumes that each fundamental wave will grow exactly in the same manner as every other fundamental wave, and should eventually lead to a break up of the jet into a stream of monosize drop with no necessary distinction between them.

The formation of distinct 'family' groupings as observed in chapter 4, provides the best clue to the possible explanation of the drop size variation in the jetting regime. The family has its own period of formation, Tg, which is always an integer multiple of the fundamental period, Tf, as can be seen in Table (3). Therefore, the group frequency, $\omega g = 2\pi/Tg$, can be compared to the beat frequency in music by the interaction of the fundamental wave with one of its harmonics. If ωf is the frequency of the fundamental wave and ωh is the frequency of the harmonic wave, then the group frequency is such that $\omega g = \omega h - \omega f$. For example, a 2N-1N family of drops with Tg = 3Tf might be formed from the interaction of the fundamental ωf with the harmonic $\omega h = 4\omega f/3$.

The qualitative picture of regular families could be explained on the basis of the interaction of the harmonic waves. However, it is still necessary to be able to characterise these patterns quantitatively. It is helpful to consider the relaxation process of the jet. Figure 26 suggests that the relaxation period, Tr, for water/decane

system is constant around a value of 6 ms while the fundamental period decreases as the flow rate increases. Therefore, a characteristic ratio Tf/Tr could be used as a criterion to relate the mean drop size in the jetting regime.

The formation of the distinct families in the early jetting regime can also be explained if we consider the interaction of the relaxing wave with that of the fundamental wave. A clear picture can emerge if we consider the growth of the fundamental wave. Tf is the time needed for the fundamental wave to grow large enough to pinch the jet at the antinode of the ultimate wave to produce a monosize stream of 1N drops. However, during the same time interval, a relaxing wave propagates backwards to interact with the fundamental wave.

Each fundamental wave could break the jet into a 1N monosize stream of drops if the relaxing and fundamental wave attain the same phase at the final antinode on the jet. Therefore, it is assumed that for an ideal situation of 1N monosize drops, Tf, should be equal to Tr.

Using the experimentally calculated value for the constant K for water into decane system as described in chapter 5, we can predict the relaxation time using equation [5.65]. The monosize stream of 1N drops will occur at a flow rate where Tf becomes equal to Tr. Replacing Tf in equation [5.63], we can estimate the critical velocity at which this stream is expected to occur. For the water into decane system this velocity was

found to be 53.5 cm/sec, which gives a critical Weber number We_m = 7.6 at which a monosize stream of IN drop is anticipated. The experimental evidence arising out of the present work and Bright (21) suggests the onset of the minimum drop size occurs around a Weber number of value8.0

The experimentally measured mean drop sizes for these families is given in Table 10. The next step is to establish the relationship between mean drop size and the characteristic ratio Tf/Tr for the family group. If D1 is the diameter of a 1N drop, D2 the diameter of a 2N drop etc, the mean drop size can be calculated for these families by adding up the numbers n_1, n_2, etc of each size of drop in each family and using the following formula ;

$$\frac{D_{32}}{D1} = [n_1 + 2n_2 + 3n_3 + ..]/[n_1 + 2^{0.67}n2 + 2^{0.67}n3 + ..] \quad [6.5]$$

To a first approximation equation [6.5] can be written as

$$\frac{D_{32}}{D_1} = [(n_1+2n_2+3n_3 + ..)/(n_1+n_2+n_3+ ...)]^{0.33} \quad [6.6]$$

or

$$\frac{D_{32}}{D_1} = [NN/ND]^{0.33} \quad [6.7]$$

For a monosize stream of 1N drops at the critical Weber number (We_m) we can write:

$$NN/ND = [Tg/Tf] = [Tf/Tr] \quad [6.8]$$

TABLE 10

EXPERIMENTAL DROP SIZE DISTRIBUTION AND VALUES OF THE RATIO Tf/Tr AT VARIOUS WEBER NUMBER FOR WATER INTO DECANE SYSTEM

S.No	WE	D32/D1	Tf/Tr
1.	1.86	1.93	3.08
2.	1.87	1.84	3.06
3.	2.73	1.58	2.26
4.	3.04	1.51	2.06
5.	3.25	1.48	1.96
6.	3.57	1.36	1.81
7.	3.66	1.32	1.71
8.	3.84	1.29	1.65
9.	4.04	1.28	1.62
10.	4.14	1.27	1.61
11.	4.19	1.22	1.60
12.	4.55	1.21	1.50
13.	4.85	1.20	1.45
14.	4.93	1.20	1.40
15.	5.29	1.19	1.30
16.	5.78	1.18	1.23

Therefore, equation [6.7] can be written as

$$\frac{D_{32}}{D_1} = [Tf/Tr]^{0.33} \qquad [6.9]$$

Now it is reasonable to assume that the fundamental period, Tf, for the fastest growing wave will depend on the Weber number. Therefore, the characteristic ratio Tf/Tr can be regarded as a function of the ratio We/We_m, where We_m is the critical Weber number at which a stream of 1N monosize drops is expected, that is the minimum drop size conditions apply. Therefore, we can write ;

$$Tf/Tr = f\,(We/We_m) \qquad [6.10]$$

Figure 43 was used to calculate the dependency of these two ratios Tf/Tr and We/We_m using Table 10. The dependency was estimated as follows

$$Tf/Tr = (We/We_m)^{-0.80} \qquad [6.11]$$

Now under the limiting case of the 1N monosize drop stream, the ratio in the equation [6.11] must be unity and using equation [6.9] we can write

$$\frac{D_{32}}{D_1} = \left([We/We_m]^{-0.80} \right)^{0.33} = [We/We_m]^{-0.47} \qquad [6.12]$$

To test equation [6.12] the mean drop size ratio against critical Weber number ratio We/We_m was plotted in Figure 44. A straight line of slope -0.50 was drawn. Thus equation [6.12] appears to possess the correct form,

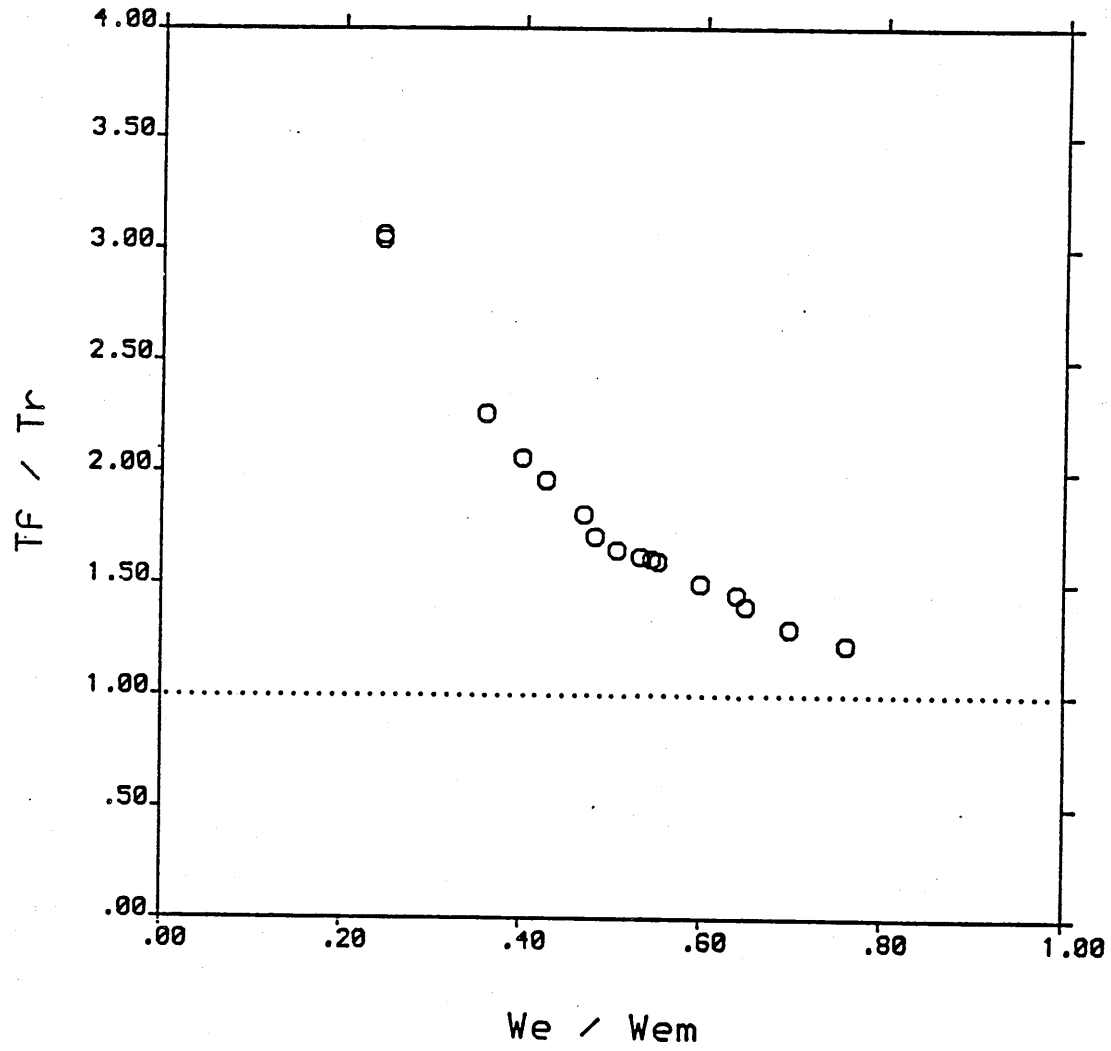

FIGURE 43 VARIATION OF THE CHARACTERISTIC RATIO WITH FLOW RATE

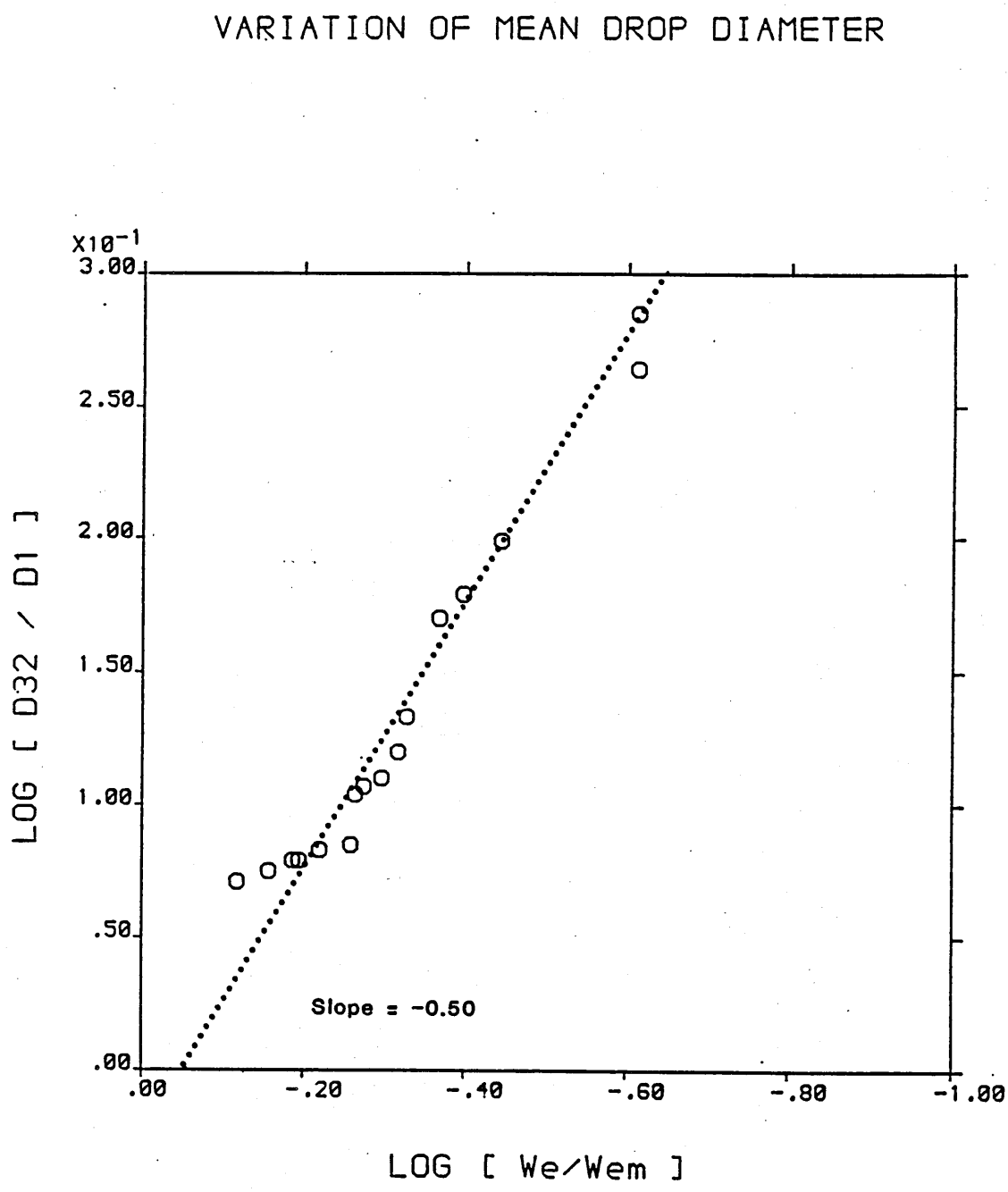

FIGURE 44 VARIATION OF MEAN DROP DIAMETER WITH FLOW RATE

which can be used to predict the mean drop size in the jetting regime up to the jet velocity where minimum drop size appears.

Considering the propagation and interaction of both the relaxing and fundamental waves on the jet one can explain the formation of a multinode drop in the intermediate regime. At a critical Weber number, where the relaxation time Tr is exactly the same as the fundamental period Tf, every fundamental wave will be in the same phase with the relaxing wave at the final antinode of the jet. The jet will break to form a one node drop due to constructive interference by every fundamental wave. But if Tr is not exactly the same as Tf then the jet might not break at the final antinode, but instead it will wait until these two waves attain the same phase again. The time these waves take to become equal in phase, determines the size of the drop.

For example, if Tf is equal to 2Tr the relaxing wave will be in the opposite phase to the fundamental wave at the final antinode and will suppress the growth of the fundamental wave; the jet will not break at this stage. The next following fundamental wave, after 2Tf, would be in the same phase and will pinch the jet to form a 2N drop. Similarly, if the Tf is equal to 3Tr then after three fundamental nodes these waves will attain the same phase and cause the jet to break to form a 3N drop. Further more, if Tr is a fraction of Tf then a combination of drops are expected depending on the Tf/Tr ratio.

CHAPTER 7

CONCLUSIONS AND RECOMMENDATIONS

In the final chapter the conclusions from the present study will be summarised. Recommendations are proposed to extend the present work in order to include aspects which have not been covered in this study.

When one liquid is injected into a second immiscible liquid through a nozzle a number of distinct regimes have been identified in the drop formation process.

7.1 DROP FORMATION REGIMES

7.1.1 PREJETTING REGIME

At low flow rates the drops of liquid grow at the nozzle tip and detach at, or close, to the nozzle. The drop's point of detachment moves increasingly away from the nozzle leaving a small residual volume of liquid at the nozzle, which becomes the seed for the growth of the next drop.

The final equation to predict the drop diameter in the prejetting condition can be written as;

$$D_d / D_n = \left[\frac{6B}{Eo} (1 + \tau) \right]^{0.33} \qquad [5.18]$$

where Eo is the Eotvos number and the values of τ and B can be calculated as given in Appendix C.

A two stage drop formation mechanism is proposed. The first stage involves a force balance on the drop

during its growth period at the nozzle. When the forces attain an equilibrium the drop leaves the nozzle and detaches from the end of a transitory liquid jet. During the second stage a new approach of the drop detachment process is proposed on the basis of the instability of the liquid column behind the drop.

The diameter and the first stage growth period of the drop decreases as the flow rate increases, while the length of the liquid column behind the drop at the time of drop detachment increases with the flow rate.The jetting starts when a flow rate is reached where the transitory liquid column behind the drop does not get time to relax towards the nozzle before a new drop start to detach.

7.1.2 JETTING REGIME

Three regimes have been identified depending on the type of the waves responsible for the eventual breakup of the jet. These regimes have been characterised by the dimensionless Weber number of the jet, We_j.

(a) $2 < We_j < 8$

This range has been given the name of "intermediate jetting regime", where the jet breaks up into families of drops of different sizes. The volumes of the individual drops are related to each other in terms of integer multiples of the fundamental minimum drop volume. The phenomenon of breakup is believed to be caused by the interaction of the fastest growing symmetrical and

relaxing wave travelling in the opposite direction on the surface of the jet.

(b) $8 < We_j < 25$

This range has been termed the "maximum jetting regime", where the length of the jet achieves its maximum value and most of the drops formed are of the minimum drop size. The jet breakup is believed to be caused by the growth of a single wave. This wave can be one of a narrow band of fast growing waves having wave length close to the fundamental wave. Within this range drop formation was irregular and no identifiable repeatable pattern was found.

(c) $We_j > 25$

This range has been given the name of "asymmetric jetting regime", where the first appearence of the asymmetric waves were observed around this Weber number. The drop sizes vary considerably due to a combination of symmetric and asymmetric wave patterns on the jet.

7.2 DROP SIZE DISTRIBUTION

The drop size varies from a maximum in the prejetting regime to a minimum in the maximum jetting regime. As the flow rate increases the mean drop size reduces in the intermediate regime, because the number of the small drops in the family increases. At the transition from intermediate to maximum jetting regimes the drop families

contain a large number of single node drops and the mean drop size approaches the minimum drop size.

7.3 WAVE PROPERTIES

A model is proposed to calculate the growth rate of the wave on the surface of the jet. The final equation used to predict the growth rate is given as;

$$\beta = (\sigma/\rho a^3)C / [A + 2qB] \qquad [5.59]$$

The dimensionless growth rate of the symmetrical waves on the surface of the jet is believed to be independent of the jet velocity. The growth rate decreases with the increasing viscosity of both the continuous and dispersed phase. The wave velocity is always less then the jet velocity and was found to satisfy the following relation.

$c = 0.60\ Uj$

7.4 RECOMMENDATIONS FOR FUTURE WORK

In the prejetting regime, the residual volume is an important parameter to be predicted accurately, in order to improve the overall drop volume prediction. To this end, more experimental information is required in order to consider the right geometry of the liquid column left behind the drop at the time of detachment. The present model assumed that during the first stage growth of the drop at the nozzle, the surface tension force adjusts itself until it reaches its maximum value, to keep the

velocity of the drop constant. To test the validity of the assumption further information about the changing behaviour of the surface tension force during the drop formation process is required. One way to achieve this is to measure the inner and the outer radii of curvature of the drop during the formation process. It would also be useful to have more information about the necking in process.

In the jetting regime, theories of instability are a long way in advance of the necessary experimental verification. Thus more direct experimental measurements of the primary variables which influence drop size, are needed. This calls for more measurements of the growth rates and wave properties of the fundamental wave on the surface of the jet. Fourier analysis of the changing wave profile might be helpful in explaining the interaction of the fundamental wave near the point of breakup.

Further to this, an extension of the results from a single to a multiple nozzle would be of direct practical importance to various chemical and biochemical industries.

The present work holds a great potential with regards to the design and development of new contacting equipment, where it is desirable to have a maximum interfacial area in order to improve the efficiency. The present work could also be adopted to produce monosize drops for various industrial applications.

BIBLIOGRAPHY

1. Harkins,W.D and Brown,F.E
Amer. Chem. Soc, 41, 499, 1919.

2. Hayworth,C.B and Treybal,R.E
Ind. Eng. Chem, 42, 1174, 1950.

3. Null,H.R and Johnson,H.F
AIChE Journal, 4, 273, 1958.

4. Meister,B.J and Sheele,G.F
AIChE Journal, 14, 9, 1968.

5. Chazal,L.E.M and Ryan,J.T
AIChE Journal, 17,1226, 197 .

6. Kumar,A and Hartland,S
Trans. IChemE Journal, 60, 35, 1982.

7. Smith,S.W and Moss,H
Proc. Roy. Soc. A93, 373, 1917.

8. Fujinawa,K; Maruyama,T and Nakaike,Y
Kagaku Kikai 21, 194, 1957.

9. Rayleigh,Lord
Proc. Lon. Math. Soc, 10, 4, 1879.

10. Tyler,E
Phil. Mag, 16, 504, 1933.

11. Keith,F.W and Hixson,A.N
Ind. Eng. Chem, 47, 258, 1955.

12. Christiansen,R.N and Hixson.A.N
Ind. Eng. Chem. 49, 1017, 1957.

13. Treybal,R.E
Liquid Extraction 2nd Ed. McGraw Hill. 1963

14. Skelland,A.H.P and Johnson,K.R
Can. J Chem. Eng. 52, 732, 1974.

15. Ryan, J T
PhD Thesis, University of Missouri 1965.

16. Rayleigh,Lord
Phil. Mag, 34, 145, 1892.

17. Weber,C
Z Angew Math Mech. 11, 136, 1931.

18. Tomotika,S
Proc. Roy. Soc, A150, 322. 1935.

19. Meister,B.J
PhD Thesis, Cornell University, NY 1966

20. Meister,B.J and Sheele,G.F
AIChE Journal 15, 701, 1969.

21. Bright,A
PhD Thesis, The Open University, U.K. 1984

22. Horvath,M; Steiner,L and Hartland,S
Can. J Chem.Eng 15, 9, 1978.

23. Van den Akker,H.E.A
Chem. Eng. Journal 19, 255, 1980.

24. Bright,A
ISEC 1982

25. Kitamura,Y., Mishima,H and Takahashi,T.
Can J Chen Eng 60, 723, 1978.

26. Lamb,H
'HYDRONAMICS' Dover Publications Inc. New York.

LIST OF SYMBOLS

a	Jet radius cm
a_0	Nozzle radius cm
c	Wave velocity = λ/τ = ω/k cm/s
$\tilde{c}$	Dimensionless wave velocity = c/U
d_j	Jet diameter cm
d_{jm}	Jet diameter at U_m cm
D_n	Nozzle diameter cm
D_d	Static drop diameter cm
D_1	Drop diameter of 1-N drop = D_m cm
D_m	Minimum drop diameter cm
D_{32}	Mean drop diameter (Sauter mean) cm
Eö	Eotvos number = $g\Delta\rho D_n^2/\sigma$
F_b	Buoyancy force N
F_m	Momemtum force N
F_s	Surface tension force N
F_p	Excess pressure force N
Fr	Froude number = $U_n/(D_n g)^{0.5}$
g	Acceleration of gravity, 9.81 m s^{-2}
h	Vibration mode number
i	Square root of -1
$I_h(x)$	Modified Bessel function of first kind of order h
$I'_h(x)$	Derivative of $I_h(x)$
I^*	$I_0(ka)/I_1(ka)$
$I^\bullet$	$\tilde{k}I^* - 1$
I^+	$\tilde{k}/I^\bullet$

I^o	$\tilde{k}I^+ - 1$
k	Wave number $= 2\pi/\lambda$ cm^{-1}
ka	Dimensionless wave number $= \tilde{k}$
ka_{max}	Wave number of the fastest growing wave cm^{-1}
$K_h(x)$	Modified Bessel function of the second kind of order h
$K_h'(x)$	Derivative of $K_h(x)$
K^*	$K_0(ka)/K_1(ka)$
$K^\bullet$	$\tilde{k}K^* + 1$
K^+	$\tilde{k}/K^\bullet$
K^o	$\tilde{k}K^+ - 1$
L	Jet length cm
L_k	Maximum jet length cm
m	ratio of viscosities (μ_c/μ_d)
ND	Number of drops in a family
NN	Number of nodes in a family
n_i	Number of drops of diameter D_i
p	Pressure mPa
$\tilde{p}$	pa_o/σ
q	Damping coefficient = $\upsilon k/a\beta$
Q	Volumetric flowrate through nozzle ml/s
r	Radial distance cm
$\tilde{r}$	r/a_o
Re	Reynold Number
s	Ratio of densities (ρ_c/ρ_d)
Tf	wave period of fundamental wave s
Tr	wave period of relaxing wave s
t	Time s

t_g	Growth time for fundamental wave to break the jet
U_n	Nozzle velocity cm/s
U_m	Nozzle velocity at minimum drop size condition cm/s
U_I	Interfacial velocity cm/s
U_A	Average jet velocity cm/s
U_j	jetting velocity cm/s
U_m'	Jet velocity at minimum drop size conditions cm/s
U_k	Jet velocity at Maximum jet length cm/s
u_r	Velocity component, r-direction
u_θ	Velocity component, θ-direction
u_z	Velocity component, z-direction
U	Axial velocity cm/s
$\tilde{U}$	U/U_n
$\bar{U}$	$\hat{U}/U$
V_d	Drop volume ml
V_f	Final drop volume in prejetting conditions ml
V_F	Fundamental drop volume ml
We	Weber number = $\rho U_n^2 D_n/\sigma$
We_j	Weber number at U_j
We_m	Weber number at U_m
z	Axial distance cm
Z	Ohnesorge number = $\mu/(\rho D_n \sigma)^{0.5}$
Z_c	Ohnesorge number of continuous phase
Z_j	Ohnesorge number of jet phase

LIST OF GREEK SYMBOLS

α	Growth rate of disturbance = $\beta - i\omega$, s^{-1}
β	Real part of α , s^{-1}
η	Disturbance amplitude = $\eta_o e^{\alpha t + i(kz + h\theta)}$, cm
η_o	Initial disturbance amplitude
λ	Wave length , cm
μ	Viscosity, mPa s
ν	kinematic viscosity cm^2/s
π	p^o/ρ
π'	$d\pi/dr$
π''	$d^2\pi/dr2$
ρ	Density , kg/m^3
$\Delta\rho$	Density difference
σ	interfacial tension , N
τ	Wave period , s
τ_n	Normal stress N/m^2
ω	Wave frequency, s^{-1}

SUBSCRIPTS

m	pertaining to fastest growing disturbance
i	pertaining to interface conditions
j	pertaining to jet conditions
n	pertaining to nozzle condition

SUPERSCRIPTS

~	Dimensionless variable
^	Continuous phase
'	Derivative with respect to r
•	Derivative with respect to z
o	fluctuating component (small scale motion)

APPENDIX A

EXPERIMENTAL DATA FOR DROP FORMATION IN PREJETTING CONDITIONS

SYMBOLS USED IN THE APPENDIX

H_t	Drop top edge
H_n	Drop neck
B	Drop expansion
V_t	Total volumetric flow
V_n	Volume of the cylinder
V_d	Volume of the drop
D_d	Drop diameter
F_b	Buoyancy force
F_m	Momentum force
F_s	Surface tension force
U_t	Drop top edge velocity
U_n	Drop neck rise velocity

TABLE 1

SYSTEM: WATER INTO DECANE D0 = 0.0602 cm Q = 0.044 cc/sec Un = 15.45 cm/sec WE = 0.0590

S.No	Time sec	H_t cm	H_n cm	B cm	V_t cc	V_n cc	V_d cc	D cm	F_b	F_m	F_s	U_t cm/sec	U_n cm/sec
1.	.000	.128	.128	.120	.00036	.000363	0.0000	.000	0.096	0.679		1.501	0.000
2.	.010	.135	.000	.135	.00081	.000000	0.0008	.118	0.211	0.679		1.501	0.000
3.	.020	.150	.000	.150	.001124	.000000	0.0012	.136	0.327	0.679		1.501	0.000
4.	.030	.165	.000	.165	.00168	.000000	0.0017	.150	0.443	0.679		1.501	0.000
5.	.040	.180	.000	.180	.00212	.000000	0.0021	.162	0.558	0.679		1.501	0.000
6.	.050	.195	.000	.185	.00256	.000000	0.0026	.173	0.674	0.679		0.750	0.000
7.	.060	.203	.000	.190	.00300	.000000	0.0030	.182	0.790	0.679		0.750	0.000
8.	.070	.210	.000	.195	.00344	.000000	0.0034	.191	0.905	0.679		0.750	0.000
9.	.080	.218	.000	.199	.00388	.000000	0.0039	.198	1.021	0.679		0.750	0.000
10.	.090	.225	.000	.204	.00432	.000000	0.0043	.205	1.137	0.679		0.750	0.000
11.	.100	.233	.000	.209	.00476	.000000	0.0048	.212	1.252	0.679		0.750	0.000
12.	.110	.240	.000	.214	.00520	.000000	0.0052	.218	1.368	0.679		0.750	0.000
13.	.120	.248	.000	.219	.00564	.000000	0.0056	.224	1.484	0.679		0.750	0.000
14.	.130	.255	.000	.223	.00602	.000000	0.0061	.230	1.599	0.679		0.750	0.000
15.	.140	.263	.000	.228	.00652	.000000	0.0065	.235	1.715	0.679		0.750	0.000
16.	.150	.270	.000	.233	.00696	.000000	0.0070	.240	1.831	0.679		0.750	0.000
17.	.160	.278	.000	.238	.00740	.000000	0.0074	.245	1.946	0.679		0.750	0.000
18.	.170	.285	.000	.243	.00784	.000000	0.0078	.250	2.062	0.679		0.750	0.000
19.	.180	.293	.000	.247	.00828	.000000	0.0083	.255	2.178	0.679		0.750	0.000
20.	.190	.300	.000	.253	.00872	.000000	0.0087	.259	2.293	0.679		0.750	0.000
21.	.200	.308	.000	.257	.00916	.000000	0.0092	.263	2.409	0.679		0.750	0.000
22.	.210	.315	.000	.262	.00960	.000000	0.0096	.267	2.525	0.679		0.750	0.000

TABLE 1 CONTINUED .....

S.No	Time sec	H_t cm	H_n cm	B cm	V_t cc	V_n cc	V_d cc	D cm	F_b	F_m	F_s	U_t cm/sec	U_n cm/sec
23.	.220	.323	.000	.267	.01004	.000000	0.0100	.271	2.640	0.679		0.750	0.000
24.	.230	.330	.000	.271	.01048	.000000	0.0105	.275	2.756	0.679		0.750	0.000
25.	.240	.338	.000	.276	.01092	.000000	0.0109	.279	2.872	0.679		0.600	0.000
26.	.250	.344	.000	.281	.01136	.000000	0.0114	.283	2.987	0.679		0.600	0.000
27.	.260	.350	.000	.286	.01180	.000000	0.0118	.286	3.103	0.679		0.600	0.000
28.	.270	.356	.000	.291	.01224	.000000	0.0122	.290	3.219	0.679		0.450	0.000
29.	.280	.360	.000	.295	.01268	.000000	0.0127	.293	3.335	0.679		0.450	0.000
30.	.290	.365	.000	.300	.01312	.000000	0.0131	.296	3.458	0.679	4.255	0.450	0.150
31.	.300	.369	.002	.305	.01356	.000043	0.0136	.299	3.566	0.679	4.255	0.300	0.150
33.	.310	.372	.003	.310	.01400	.000085	0.0140	.303	3.682	0.679	4.255	0.300	0.300
33.	.320	.375	.006	.315	.01444	.000171	0.0144	.306	3.797	0.679	4.255	0.300	0.300
34.	.330	.378	.009	.320	.01488	.000256	0.0149	.309	3.913	0.679	4.255	0.300	0.300
35.	.340	.381	.012	.324	.01532	.000342	0.0153	.312	4.029	0.679	4.255	0.300	0.300
36.	.350	.384	.015	.327	.01576	.000427	0.0157	.314	4.144	0.679	4.255	0.750	0.750
37.	.360	.392	.023	.330	.01620	.000641	0.0161	.317	4.260	0.679	4.255	0.750	0.750
38.	.370	.399	.030	.333	.01664	.000855	0.0166	.320	4.376	0.679	4.255	0.750	0.750
39.	.380	.407	.038	.336	.01708	.001060	0.0170	.323	4.491	0.679	4.255	0.750	0.750
40.	.390	.414	.045	.338	.01752	.001282	0.0174	.325	4.607	0.679	4.255	1.801	1.501
41.	.400	.432	.060	.338	.01796	.001709	0.0178	.328	4.723	0.679	4.255	3.003	3.003
42.	.410	.462	.090	.339	.01840	.002564	0.0181	.330	4.838	0.679	4.255	3.303	3.003
43.	.420	.495	.120	.339	.01884	.003419	0.0185	.332	4.954	0.679	4.255	3.303	3.003

TABLE 2

SYSTEM: WATER INTO DECANE D0 = 0.0602 cm Q = 0.057 cc/sec Un = 20.02 cm/sec WE = 1.0719

S.No	Time sec	H_t cm	H_n cm	B cm	V_t cc	V_n cc	V_d cc	D cm	F_b	F_m	F_s	U_t cm/sec	U_n cm/sec
1.	.000	.150	.150	.128	.00043	.000427	0.0000	.000	0.112	1.140		1.501	0.000
2.	.010	.165	.000	.135	.00100	.000000	0.0000	.127	0.262	1.140		1.501	0.000
3.	.020	.180	.000	.150	.00157	.000000	0.0016	.147	0.412	1.140		1.501	0.000
4.	.030	.195	.000	.165	.00214	.000000	0.0021	.163	0.562	1.140		1.501	0.000
5.	.040	.210	.000	.180	.00271	.000000	0.0027	.176	0.712	1.140		1.501	0.000
6.	.050	.225	.000	.195	.00328	.000000	0.0033	.187	0.862	1.140		1.501	0.000
7.	.060	.240	.000	.201	.00385	.000000	0.0038	.198	1.012	1.140		1.501	0.000
8.	.070	.255	.000	.207	.00442	.000000	0.0042	.207	1.161	1.140		1.501	0.000
9.	.080	.270	.000	.212	.00499	.000000	0.0050	.215	1.311	1.140		1.501	0.000
10.	.090	.285	.000	.218	.00556	.000000	0.0056	.223	1.462	1.140		1.501	0.000
11.	.100	.300	.000	.224	.00613	.000000	0.0061	.230	1.611	1.140		0.750	0.000
12.	.110	.308	.000	.230	.00670	.000000	0.0067	.237	1.761	1.140		0.750	0.000
13.	.120	.315	.000	.236	.00727	.000000	0.0073	.244	1.911	1.140		0.750	0.000
14.	.130	.323	.000	.242	.00784	.000000	0.0078	.250	2.061	1.140		0.750	0.000
15.	.140	.330	.000	.248	.00841	.000000	0.0084	.256	2.210	1.140		0.750	0.000
16.	.150	.338	.000	.254	.00898	.000000	0.0090	.261	2.360	1.140		0.750	0.000
17.	.160	.345	.000	.260	.00955	.000000	0.0095	.267	2.510	1.140		0.750	0.000
18.	.170	.353	.000	.266	.01012	.000000	0.0101	.272	2.660	1.140		0.750	0.000
19.	.180	.360	.000	.273	.01069	.000000	0.0107	.277	2.810	1.140		0.750	0.000
20.	.190	.368	.000	.278	.01126	.000000	0.0113	.282	2.960	1.140	4.255	0.750	0.075

TABLE 2 CONTINUED ...

S.No	Time sec	H_t cm	H_n cm	B cm	V_t cc	V_n cc	V_d cc	D cm	F_b	F_m	F_s	U_t cm/sec	U_n cm/sec
21.	.200	.375	.001	.284	.01183	.000002	0.0118	.286	3.110	1.140	4.255	0.750	0.075
22.	.210	.383	.002	.290	.01240	.000004	0.0124	.291	3.259	1.140	4.255	0.750	0.075
23.	.220	.390	.002	.296	.01297	.000006	0.0130	.295	3.409	1.140	4.255	0.750	0.525
24.	.230	.398	.008	.303	.01123	.000021	0.0135	.299	3.559	1.140	4.255	1.201	0.750
25.	.240	.410	.015	.310	.01190	.000042	0.0141	.303	3.709	1.140	4.255	1.501	1.501
26.	.250	.425	.030	.313	.01257	.000085	0.0146	.307	3.859	1.140	4.255	2.252	2.252
27.	.260	.447	.053	.316	.01324	.000149	0.0151	.310	4.009	1.140	4.255	2.852	2.252
28.	.270	.476	.075	.319	.01391	.000213	0.0156	.314	4.159	1.140	4.255	4.504	3.003
29.	.280	.521	.105	.320	.01445	.000299	0.0161	.317	4.308	1.140	4.255	4.692	7.507
30.	.288	.559	.165	.321		.000470	0.0164	.319	4.428	1.140	4.255	4.692	7.507

TABLE 3

SYSTEM: WATER INTO DECANE D0 = 0.0602 cm Q = 0.067 cc/sec Un = 23.53 cm/sec WE = 1.4810

S.No	Time sec	H_t cm	H_n cm	B cm	V_t cc	V_n cc	V_d cc	D cm	F_b	F_m	F_s	U_t cm/sec	U_n cm/sec
1.	.000	.180	.180	.120	.00051	.000512	0.0000	.000	0.000	1.576		0.000	0.000
2.	.010	.180	.000	.135	.00118	.000000	0.0012	.134	0.311	1.576		1.501	0.000
3.	.020	.195	.000	.150	.00185	.000000	0.0019	.155	0.487	1.576		1.501	0.000
4.	.030	.210	.000	.165	.00252	.000000	0.0025	.172	0.663	1.576		1.501	0.000
5.	.040	.225	.000	.180	.00319	.000000	0.0032	.186	0.839	1.576		1.501	0.000
6.	.050	.240	.000	.195	.00386	.00000	0.0039	.198	1.016	1.576		1.501	0.000
7.	.060	.255	.000	.203	.00453	.00000	0.0045	.209	1.192	1.576		1.501	0.000
8.	.070	.270	.000	.210	.00520	.00000	0.0052	.218	1.368	1.576		1.501	0.000
9.	.080	.285	.000	.218	.00587	.00000	0.0059	.227	1.544	1.576		1.501	0.000
10.	.090	.300	.000	.225	.00654	.00000	0.0065	.235	1.720	1.576		1.501	0.000
11.	.100	.315	.000	.233	.00721	.00000	0.0072	.243	1.896	1.576		1.501	0.000
12.	.110	.330	.000	.240	.00788	.00000	0.0079	.250	2.072	1.576		1.501	0.000
13.	.120	.345	.000	.248	.00855	.00000	0.0086	.257	2.249	1.576		1.501	0.000
14.	.130	.360	.000	.255	.00922	.00000	0.0092	.264	2.425	1.576		1.501	0.000
15.	.140	.375	.000	.263	.00989	.00000	0.0099	.270	2.601	1.576	4.255	1.501	0.000
16.	.150	.390	.008	.270	.01056	.00002	0.0105	.276	2.777	1.576	4.255	1.501	0.750
17.	.160	.405	.018	.278	.01123	.00005	0.0112	.281	2.953	1.576	4.255	1.411	1.051
18.	.170	.423	.038	.285	.01190	.00010	0.0118	.286	3.129	1.576	4.255	1.801	1.952
19.	.180	.445	.060	.293	.01257	.00017	0.0124	.291	3.306	1.576	4.255	2.252	2.252
20.	.190	.470	.092	.300	.01324	.00026	0.0130	.295	3.482	1.576	4.255	2.492	3.153
21.	.200	.511	.132	.315	.01391	.00037	0.0135	.299	3.658	1.576	4.255	4.054	4.054
22.	.208	.571	.176	.316	.01445	.00050	0.0139	.302	3.799	1.576	4.255	7.507	5.443

APPENDIX B

EXPERIMENTAL DATA ON WAVE PROPERTIES FOR VARIOUS SYSTEMS

SYMBOLS USED IN THE APPENDIX

A - Growth rate

B - Dimensionless growth rate

D_o - Nozzle diameter

ρ_c - Continuous phase density

ρ_d - Dispersed phase density

μ_c - Continuous phase viscosity

μ_d - Dispersed phase viscosity

σ - Surface tension

U_n - Nozzle velocity

We - Weber Number

JL Jet length

CVE - Exp. wave velocity

DIM - Dimensionless group

SYSTEM : DECANE INTO WATER

Do = 0.0602 cm ρ_c = 0.999 ρ_d = 0.732 μ_c = 0.011 μ_d = .009 σ = 22.5

SET 1

Un =56.0cm/sec WE = 6.14 JL = 0.65cm CVE = 27.5cm/sec DIM = 1013

S.No	Dist from nozzle Y in cm	Ave. Peak Amp in cm	Log(Ave. Peak Amp)
1.	0.14811	0.000642	-7.3536
2.	0.24680	0.000471	-7.6664
3.	0.35056	0.001939	-6.8189
4.	0.40018	0.002967	-5.8275
5.	0.44595	0.007226	-4.9390
6.	0.49895	0.008565	-4.7696
7.	0.50798	0.010764	-4.5315
8.	0.60026	0.011795	-4.4406
9.	0.65000	0.013980	-4.2762

A = 229 B = A/DIM = 0.2262

SET 2

Un = 72.0cm/sec WE = 10.15 JL = 1.25cm CVE = 43.6cm/sec DIM = 916

S.No	Dist from nozzle Y in cm	Ave. Peak Amp in cm	Log(Ave. Peak Amp)
1.	0.85575	0.002754	-5.8946
2.	0.92221	0.003625	-5.6199
3.	0.95843	0.004339	-5.4404
4.	1.00960	0.006243	-5.0763
5.	1.05860	0.007459	-4.9055
6.	1.10790	0.007694	-4.8672
7.	1.15840	0.008401	-4.7793
8.	1.20800	0.011201	-4.4917
9	1.25000	0.011621	-4.4549

A = 207 B = A/DIM = 0.2259

SET 3

Un = 98.0cm/sec WE = 18.81 JL = 2.4cm CVE = 59.17cm/sec DIM = 843

S.No	Dist from nozzle Y in cm	Ave. Peak Amp in cm	Log(Ave. Peak Amp)
1.	2.20150	0.007084	-4.9542
2.	2.25150	0.008738	-4.7482
3.	2.29960	0.009279	-4.6873
4.	2.34930	0.010998	-4.5114
5.	2.40030	0.012130	-4.4126

A = 189 B = A/DIM = 0.2241

SYSTEM : DECANOL INTO WATER

Do = 0.0602 cm ρ_c = 0.999 ρ_d = 0.836 μ_c = 0.015 μ_d =0.18 σ= 6.9

SET 1
Un = 19.2cm/sec WE = 5.98 JL = 0.90cm CVE = 12.8cm/sec DIM = 438

S.No	Dist from nozzle Y in cm	Ave. Peak Amp in cm	Log(Ave. Peak Amp)
1.	0.50759	0.002579	-5.9617
2.	0.60611	0.007828	-4.8596
3.	0.70421	0.011678	-4.4545
4.	0.80429	0.008246	-4.7983
5.	0.90000	0.023190	-3.7647

A = 78 B = A/DIM = .1777

SET 2
Un = 24.8cm/sec WE = 9.98 JL = 1.05cm CVE = 13.7cm/sec DIM = 405

S.No	Dist from nozzle Y in cm	Ave. Peak Amp in cm	Log(Ave. Peak Amp)
1.	0.75057	0.006360	-5.1112
2.	0.84894	0.007129	-4.9660
3.	0.94634	0.014264	-4.2595
4.	0.99912	0.019448	-3.9481
5.	1.05000	0.024079	-3.7244

A = 73.8 B = A/DIM = 0.1822

SET 3
Un = 35.0cm/sec WE = 19.89 JL = 1.95cm CVE = 19.3cm/sec DIM = 359

S.No	Dist from nozzle Y in cm	Ave. Peak Amp in cm	Log(Ave. Peak Amp)
1.	1.6016	0.010672	-4.5530
2.	1.7002	0.013420	-4.3110
3.	1.8001	0.018006	-4.0171
4.	1.8507	0.021927	-3.8257
5.	1.8990	0.027051	-3.6139
6.	1.9500	0.026252	-3.6420

A = 64.5 B = A/DIM = 0.1796

SYSTEM : PARAFFIN INTO WATER

Do = 0.0602 cm ρ_c = 0.999 ρ_d = 0.882 μ_c = 0.015 μ_d = .102 σ = 27.5

SET 1
Un = 52.0cm/sec WE = 5.22 JL = 0.85cm CVE = 23.3cm/sec DIM = 845

S.No	Dist from nozzle Y in cm	Ave. Peak Amp in cm	Log(Ave. Peak Amp)
1.	0.55097	0.004296	-5.4512
2.	0.60071	0.005247	-5.2554
3.	0.64995	0.006156	-5.0963
4.	0.70079	0.007083	-4.9560
5.	0.74992	0.009466	-4.6673
6.	0.79996	0.014696	-4.2210
7.	0.85000	0.018169	-4.0028

A = 150 B = A/DIM = 0.1780

SET 2
Un = 74.5cm/sec WE = 10.7 JL = 1.30cm CVE = 30.0cm/sec DIM = 829

S.No	Dist from nozzle Y in cm	Ave. Peak Amp in cm	Log(Ave. Peak Amp)
1.	0.905521	0.007153	-4.9439
2.	1.053310	0.012548	-4.5802
3.	1.149470	0.015422	-4.1763
4.	1.200580	0.018297	-4.0012
5.	1.251460	0.021927	-3.8269
6.	1.300000	0.026252	-3.6406

A = 147 B = A/DIM = 0.1773

SET 3
Un = 105.5cm/sec WE = 21.49 JL = 2.20cm CVE = 45.1cm/sec DIM = 698

S.No	Dist from nozzle Y in cm	Ave. Peak Amp in cm	Log(Ave. Peak Amp)
1.	1.9020	0.008829	-4.7276
2.	2.0015	0.010357	-4.5708
3.	2.0524	0.011562	-4.4616
4.	2.1027	0.013296	-4.3275
5.	2.1505	0.014698	-4.2254
6.	2.2000	0.016082	-4.1306

A = 121 B = A/DIM = 0.1733

SYSTEM : WATER INTO DECANE

Do = 0.0602 cm ρ_c = 0.732 ρ_d = 0.999 μ_c = 0.009 μ_d = .011 σ = 22.5

SET 1

Un = 47.3cm/sec WE = 5.98 JL = 0.70cm CVE = 33.3cm/sec DIM = 924

S.No	Dist from nozzle Y in cm	Ave. Peak Amp in cm	Log(Ave. Peak Amp)
1.	0.25546	0.000496	-7.6255
2.	0.35319	0.001281	-6.6622
3.	0.45341	0.001490	-6.5356
4.	0.50371	0.004087	-5.5002
5.	0.55545	0.005742	-5.1585
6.	0.60494	0.007226	-4.9346
7.	0.65380	0.019259	-4.5887
8.	0.70000	0.013842	-4.2884

A = 254 B = A/DIM = 0.2753

SET 2

Un = 61.2cm/sec WE = 10.0 JL = 1.60cm CVE = 42.2cm/sec DIM = 917

S.No	Dist from nozzle Y in cm	Ave. Peak Amp in cm	Log(Ave. Peak Amp)
1.	1.301521	0.005165	-5.1354
2.	1.399310	0.007299	-4.9223
3.	1.490970	0.010567	-4.5537
4.	1.499680	0.012525	-4.3825
5.	1.550560	0.013847	-4.2856
6.	1.600000	0.059228	-4.1468

A = 248 B = A/DIM = 0.2704

SET 3

Un = 86.55cm/sec WE = 20.02 JL = 3.00cm CVE = 459.2m/sec DIM = 804

S.No	Dist from nozzle Y in cm	Ave. Peak Amp in cm	Log(Ave. Peak Amp)
1.	2.8055	0.012779	-4.3680
2.	2.8562	0.011108	-4.5016
3.	2.9079	0.013334	-4.4821
4.	2.9545	0.015922	-4.1411
5.	3.0000	0.016739	-4.0977

A = 200 B = A/DIM = 0.2487

SYSTEM : WATER INTO DECANOL

Do = 0.0602 cm ρ_c = 0.836 ρ_d = 0.999 μ_c = 0.180 μ_d = .015 σ = 6.90

SET 1
Un = 17.2cm/sec WE = 5.73 JL = 0.75cm CVE = 8.80cm/sec DIM = 384

S.No	Dist from nozzle Y in cm	Ave. Peak Amp in cm	Log(Ave. Peak Amp)
1.	0.24196	0.001080	-6.8301
2.	0.25564	0.001821	-6.7449
3.	0.35625	0.002554	-5.9763
4.	0.45467	0.004797	-5.3493
5.	0.55195	0.007012	-4.9631
6.	0.65419	0.009377	-4.6722
7.	0.75000	0.011108	-4.5017

A = 64.4 B = A/DIM = 0.1677

SET 2
Un = 22.2cm/sec WE = 9.56 JL = 1.15cm CVE = 9.92cm/sec DIM = 341

S.No	Dist from nozzle Y in cm	Ave. Peak Amp in cm	Log(Ave. Peak Amp)
1.	0.772301	0.002469	-6.0067
2.	0.852000	0.003926	-5.5439
3.	0.958210	0.004748	-5.3533
4.	1.150000	0.010985	-4.5162

A = 59.3 B = A/DIM = 0.1739

SET 3
Un = 32.25cm/sec WE = 20.11 JL = 2.00cm CVE = 14.12m/sec DIM = 304

S.No	Dist from nozzle Y in cm	Ave. Peak Amp in cm	Log(Ave. Peak Amp)
1.	1.50561	0.004700	-5.3690
2.	1.60619	0.005092	-5.2819
3.	1.70640	0.007504	-4.8626
4.	1.80675	0.007306	-4.9192
5.	1.90675	0.010462	-4.5610
6.	2.00000	0.011562	-4.4690

A = 52.0 B = A/DIM = 0.1710

SYSTEM : WATER INTO PARAFFIN

Do = 0.0602 cm ρ_c = 0.882 ρ_d = 0.999 μ_c = 0.102 μ_d = .015 σ = 27.5

SET 1
Un = 52.3cm/sec WE = 5.98 JL = 1.40cm CVE = 36.0cm/sec DIM = 865

S.No	Dist from nozzle Y in cm	Ave. Peak Amp in cm	Log(Ave. Peak Amp)
1.	0.73901	0.002112	-6.1659
2.	0.83895	0.002091	-6.1788
3.	0.93782	0.004086	-5.5001
4.	1.03827	0.006036	-5.1173
5.	1.14165	0.007592	-4.8853
6.	1.23659	0.009757	-4.6385
7.	1.33480	0.012038	-4.4283
8.	1.40000	0.013704	-4.2938

A = 141 B = A/DIM = 0.1630

SET 2
Un = 67.5cm/sec WE = 9.99 JL = 1.90cm CVE = 41.7cm/sec DIM = 840

S.No	Dist from nozzle Y in cm	Ave. Peak Amp in cm	Log(Ave. Peak Amp)
1.	1.403801	0.003588	-5.6382
2.	1.503300	0.005790	-5.1509
3.	1.603710	0.008066	-4.8232
4.	1.704600	0.010254	-4.7020
5.	1.801200	0.010254	-4.5838
6.	1.900000	0.014407	-4.2470

A = 136 B = A/DIM = 0.1619

SET 3
Un = 95.55cm/sec WE = 19.91 JL = 3.00cm CVE = 50.02m/sec DIM = 694

S.No	Dist from nozzle Y in cm	Ave. Peak Amp in cm	Log(Ave. Peak Amp)
1.	2.50351	0.005390	-5.2226
2.	2.60149	0.008069	-4.8200
3.	2.70240	0.008004	-4.8289
4.	2.79915	0.007446	-4.9003
5.	2.89895	0.010352	-4.5720
6.	3.00000	0.014122	-4.2655

A = 113 B = A/DIM = 0.1628

APPENDIX C

PREDICTION OF DROP DIAMETER AT LOW FLOW RATES

The drop diameter in the prejetting condition can be predicted using equation 5.18 provided the values of τ, B and Eö are known. These values can be estimated as follows :

1. Measure flow rate of liquid through the nozzle. Q
2. Calculate nozzle velocity, $Un = 4Q/\pi Dn^2$
3. Calculate Weber number, $We = \rho Un^2 Dn/\sigma$
4. Calculate Eotvos number, $Eö = g\Delta\rho Dn/\sigma$
5. Calculate Vo/Vs using Figure A.
6. Calculate B =(1 - We/4 - Vo/Vs)
7. Calculate L/Dn using Figure B
8. Calculate τ using equation 5.17
9. Put values of τ , B and Eö in equation 5.18 to predict the drop diameter in prejetting conditions.

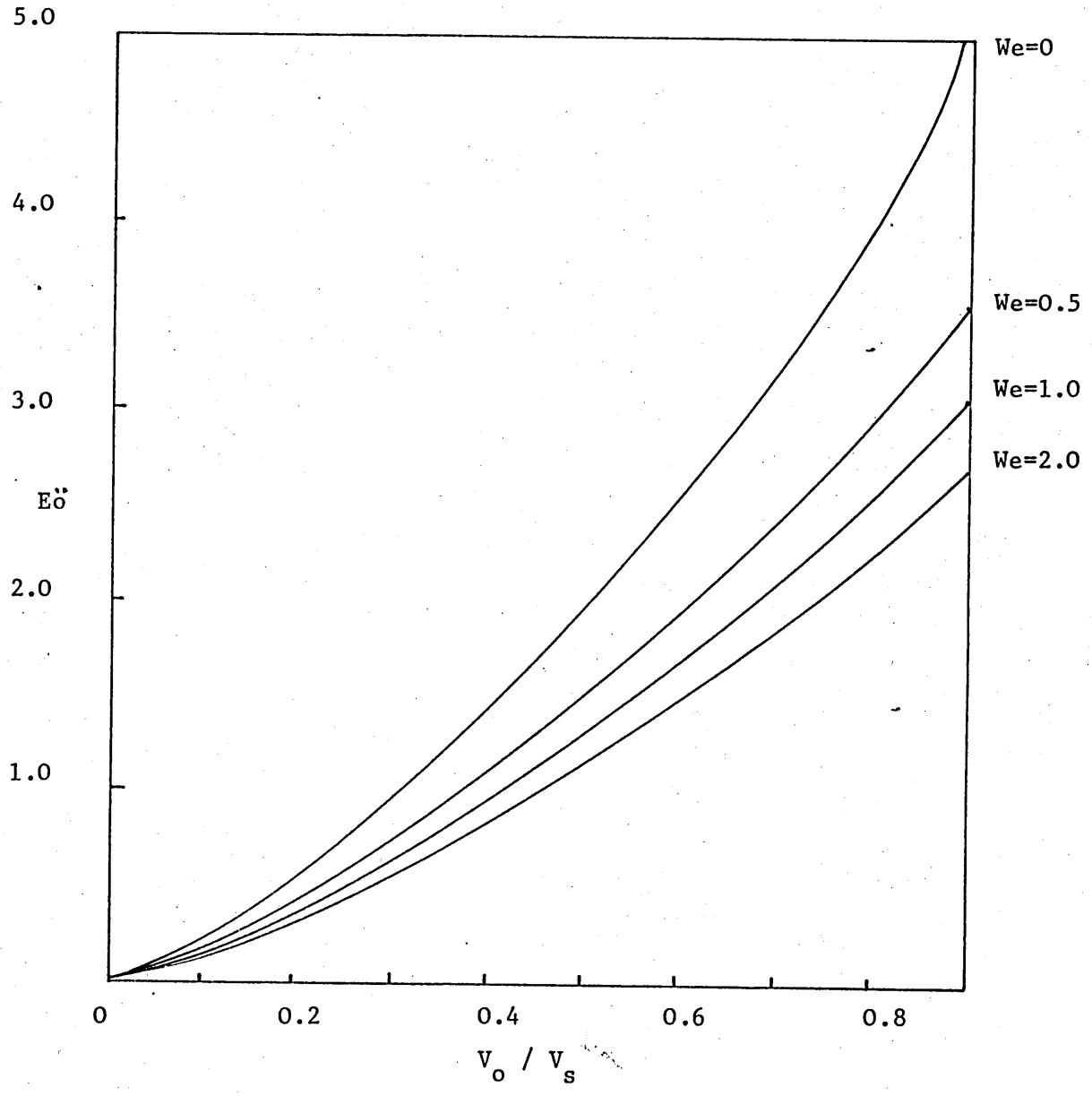

FIGURE A

Relationship between Vo/Vs and Eö at various We

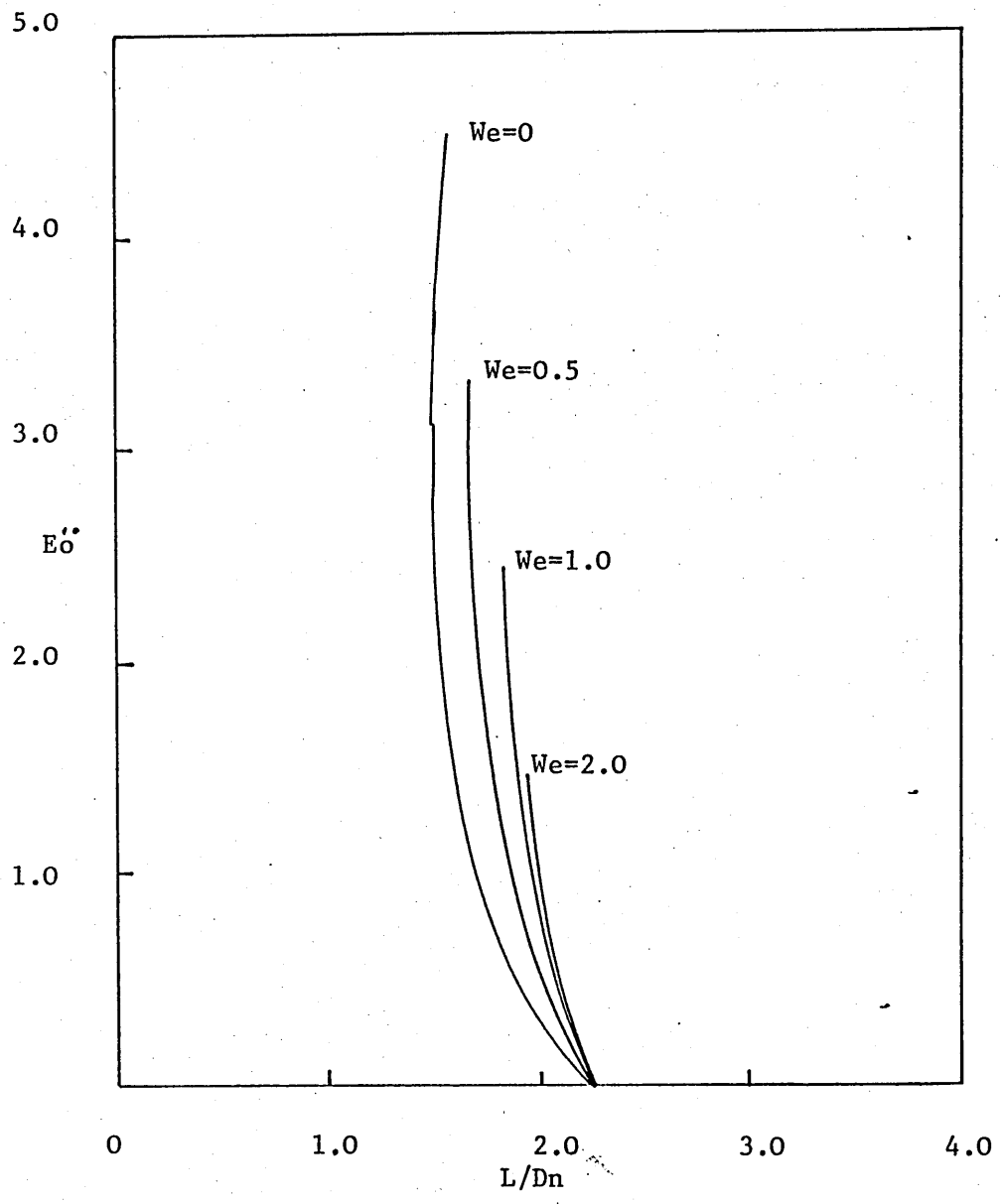

FIGURE B

Relationship between L/Dn and Eö at various We

f	L/Dn		We										
			0	0.2	0.4	0.6	0.8	1.0	1.2	1.4	1.6	1.8	2.0
1	2.25	Eö B, Vo/Vs	0 1 0	0 0.95 0	0 0.90 0	0 0.85 0	0 0.80 0	0 0.75 0	0 0.70 0	0 0.65 0	0 0.60 0	0 0.55 0	0 0.50 0
0.90	2.14	Eö B Vo/Vs	0.42 0.90 0.10	0.47 0.83 0.11	0.51 0.77 0.12	0.56 0.71 0.13	0.61 0.65 0.14	0.66 0.59 0.15	0.71 0.52 0.17	0.76 0.46 0.18	0.81 0.40 0.19	0.86 0.34 0.20	0.91 0.28 0.21
0.80	2.04	Eö B Vo/Vs	0.88 0.80 0.20	1.00 0.72 0.22	1.13 0.64 0.25	1.25 0.56 0.28	1.38 0.48 0.31	1.50 0.40 0.34	1.63 0.33 0.36	1.75 0.25 0.39	1.88 0.17 0.42	2.00 0.09 0.43	2.13 1.87 0.48
0.70	1.95	Eö B Vo/Vs	1.39 0.70 0.30	1.63 0.59 0.35	1.88 0.49 0.40	2.12 0.39 0.45	2.36 0.29 0.50	2.60 0.18 0.56	2.85 0.08 0.61	3.09 -0.01 0.66	3.33 -0.11 0.71	3.57 -0.21 0.76	3.82 -0.32 0.82
0.60	1.87	Eö B Vo/Vs	1.95 0.60 0.40	2.39 0.46 0.46	2.82 0.32 0.57	3.26 0.18 0.66	3.70 0.04 0.75	4.13 -0.09 0.84	4.57 -0.23 0.93	5.00 -0.37 1.02	5.44 -0.51 1.11	5.87 -0.65 1.20	6.31 -0.78 1.28
0.50	1.81	Eö B Vo/Vs	2.57 0.50 0.50	3.34 0.30 0.65	4.11 0.10 0.80	4.88 -0.10 0.95	5.65 -0.30 1.10	6.42 -0.50 1.25	7.20 -0.70 1.40	7.97 -0.90 1.55	8.74 -1.10 1.70	9.51 -1.30 1.85	10.25 -1.50 2.00
0.40	1.77	Eö B Vo/Vs	3.23 0.40 0.60	4.64 0.05 0.80	6.05 -0.22 1.12	7.47 -0.53 1.38	8.88 -0.85 1.65	10.29 -1.16 1.91	11.71 -1.47 2.17	13.12 -1.78 2.43	14.53 -2.10 2.70	15.95 -2.41 2.96	17.36 -2.72 3.22
0.30	1.75	Eö B Vo/Vs	3.92 0.30 0.70	5.76 -0.25 1.20	7.60 -0.81 1.71	12.43 -1.36 2.21	15.27 -1.92 2.72	18.11 -2.47 3.22	20.94 -3.03 3.73	23.78 -3.58 4.23	26.62 -4.14 4.74	29.46 -4.70 5.25	32.29 -5.25 5.75
0.20	1.77	Eö B Vo/Vs	4.64 0.20 0.80	11.61 -1.05 2.00	18.58 -2.30 3.20	25.54 -3.55 4.40	32.51 -4.80 5.60	39.48 -6.05 6.80	46.45 -7.30 8.00	53.41 -8.55 9.20	60.38 -9.80 10.40	67.35 -11.05 11.60	74.32 -12.30 12.86
0.10	1.85	Eö B Vo/Vs	5.35 0.10 0.90	34.78 -4.88 -5.54	64.21 -9.89 10.80	93.64 -14.90 15.75	123.08 -19.90 20.70	152.51 -24.90 25.65	181.94 -29.89 30.59	211.37 -34.89 35.54	240.81 -39.89 40.49	270.24 -44.89 45.44	299.67 -49.89 50.39

TABLE A COMPUTER SOLUTION FOR EQUATIONS 5.37, 5.38 and 5.39 TO PLOT Vo/Vs and L/Dn AS FUNCTIONS OF Eo and We.